Alma Mater Studiorum · Università di Bologna

Scuola di Scienze

Corso di Laurea Magistrale in Fisica

RADIOTHERAPY WITH SCANNING CARBON ION BEAMS: BIOLOGICAL DOSE ANALYSIS FOR PARTIAL TREATMENT DELIVERY

Relatore:

Prof. Gastone Castellani

Presentata da:

Lucio Alticozzi

Correlatori:

Dott. Mario Ciocca

Dott. Simona Giordanengo

Sessione III

Anno Accademico 2014/2015

Abstract

L'uso di particelle cariche pesanti in radioterapia prende il nome di adroterapia.
L'adroterapia permette l'irraggiamento di un volume bersaglio minimizzando il danno ai tessuti sani circostanti rispetto alla radioterapia tradizionale a raggi X.
Le proprietà radiobiologiche degli ioni carbonio rappresentano un problema per i modelli radiobiologici a causa della non linearità della loro efficacia biologica.
In questa tesi presenteremo gli algoritmi che possono essere usati per calcolare la dose fisica e biologica per un piano di trattamento del CNAO (Centro Nazionale Adroterapia Oncologica).
Un caso di particolare interesse è l'eventualità che un piano di trattamento venga interrotto prima del dovuto. A causa della non linearità della sopravvivenza cellulare al variare della quantità di dose ricevuta giornalmente, è necessario studiare gli effetti degli irraggiamenti parziali utilizzando algoritmi che tengano conto delle tante variabili che caratterizzano sia i fasci di ioni che i tessuti irraggiati.
Nell'ambito di questa tesi, appositi algoritmi in MATLAB sono stati sviluppati e implementati per confrontare la dose biologica e fisica assorbita nei casi di trattamento parziale.

Abstract

The use of heavy charged particles in radiotherapy is called hadron therapy.
Hadron therapy allows irradiation of target volume with much less damage to healthy tissue compared to x-ray therapy.
The radiobiological properties of carbon ions represent a problem for radiobiological models due to the non linearity of the biological effectiveness of carbon ions.
In this thesis, we will present the algorithms that can be used to calculate physical and biological dose for a given treatment plan at CNAO (National Center for Oncological Hadron therapy).
A case of particular interest is the eventuality of a treatment plan being interrupted before the end of the daily irradiation. Dedicated algorithms have to be used to calculate the actual biological dose delivered to the patient when parts of the the planned dose is missed.
For this thesis, special MATLAB scripts have been developed and use to compare physical and biological dose in the case of partial treatment.

Contents

Introduction

The use of heavy charged particles – hadrons – for cancer radiotherapy purpose is called *hadron therapy*.
Compared to conventional, X-ray based radiotherapy, this kind of treatment potentially allows for a more efficient tumor irradiation, while reducing damage to healthy tissue. This is due to a better spatial control on dose deposition, a characteristic of ions. During the last 5 years, the number of hadron therapy dedicated centers quickly increased thanks to good clinical results and subsequent interest by businesses.
Italian reasearch has contributed to the technological and scientific development of this thecnology for the last 20 years and obtained three active hadron therapy centers within the country. The first was born in Catania, at INFN's Laboratori Nazionali del Sud, where eye tumors have been treated since 2002 using ciclotron-accelerated proton beams. The second – and first to be a dedicated hospital center – is CNAO, the National Centre for Oncological Hadron therapy, situated in Pavia, which has been treating patients since September 2011 using both protons and carbon ions. Finally, the proton therapy center in Trento has been operating since 2014, and has been bought by Belgian Ion Beam Applications (IBA) company.
This thesis work has been conducted with CNAO and the Turin section of the INFN. The main goal is to realize a suite of programs, in MATLAB, to easy compute and analyze the delivered biological dose in case of interrupted treatment – i.e, if a part of the daily irradiation session is missed. This situation, despite being rare, happens on occasion due to machine related or patient related issues. When it happens, because of the non linearity in the biological efficacy of carbon ions treatment, the actual delivered dose must be recalculated, taking into account the reduced number of ions delivered and the partial

target coverage.
To evaluate the dose delivered to a patient in a carbon ion treatment, an algorithm is required to simulate the dose distribution taking into account the physical interactions of particles with traversed tissues and subsequent biological effects.

In chapter 1 of this thesis we will see the physical and biological aspects of ionizing radiation, we will approach the field called *dosimetry* and study the biological effects of the radiation-matter interaction.
In chapter 2 we will introduce CNAO, where certain kinds of tumors are treated with protons and carbon ions accelerated by a synchrotron. We will introduce the structure and techniques used at CNAO.
In chapter 3 we will consider in more detail treatment plans used in hadron therapy, the techniques employed and the radiobiology of carbon ions. The Local Effect Model, LEM, will be introduced; it is the model used at CNAO that describes the radiobiological effects of carbon ions.
In Chapter 4 we will learn Treatment Planning System, TPS, and in particular about the TPS DEK (Dose Engine Kernel) used for this thesis. DEK is developed by INFN, in particular at the Turin section in collaboration with the IBA, mentioned above.
Then we will consider the methods used to compare the biological dose distribution in case of partial treatment introducing the Dose Volume Histogram, DVH.
Finally, in Chapter 5 we will analyze the plots that we obtained to evaluate the effects of the relative biological effectiveness (RBE) in case of partial treatment for two patients treated at CNAO.

Chapter 1

Biological and physical aspects of hadron therapy

Radiation therapy is the medical use of ionizing radiation to treat cancer. In conventional radiation therapy, beams of X rays (high energy photons) are produced by accelerated electrons and then delivered to the patient to destroy tumour cells. Using crossing beams from many angles, radiation oncologists irradiate the tumour target while trying to spare surrounding normal tissues. Inevitably some radiation dose is always deposited in the healthy tissues.

When the irradiating beams are made of charged particles (protons and other ions, such as carbon), radiation therapy is called **hadron therapy**. The strength of hadron therapy lies in the unique physical and radiobiological properties of these particles; they can penetrate the tissues with little diffusion and deposit maximum energy just before stopping. This allows a precise definition of the specific region to be irradiated. The peaked shape of the hadron energy deposition is called *Bragg peak* and has become the symbol of hadron therapy. With the use of hadrons the tumour can be irradiated with less damage to surrounding tissues than with X-rays.

The idea of using beams of high-energy charged particles in radiotherapy dates back to 1946 and is due to Robert R. Wilson, who first investigated the depth profile of the dose achieved with proton beams, initially for shielding applications. Wilson was able to guess the potential clinical benefits of this particular radiation, and predicted that an exact small and well-defined portions of the body as target would soon be possible. Two years later, at Lawrence Berkeley Laboratory in the USA, a sicrotrone was employed for pro-

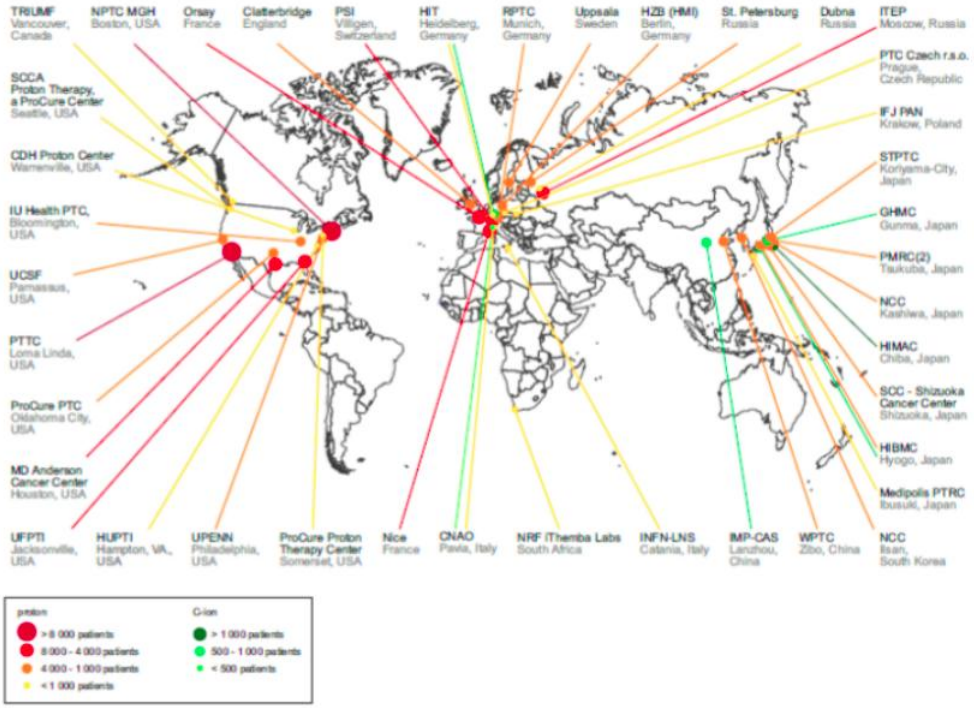

Figure 1.1: Proton (red-orange) and C-ion (green) centers active worldwide. The size of the spot is proportional to the number of patients treated as indi- cated in the figure legend

ton beams physical and radiobiological experiments. Initially, in 1954 the first patients were treated with proton beams, then helium. From that moment, the use of protons for therapeutic purposes and biological research has spread quite rapidly throughout the world; because of complexity and cost of the accelerators to light ions, treatment by ion beams was conducted initially using accelerators dedicated to fundamental research in nuclear and particle physics. In 1993, the first hospital to become operationally dedicated to hadrotherapy was the Loma Linda University Medical Center in California, currrently about thirty proton centres are either in operation or in construction worldwide. Although protons are used in several hospitals, the next step in radiation therapy is the use of carbon ions. In Fig. 1.1 centres which are actually active worldwide are showed.
Conventional radiotherapy has two intrinsic drawbacks which arise from the shape of the natural attenuation of the beam entering the body and its lateral diffusion. The attenuation leads most of the overall dose being deposited before the target depth, while lateral

diffusion limits the collimation of photon beams. These aspects make photon beams scarcely apt to treat deep-seated tumors resulting in a substantial dose being delivered to critical organs (Organs At Risk = OAR) in contrast to having just the required dose deposited in the tumor. Hadron Therapy is ideally suited to treat tumors that are deep-seated, located close to critical organs and which respond poorly to conventional photon or electron radiotherapy. The clinical goal of a good radiotherapy technique is to maximize the damage to the tumor, and to minimize dose in the healthy tissues. Thanks to their features, proton and carbon ion beams for therapy will not only improve the tumor control probability for certain malignant diseases, but also reduce long-term complications in the surrounding healthy tissue. This "conformational therapy" is particularly advantageous in the case of ocular, brain, salivary glands, backbone tumors and some tumors at prostate and uterus. Well collimated protons beams and heavier ions permit a conform irradiation of the target, following the contour with a millimetric precision and sparing healthy tissue sourrounding the tumor in a better way than conventional radiation. Treatment with protons permits to increase the prescribed dose to the tumor without increasing exposition of vital organs. This largely increases the probability of cure and optimizes the therapeutic outcome of critical organs. Although they have a ballistic accuracy, protons are not more efficient, in term of biological damage induced, than photons or electrons in the treatment of radio-resistant tumors. Those tumors appear to be more sensitive to beams which show an intense local ionization, as carbon, oxygen or neon beams. These ions are said to have an high linear energy transfer (LET) and are interesting in radiotherapy not only for their ballistic accuracy but also for their high biologic effectiveness in comparison with γ radiation (RBE) and the reduced dependence of the oxygen effect at cellular level (OER).

1.1 Biological effects of ionizing radiation

The term **radiation** defines the particular mode in which energy is propagated from one point to another in space, in absence of macroscopic matter transport and without the need of a substrate material support. Radiation can be divided into electromagnetic and corpuscular: the former is constituted by electromagnetic fields oscillating with a certain frequency (electromagnetic waves) which propagate in vacuum at speed of light, the latter are constituted by particles of atomic or subatomic matter at high kinetic energy..

Radiation is classified into *ionizing* and *not ionizing* based on its ability to ionize the medium.
Ionizing radiation can be divided into two main categories:

- Directly ionizing: produces ions directly (particles α, $\beta^{\pm}$)
- Indirectly ionizing: produces ions in an indirect way (X-rays, γ, neutrons)

1.1.1 DNA damage induced by ionizing radiation

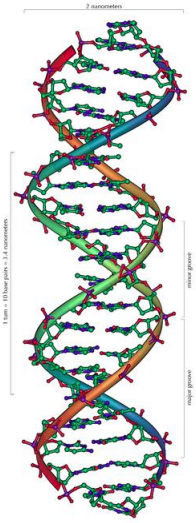

Biological damage caused by radiations results from the ionization of atoms forming the molecular structures of cells in living organisms. A ionized atom will tend to produce new chemical bonds within the molecule to which it belongs. The vital functions of the cell can be compromised if the damaged molecule is critical within the cell.
Deoxyribonucleic acid, **DNA**, is a nucleic acid that contains the genetic information necessary to the biosynthesis of RNA and protein molecules essential for the development and proper functioning of most living organisms. DNA is formed by four different nitrogenous bases: two purine bases (Adenine and Guanine) and two pyrimidine bases (thymine and cytosine) which, assembled in groups of three (triplets), are organized into chains of nucleotides forming the various genes located on chromosomes. Each gene provides for the coding of a particular protein. Each triplet determines a well defined amino acid into the protein. Any errors occurring in response to radiation can lead to position changes of the triplets in DNA molecules, resulting in coding errors for protein building. Such changes can lead to diseases of genetic origin.
The radioinduced structural alteration of nucleic acids has a lethal effect on the cell when the cell loses its ability to divide. This occurs because of an irreparable impairment of hereditary information encoded in the nucleotide sequence of the DNA. It can occur through three main mechanisms:

- Breaking of the main chain.
- Intramolecular bridges formation (covalent bonds, cross-link) that block the duplication process, preventing the separation of the two strands of nucleic acid.

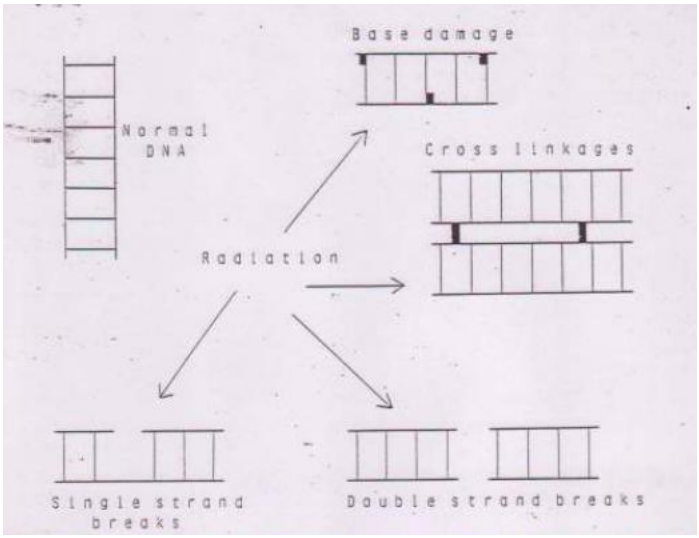

Figure 1.2: Principal DNA damage types induced by ionizing radiation.

- Structural modification of purine and pyrimidine bases. This can lead to a gene mutation of greater or lesser gravity in function of the character-dependent gene concerned.

Breaking of a single chain occurs when damage to one of the two chains leaves the complementary strand intact. The repair mechanism of this kind of damage is quite simple: the section of chain containing the breakage is removed and then rebuilt employing the complementary chain as a reference and finally reconnected by an enzyme called ligase. The number of broken individual strands has been shown to be linearly related to the dose of radiation within a very wide range (from 0.2 to 60000 Gy), the average energy required to produce a single break is comprised between 10 and 20 eV in the case of weakly ionizing radiation.
Breaking of the double chain occurs when two breakages on individual adjacent chains cause the detachment of part of the DNA. A double breakage can derive from a single ionizing event due to the radiation itself, affecting two chains at once or to the combination of two events due to different single breaking events which, incidentally, affect two nearby points of two chains of the same macromolecule. The former happens especially with highly ionizing radiation; in fact, the high density of delivered dose makes a double breaking event quite probable. The latter occurs when the second radiaton damage is dealt before the firse can be repaired. This most likely occurs in the presence of high dose

rate. Has been experimentally sought the relationship between dose and number of double breakage; the model more accepted is the linear-quadratic. It seems that a double chain breaking can not be repaired or possibly can be repaired by an "error-prone" mechanism. The dose dependence is linear-quadratic.

1.1.2 Cell survival curves

After a single dose of ionizing radiation, the number of living cells (surviving fraction) decreases with increasing dose. The graphic expression of this phenomenon is the **cell survival curve**.

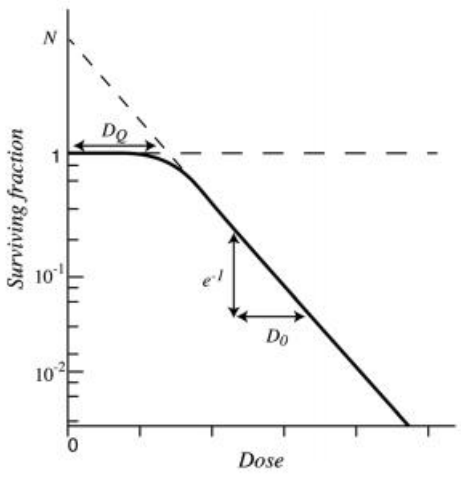

The typical survival curve for mammalian cells has a "shoulder" at low doses and becomes exponential only for higher doses. D_0 determines the slope of the linear part of the curve and indicates the dose which reduces the surviving fraction to a factor equal to 0.37. The number of extrapolation N, wich is obtained by extrapolating the linear portion of the curve until it intersects the y-axis, is an index of the cell's ability to store and repair the subletha damage and represents the number of targets to hit. Typically D_0 has values between 1-2 Gy and N between 1 and 5. The width of the shoulder is indicated by the parameter D_q (quasi-threshold dose), which is the intersection between the extension of the exponential part, straight part of the curve and the horizontal line passing through the 100% of survival. To interpret the behavior of survival curves in which a shoulder is present, a theoretical model has developed based on the assumption that inactivation of a cell requires the inactivation inside the cell of a number $n \geq 1$ of targets, each of which requires a single shot to be inactivated (hypothesis of multiple targets single-shot). The inactivation of the cell occurs only when a number of sublethal events occur within a short period of time. At low dose, only a few events per cell will occur, thus making cell death unlikely.. There will be a dose range in which inactivation is not experienced (part of the shoulder).

At higher dose, interaction events within cells begin to add up, until the first inactivations occur. The survival curve will begin to trend downward (passage between shoulder and linear region). Increasing the dose again, the number of events per cell will keep growing, trending to be n-1 in each of them. Above this dose, the behavior is identical to a system of elements inactivable with a single blow, as a single additional event per cell will reach the N threshold and cause inactivation.
The analytical expression corresponding to this theoretical model is the following:

$$f = 1 - (1 - e^{-\frac{D}{D_0}})^n \tag{1.1}$$

This model implies a zero slope at low dose; however, experimental data is often not in agreement with it. The suitable model for the majority of survival curves for mammalian cells posits that cell death can be determined by a variety of processes. It then combines the principles of the multiple targets model with a single event component. The corresponding analytical expression is the following:

$$f = e^{-\frac{D}{D_1}} \left[1 - (1 - e^{-\frac{D}{D_2}})^n\right] \tag{1.2}$$

A model widely used in radiotherapy is the textbf linear quadratic. In this model, the fraction of surviving cells is

$$f = e^{-\left(\alpha D + \beta D^2\right)} \tag{1.3}$$

where D is the dose, α and β are two constants:

- α: log of cells killed per Gy, is the constant of proportionality linearly linking the cellular lethality to single hit damage
- β: log of cells killed per Gy^2, is the constant of proportionality quadratically linking the cellular lethality to damage due to the sum of sub-lethal events

The ratio α/β is the dose in Gy at which lethality is equally likely to be due to single events and to accumulation of sublethal damage.
According to this model there are two components that determine cell death by radiation: a component proportional to the dose administered (α) and a component proportional to the square of the dose (β). The component αD represents a non-repairable damage (the dose / effect relationship is linear, from single shot, and therefore even small

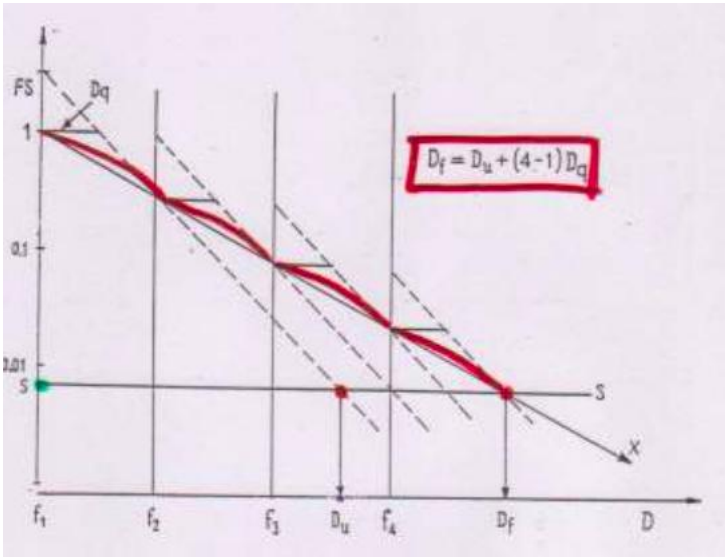

Figure 1.3: Fractionated irradiation: the overall dose is given by $D_f = D_u + (n-1)D_q$, where n is the number of fractionations.

doses are able to cause damage). The component βD^2 indicates the existence of recovery processes (more hit events), the dose should increase quadratically to surmount them.

In the case of *fractionated irradiation*, Fig. 1.3, at each subsequent irradiation reoccurs the shoulder, because of a repair of sublethal damage by the elements of the system. The overall dose, necessary to obtain the same degree of cell inactivation, must be increased by ìD_q times fractions -1.
The dose fractionation in radiation therapy involves a "therapeutic gain", in fact it increases tolerance in normal tissues (due to repair and restocking phenomena) and at the same time eliminates the radioprotective effects of hypoxia on tumor (due to reoxygenation phenomena).

1.1.3 Radiation quality

Although all ionizing radiations interact with living matter in a similar manner, different types of radiation differ in their effectiveness, or ability to do harm to a biological system. The various radiations, in fact, interact with matter in a different way in relation to the amount of energy deposited along their path.
The transfer of energy of the radiation is defined by the **LET** (*linear energy transfer*)

and denoted by the symbol L_Δ

$$L_\Delta = \left(\frac{dE}{dl}\right)_\Delta \tag{1.4}$$

where dE is the local energy loss due to collisions for a charged particle along a track segment dl, considering only collisions involving transfer of energy less than Δ (in eV). L_Δ is habitually expressed in $keV \cdot \mu m^{-1}$. If $\Delta = \infty$ all energy losses are considered.
High LET means high specific ionization. A particle can have a low LET at high energy and a high LET at low energy.

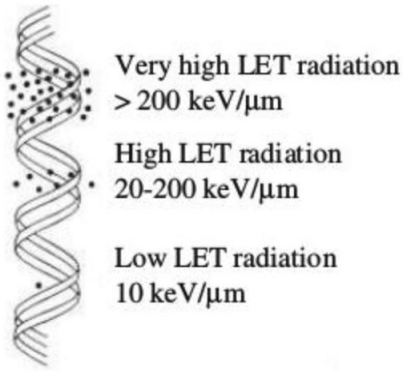

- Low-LET radiations have tracks with primary events (collisions) well separated in space, it is the case of X-rays which are said to be *sparsely ionizing*.
- High-LET radiations have tracks with primary events not well separated in space, a dense column of ionization is produced. It is the case of ions and heavy particles which are said to be *densely ionizing*.

So a different LET leads, at equal doses, to different biological effects and to take account of this fact the *relative biological effectiveness*, **RBE**, has been introduced. The intent is to quantify the effect, at the same imparted dose, of a radiation r in comparison with a reference radiation which is assumed to be that of X-rays at 250 kV. By this definition, the reference radiation has RBE equal to 1. This way RBE, or weighting factors, quantify the increment of biological effects of highly ionizing radiations with respect to X-rays at the same physical dose.
Its follows: the RBE of some test radiation (r) compared with X-rays is defined by the ratio

$$RBE = \frac{D_{250}}{D_r} \tag{1.5}$$

where D_{250} and D_r are respectively, the doses of X-rays of 250 kV, and the test radiation required for equal biological effect. The higher the LET, the higher the biological effectiveness (RBE), as it is shown in Fig. 1.4 for radiations of different LET.

DRBE defined as the product of hadron absorbed dose, D, and hadron RBE

$$DRBE = D \times RBE \tag{1.6}$$

is introduced to estimate the photon dose that would produce the same therapeutic effect as the hadron absorbed dose, D, given under identical conditions.
An essential goal for the development of heavy ion therapy is not only to select with the Bragg peak the tumor area, but also to maximize the difference in the biological effectiveness between entrance channel and tumor area. The advantage of heavy ions beams like carbon ions, in comparison with protons, is the higher relative biological effectiveness at the beam range (about three times the RBE effectiveness at the end of the range of the beam). At the entrance channel, the RBE is only slightly elevated. The low dose in the entrance channel produces less and more reparable damage than the more significant damage in the target volume. RBE is a function of radiation quality (LET) (Fig. 1.4), radiation dose, fractionation, dose rate, cell tissue type, and end-point.

At last, because the presence or absence of molecular oxygen dramatically influences the biologic effect of x-rays, has been introduced the oxygen enhancement ratio, **OER**, defined as the ratio of doses under hypoxic to aerated conditions that produce the same biological effect. Oxigen presence (aerated cells) increases radiation effectiveness for cell killing, lack of oxygen (hypoxic cells) results in more radio resistant cells.

1.2 Radiation and dosimetric fields

When in a certain region of space radiations propagate (of any kind) it is said that this region is the seat of a *radiation field*, described by field quantities. A simple way to describe the radiation field consists counting the number of particles that pass through a sphere of maximum section dA in a finite time interval. We define *fluence of the radiation field* the number of particles dN crossing the ball during the experiment

$$\Phi = \frac{dN}{dA} \quad \left[\frac{particle}{cm}\right] \tag{1.7}$$

The fluence rate is the time derivative of the fluence:

$$\phi = \frac{d\Phi}{dt} \quad \left[\frac{particle}{cm\,s}\right] \tag{1.8}$$

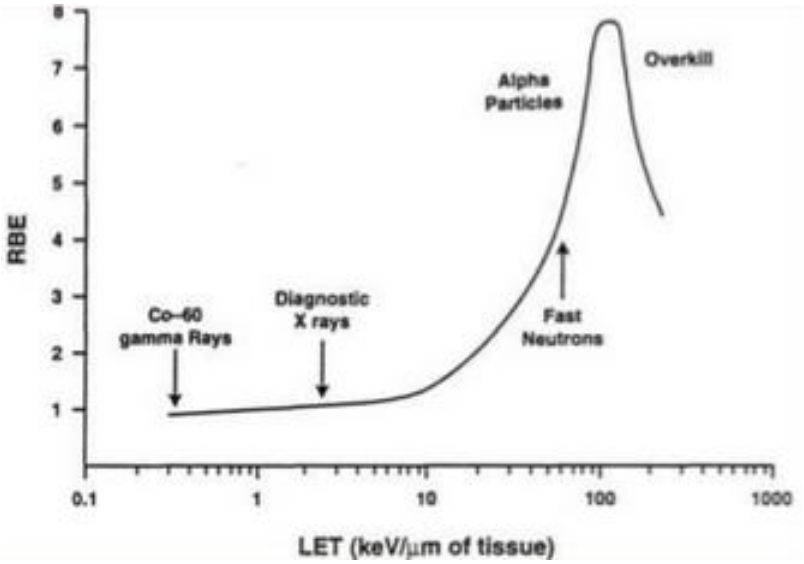

Figure 1.4: The LET at wich the RBE reaches a peak is much the same (about 100 $keV/\mu m$) for a wide range of mammalian cells; as the LET increases, the RBE increases slowly at first, and then more rapidly as the LET increases beyond 10 $keV/\mu m$, beyond 100 $keV/\mu m$, the RBE again falls to lower values. In the case of sparsely ionizing X-rays the probability of a single track causing a DSB is low, thus X-rays have a low RBE. At the other extreme, densely ionizing radiation (ex. LET of 200 $keV/\mu m$) readily produce DSB, but energy is "wasted" because the ionizing events are too close together; thus, RBE is lower than optimal LET radiation.

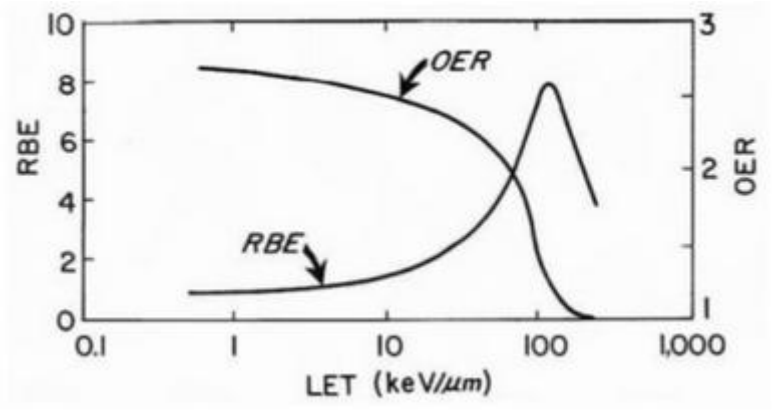

Figure 1.5: Variation oof OER and RBE as a function of LET of the radiation involved.

Another important quantity is the stopping power, which is the rate (in terms of length) with which a particle loses kinetic energy:

$$S = -\frac{dE}{dx} \quad \left[\frac{MeV}{cm}\right] \tag{1.9}$$

usually we use the massive stopping power, that is the proper stopping power depending on the density of the material:

$$\frac{S}{\rho} = -\frac{dE}{\rho dx} \quad \left[\frac{MeV}{g/cm^2}\right] \tag{1.10}$$

this quantity often loses its dependence on material crossed because dE/dx is divided by the density ρ of the target.

The purpose of the *dosimetry* is to identify physical quantities to be put to quantitative relationship with the effects (deterministic and stochastic) induced by ionizing radiation. The oldest of the dosimetric quantities is the *exposure* and was introduced to describe the ability of electromagnetic radiation to produce ionization in air

$$X = \frac{dQ}{dm} \tag{1.11}$$

where dQ is the absolute value of the total charge of the ions, produced in the air when all the electrons (positive and negative) released by the photons in the element of volume of mass dm are completely stopped in the air. In SI exposure is measured in $C\,kg^{-1}$. The most commonly used, however, is the old special unit, the *roentgen*, R, whose value is: $1R = 2.58 \times 10^{-4} CKg^{-1}$.
We define the *absorbed dose*

$$D = \frac{d\bar{\epsilon}}{dm} \tag{1.12}$$

as the mean energy imparted by ionizing radiation to a volume element of mass dm. For purposes of radiation protection it is useful to define a mean absorbed dose to tissue or organ, called *organ dose*

$$D_T = \frac{d\epsilon_T}{dm} \tag{1.13}$$

Where ϵ_T is the total energy imparted in a tissue or organ and m_T is the mass of that tissue or organ. The unit of measurement is the *Gray* ($1\,Gy = 1\,J/Kg$).

$L_\infty\,(keV\cdot\mu m^{-1})$	Q(L)
L<10	1
$10 \leq L \leq 100$	0.32L-2.2
L<100	$300L^{-1/2}$

Table 1.1

The probability of stochastic effects depends not only on the absorbed dose, but also on the type and energy of radiation. This fact is taken into account by weighing the absorbed dose by a factor related to the quality of radiation. In the past this factor has been applied to the absorbed dose at one certain point and called *quality factor*, Q, related to LET radiation (table 1.1). The weight factor is now called *weight factor of radiation* w_R and depends on the type and energy of radiation. We call *equivalent dose*:

$$H_T = \sum_R w_R D_{T,R} \tag{1.14}$$

where $D_{T,R}$ is the absorbed dose averaged over tissue or organ T, due to radiation R. The value of the radiation weight factor is indicative of the relative biological effectiveness value of that radiation to induce stochastic effects at low doses. The values of w_R are broadly compatible with the values of Q, related to the linear energy transfer (LET), a measure of the ionization density along the track of a particle. The unit of measurement is the *Sievert*, Sv.

The relationship between the probability of stochastic effects and the equivalent dose also depends on the organ or the tissue irradiated. The equivalent dose in tissue or organ T is then weighed with the tissue weight factor, w_T, representing the contribution of that organ or tissue to the total detriment resulting from uniform irradiation of the whole body. Is then introduced the *effective dose*, as the sum of the weighted equivalent doses in all the tissues and organs of the body:

$$E = \sum_T w_T H_T \tag{1.15}$$

where H_T is the equivalent dose in tissue or organ T and w_T is the weight factor for the tissue T. The values of w_T are chosen so that a equivalent uniform dose over the entire body gives an effective dose numerically equal to the equivalent uniform dose. The sum of the weight factors is therefore equal to 1 (see table 1.3.

Type and energy range	Weight factor
Photons of all energies	1
Electrons and muons of all energies	1
Neutrons, of energy < 10 keV	5
Neutrons, of energy from 10 keV to 100 keV	10
Neutrons, of energy from 100 keV to 2 MeV	20
Neutrons, of energy from 2 MeV to 20 MeV	10
Neutrons, of energy > 20 MeV	5
Alpha particles, fission fragments, heavy nuclei	20
Protons, of energy > 2 MeV	5

Table 1.2: All values are related to the incident radiation on body or, for inside sources, emitted from the source.

1.3 Charged heavy particles interaction with matter

A charged particle passing through matter undergoes many collisions before being stopped. To a first approximation we can assume that the slowdown occurs continuously (zig-zag for electrons, straightforward for a heavy particle). The loss of energy is given by:

- Ionization and excitation of electrons in the medium.
- Molecular bonds breakage (radical formation).
- Radiation emission.

According to classical electrodynamics, a charged particle subjected to an acceleration a emits radiation proportional to a^2. For a particle that passes near a nucleus, $a \propto Z/M$ where Z is the atomic number of the nucleus and M the mass of the particle, the emitted radiation is proportional. to $(Z/M)^2$. Due to the term $\left(\frac{1}{M}\right)^2$, the radiative loss is significant only for electrons.
The mode of interaction of charged particles depends on the energy of the particles and the minimum distance they reach from the nucleus.

- Distant collisions: the atom is excited or ionized.
- Nearby collisions: peripheral electrons extraction and energy loss.

Organ or tissue	Weight factor
Gonads	0.20
Red bone marrow	0.12
Colon	0.12
Lung	0.12
Stomach	0.12
Bladder	0.05
Breasts	0.05
Liver	0.05
Esophagus	0.05
Thyroid	0.05
Skin	0.01
Bone surface	0.01
Remaining organs and tissues	0.05

Table 1.3: These values were derived from a reference population, comprising an equal number of individuals of both sexes and a wide range of ages. These values apply to workers, to population and to both sexes.

1.3.1 Bethe-Block formula

When a heavy charged particle passes through a material, the average loss of energy per unit path length is given by the following theoretical expression (**Bethe-Bloch formula**):

$$-\frac{dE}{dx} = \frac{4\pi e^4 z^2 ZNB}{mv^2} \tag{1.16}$$

with

$$B = ln\left[\frac{2mv^2}{I(1-\beta^2)}\right] - \beta^2$$

where z is the charge of the particle, Z the atomic number of the medium, N is the number of atoms per cm^3 of the absorbing material, M is the mass of the electron, I the average potential of ionizationl of the absorbent substance atoms and $\beta = v/c$.
The formula of Bethe-Bloch is independent of the mass of the particle and is valid as long as the energy of the incident particle is much higher than the ionization potential of the

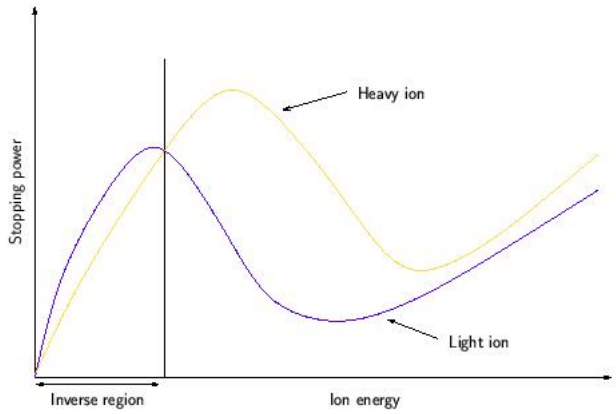

Figure 1.6: Energy loss as function of the particle energy.

electrons.

The trend of the energy as a function of energy loss (dE/dx) depends strongly on the energy of the particle. As you see in Fig. 1.6, at low energy the term $1/\beta^2$ dominates, reaching a minimum ionization point and for higher energies there is a relativistic lift. For very low energies, when the speed of the primary particle becomes of the same order of magnitude as the velocity of the electron orbital, the formula is no longer valid.

1.3.2 Bragg curve

The increase in ionization near the end of the path is explained by the dependence of the stopping power by the term $\frac{1}{v^2}$ in the formula 1.16. The specific ionization remains almost constant until near the checkpoint of the particle, where it rapidly increases, giving rise to the so-called **Bragg peak**.

The stopping power is an additive quantity, therefore, for a material that is a mixture of elements, it can be rewritten as:

$$\frac{S}{\rho} = \sum w_i \left(\frac{S}{\rho}\right)_i \tag{1.17}$$

See Fig. 1.8 to understand the use of Bragg peak to achieve the tumor depth with respect conventional radiotherapy.

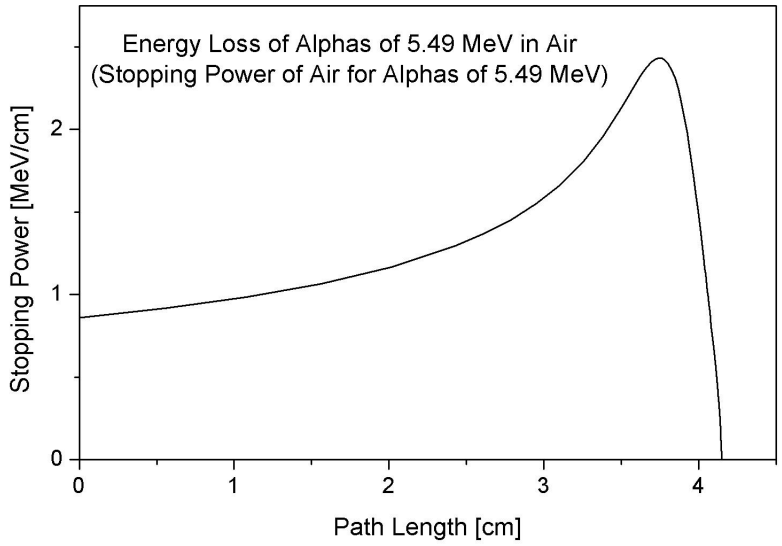

Figure 1.7: The Bragg curve of 5.49 MeV alphas in air has its peak to the right and is skewed to the left.

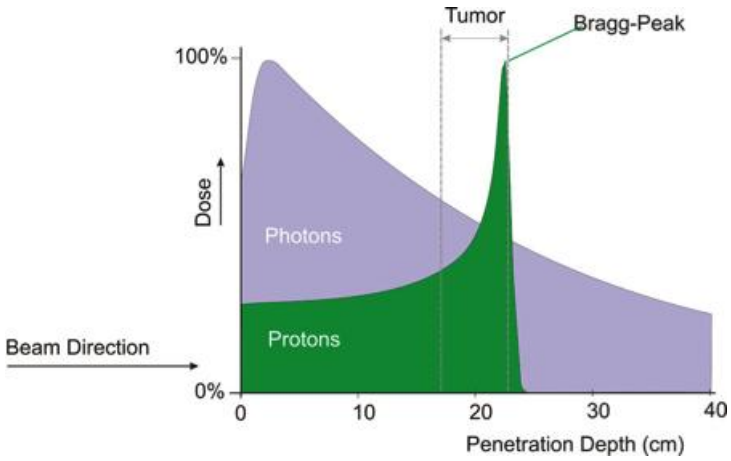

Figure 1.8: Use of Bragg peak in hadron theraphy.

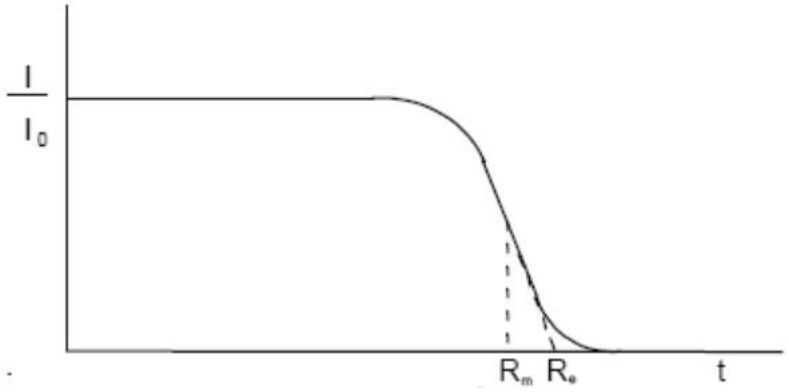

Figure 1.9: Dispersion across the track, R_m is the average range, R_e the extrapolated range.

1.3.3 Energy and range straggling

The heavy charged particles lose energy in collisions with continuity and, mainly because they interact with atomic electrons, are slightly deflected from their trajectory while maintaining a nearly straight path until they stop. This behavior explains the trend of *attenuation curve*.
Each particle has a trajectory of its own and all the particles having the same initial energy have a path that differs statistically from each other.

Average range: Absorber thickness which reduces to 50% the number of particles α transmitted.

Extrapolated range: It is obtained by extrapolating to zero the linear portion of the transmission curve.

The difference, δ, between middle path and extrapolated path is called *straggling*. For α of 5 MeV it is $\sim 1\%$.
The range of the charged particles can be expressed as:

$$R_{calc} = \int_0^{L_f} dx = \int_{E_i}^{0} \frac{1}{(dE/dx)} dE \tag{1.18}$$

In first approximation, neglecting the variation of B with v, you have there the average path of a charged particle of mass M and charge ze (from energy E_0 to 0) is given by:

$$R_{z,M} = \int_{E_0}^{0} \frac{dE}{\frac{dE}{dx}} = \int_{0}^{E_0} \frac{Mmv^2 AdE}{M4\pi e^4 z^2 Z\rho N_0 B} \approx \frac{mA}{2\pi e^4 z^2 Z\rho N_0 BM} \int_{0}^{E_0} EdE = \frac{mAE_0^2}{4\pi e^4 z^2 \rho MZ N_0 B} \tag{1.19}$$

A, ρ and Z are material properties; in two different materials, for particles of a certain type and of a given energy, you have:

$$\frac{R_1}{R_2} = \frac{Z_2\rho_2 A1}{Z_1\rho_1 A_2} \approx \frac{\rho_2}{\rho_1} \quad \left(\Rightarrow \frac{Z_2}{A_2} \approx \frac{Z_1}{A_1}\right) \tag{1.20}$$

When it is known the relationship between the energy and the penetration depth for a certain particle type and for a given material, one can determine the corresponding relationship for a different type of particle in the same material. Considering the dependence of B on the speed v, instead of 1.19 you get:

$$R_{z,M}(E_0) = \int_{E_0}^{0} \frac{dE}{\frac{dE}{dx}} = \frac{Mm}{4\pi e^4 z^2 ZN} \int_{0}^{v} \frac{v^3 dv}{B(v)} \tag{1.21}$$

dove si è usata where is used the relation $E = \frac{1}{2}Mv^2$ $Rightarrow dE = d\left(\frac{1}{2}Mv^2\right) = Mvdv$. You can then rewrite:

$$R_{z,M}(v) = \frac{M}{z^2} F(v) \tag{1.22}$$

where F(v) is essentially the integral 1.21, evaluated between the limits 0 and v. The equation 1.22 shows that for different types of fast particles in an absorbent material, the penetration depth depends only on the velocity of the particle, from its mass M and the charge z.

Using the 1.22 we can relate $R_p(v)$, depth of penetration of a proton with speed v, with the depth of penetration of a particle of mass M and charge z, equipped with the same speed:

$$R_{z,M}(v) = \frac{Mz_p^2 R_p(v)}{m_p z^2} \Rightarrow R_{z,M}(v) = \frac{MR_p(v)}{z^2} \tag{1.23}$$

At constant speed the energies, in the non-relativistic case , are linked by the relation:

$$\begin{aligned} E_p &= \frac{1}{2} m_p v^2 \\ E_M &= \frac{1}{2} M v^2 \end{aligned} \Rightarrow E_p = \frac{m_p}{M} E_M \Rightarrow E_p = \frac{E_M}{M} \tag{1.24}$$

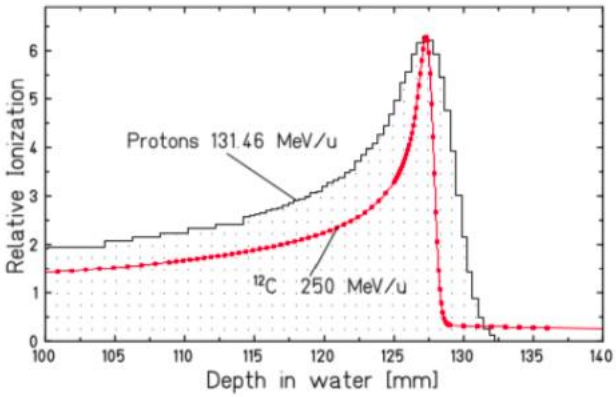

Figure 1.10: Measured Bragg peaks of protons and ^{12}C ions having the same mean range in water Schardt et al.,2008

and then

$$R_{z,M}(E) = \frac{MR_p(E/M)}{z^2} \tag{1.25}$$

Known the range of a proton in a given material, it's possible calculate the range for different mass particles, having the same speed.

In typical biological tissue, range straggling amounts to about 1% of the mean range for protons and only to 0.3% for carbon ions (Fig. 1.10).

The variance σ_R^2 of the range straggling is related to the variance σ_E^2 of the energy-loss straggling by:

$$\sigma_R^2 = \int_0^{E_i} \left(\frac{d\sigma_E}{dx}\right) \left(\frac{dE}{dx}\right)^{-3} dE \tag{1.26}$$

The ratio of the straggling width σ_R^2 and the mean range R is nearly constant and can be described by:

$$\frac{\sigma_R^2}{R} = \frac{1}{\sqrt{m}} f\left(\frac{E}{mc^2}\right) \tag{1.27}$$

where f is a slowly varying function depending on the absorber and E and m are the particle energy and mass.

In practice, the profile of the Bragg peaks is broader, mainly due to the density inhomogeneities of the penetrated tissue. Furthermore, for scanning beam delivery systems using slice-by-slice irradiation of the target volume, it can be even advantageous to widen the sharp Bragg peaks by passive systems in order to reduce the treatment time.

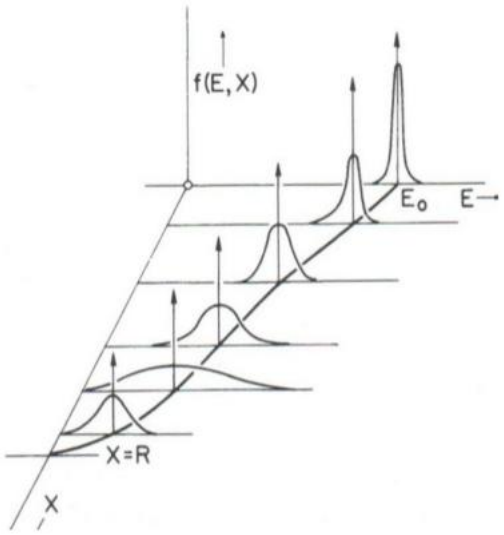

Figure 1.11: Plot of energy distribution of a beam of initially monoenergetic charged particles at various penetration distances. E is the particle energy and X is the distance along the track. Over the first portion, the distribution becomes wider (and more skewed) with penetration distance, showing the increasing importance of energy straggling. Near the end of the range distribution narrows again because the mean particle energy has greatly been reduced.

1.4 Nuclear reactions

Unlike e^+, $^-$ and γ, heavy particles can interact with matter also via strong nuclear force. Different nuclear process dominate at different energies: interaction mechanisms vary from transfer reactions, observed at low energies, to fragmentation processes, observed at the highest energies around 1 GeV/u. In therapeutic applications peripheral collisions, in which fragments are stripped of only few nucleons, are the most frequent reactions, especially in the first few centimeters of depth. Because of the reaction kinematics, projectile fragments travel nearly in forward direction at almost the same velocity as the incident particle and may therefore cause further fragmentation reactions, while the target nuclei remain approximately at rest. The secondary fragments, due to have lower charge, and the same velocity of the projectile, have a longer range than the primary beam particles, giving rise to an undesirable dose deposition beyond the Bragg peak. Dose tails are problematic, because they affect healthy tissues beyond the tumoral volume. The ratio between deposited dose at peak and at tail depends on the particle, primary or secondary, mass. For Lithium and Carbon ions this crucial ratio is of the order of 15%, for Neon ions it is about 30%. The fragments associated must be summed to the one from primary beam at the energy of treatment planning, and finally must be multiplied by the RBE of the various nuclear species generated.
For protons beam, only target fragmentation is possible; although EM interactions of protons dominate, nuclear interactions are not quite rare enough to be neglected. They are more difficult to model but they can be taken into account well enough by using experimentally measured Bragg Peaks. However, their biological effect turns out to be small. According to ICRU63 definitions they are divided in:

- *Elastic*, which are reactions where the incident particle scatter off the target nucleus conserving total kinetics energy. The internal state of both target nucleus and the projectile does not change.

$$p + {}^{16}O \longrightarrow p + {}^{16}O \tag{1.28}$$

- *Inelastic*, which are a subcategory of the nonelastic reactions because the kinetic energy is not conserved but the final nucleus is the same as the bombarded nucleus.

$$p + {}^{16}O \longrightarrow p + {}^{16}O^* \tag{1.29}$$

- *Nonelastic*, which are nuclear reactions that are not elastic, so the kinetic energy is not conserved, and the target nucleus may breakup, or be excited into an higher quantum state... etc.

$$p + {}^{16}O \longrightarrow p + p + {}^{15}N \tag{1.30}$$

p	**d**	**t**	**He-3**	$\boldsymbol{\alpha}$	**Recoils**	**n**	$\boldsymbol{\gamma}$
0.57	0.016	0.002	0.002	0.029	0.016	0.20	0.16

Table 1.4: Percentage of secondaries produced by 150 MeV protons with ^{16}O.

Protons that slow down and stop in matter are called primaries, instead particles from inelastic and nonelastic nuclear reactions are called secondaries. Possible secondaries from nonelastic reactions at therapy energies are protons, neutrons, gamma rays, heavy fragments and recoiling residual nuclei. The importance of each is the fraction of the initial energy carried away. Table 1.4 shows relative energy fraction for 150 MeV protons impacting on ^{16}O nuclei. Total energy imparted to charged particles is 0.64 MeV, and alphas take away only 2.9% of total energy. The RBE enhancement comes from the abundant secondary and, at the distal end of the Bragg Peak, primary low-energy protons. Thanks to the fact that secondaries typically make large angles with the beam axis, unlike primaries which despite multiple scattering rarely exceed a few degrees, secondaries produced in scatterers or absorbers will clear out of the beam before they reach the patient.
For heavier ions, fragmentation is the most important process leading to the build-up of the secondary particles along the penetration depth. Some important conclusions can be drawn on the effects of fragmentation relevant to high-energy ion beam radiotherapy:

- Nuclear reactions cause a loss of primary beam particles and a buildup of lower-Z fragments. These effects become more and more important with increasing penetration depth, or initial beam energy.

- Secondary (or higher-order) projectile-like fragments move with about the same velocity as the primary ions. They have in general longer ranges and produce a dose tail behind the Bragg peak.

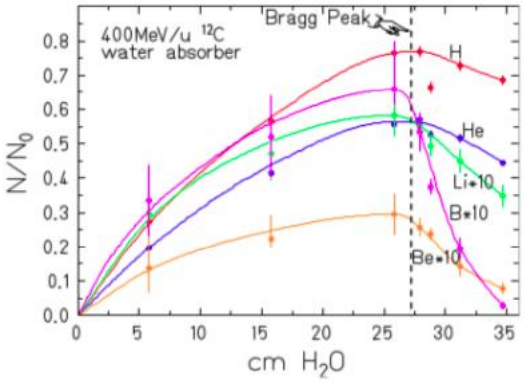

Figure 1.12: Buildup of secondary fragments produced by 400 MeV/ u C-12 ions stopping in water.

- The angular distribution of fragments is mainly determined by reaction kinematics and forward directed, but is much broader than the lateral spread of the primary ions caused by multiple Coulomb Scattering.

See Fig. 1.12 to have an idea of the build up of secondary fragments produced by 400 MeV/u 12 C ions stopping in water.
The impact of nuclear fragmentation on depth dose profile is shown in Fig. 1.13. As already mentioned, with increasing penetration depth the peak-to-entrance dose ratio becomes gradually smaller, mainly due to the exponentially diminishing flux of primary ions. The buildup of lower-Z fragments is clearly visible in the dose tail behind the Bragg peak at larger depths. Additionally, Bragg peaks are increasingly broadened by straggling. In comparison to ^{12}C ions these effects are much more pronounced in the example shown in Fig. 1.14 for 670 MeV/u ^{20}Ne ions with a range of about 36 cm in water. The peak-to-entrance dose ratio is only 1.5 in this case. The calculated contributions of the primary ions and second and third generation fragments are based on a semi-empirical fragmentation cross-section formula (Sihver et al., 1998).
Clinical applications require a relatively uniform release of the dose at target volume. Therefore the beam must be spread out laterally and along the depth. This is obtained by overlapping different Bragg peaks of specific intensities and energies, both with the active and passive technique, and the resulting dose distribution is called *Spread-Out-Bragg-Peak* (**SOBP**), see Fig. 1.16. The SOBP amplitude is defined as the distance between the dose level at 90% proximal and the 90% distal on the depth-dose curve. In

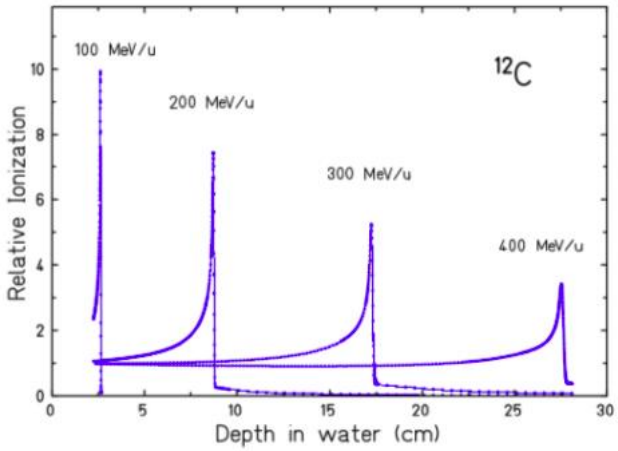

Figure 1.13: Measured Bragg curves of ^{12}C ions stopping in water.

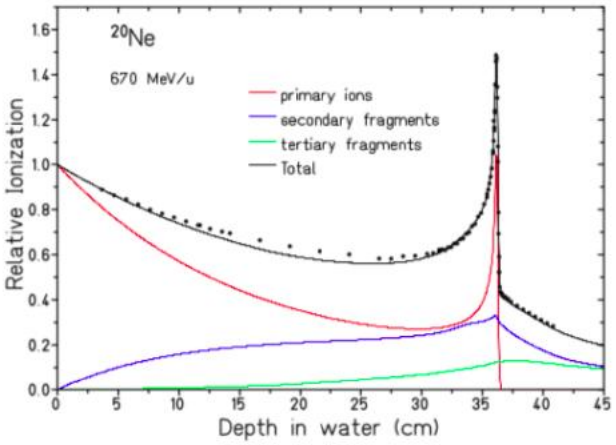

Figure 1.14: Bragg curve for 670 MeV/u Ne-20 ions in water at GSI (circles) and calculated contributions of primary ions, secondary and tertiary fragments.

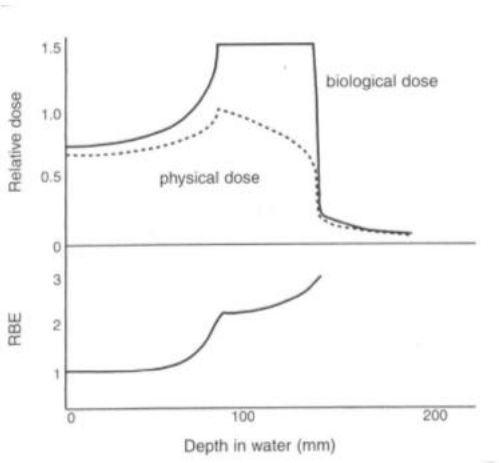

Figure 1.15: Schematic representation of the variation with depth of RBE, showing the profile of the (physical) dose required to obtain a flat SOBP in term of "biological dose".

order to obtain a uniform release of the dose at target volume the rise of RBE over the SOBP must be considered, clearly related to the presence at the end of the range of low-energy, thus high-LET, particles. In general, at the "entrance channel" of a hadron beam the high-LET component is small. Here, for example, protons behaves much like a photon beam and the subsequent LET rise is quite limited so that only over the last millimeters or fractions of millimeters the low-energy, high-LET, component is large enough to give an RBE significantly larger than 1. For carbon ions there is a significant increase in RBE over all the SOBP. If an homogeneous biological effect is desired over the tumor volume, then the physical dose of the carbon beam has to decrease towards the distal edge (Fig. 1.15). The ratio between RBE around the Bragg peak and that in the entrance plateau region is a significant factor determining how much the traversed tissue can be spared. The proportion of low-energy, high-LET, particles varies with depth and strongly depends on the beam initial energy, as it can be seen from the example shown in Fig. 1.13. For protons with 200-250 MeV initial energy only over the last millimeters, or fraction of a millimeter, this component is significant, giving an RBE significantly larger than 1. Slightly larger variation, though still of limited amount, along the SOBP are expected for protons beams with lower initial energy, such as those used for ocular treatment (typically around 60 MeV). Therefore, in an extended Bragg maximum the RBE critically depends on the local compositions of the beam energy, atomic number and intensity. This is illustrated in Fig. 1.16 where extended Bragg curves of different physical dose shapes

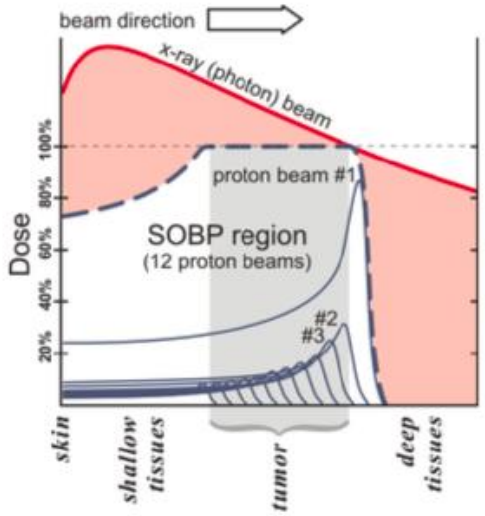

Figure 1.16: In a typical treatment plan for proton therapy, the Spread Out Bragg Peak (SOBP, dashed blue line), is the therapeutic radiation distribution. The SOBP is the sum of several individual Bragg peaks (thin blue lines) at staggered depths. The depth-dose plot of an X-ray beam (red line) is provided for comparison. The pink area represents the additional dose delivered by X-ray radiotherapy which can cause damage to normal tissue and secondary cancers, especially of the skin.

are used to determine survival and RBE with the goal was to achieve a flat top of cells survival over the target volume.

Chapter 2

The status of CNAO

The CNAO (Italian acronym that stands for National Centre for Oncological Hadron therapy) is situated in Pavia, Italy. It is a clinical facility created and financed by the Italian Ministry of Health and conceived to supply hadron therapy treatments to patients from all over the Country. A qualified network of clinical and research institutes, the CNAO Collaboration, has been created to build and run the centre. This organizational model turned out to be very efficient and fruitful to reach the goal of introducing the most advanced techniques and procedures of hadron therapy. Three treatment rooms with four beam ports (three horizontal and one vertical) are operational and one experimental room has been built. Beams of protons with kinetic energies up to 250 MeV and beams of carbon ions with maximum kinetic energy of 400 MeV/u are transported and delivered by active scanning systems. This operation started in 2009 with the commissioning of the high-technology components that form the acceleration chain from the sources to the patient. The dosimetry and radiobiology tests have been completed with proton beams and CNAO obtained the authorisation to start treating patients. Statistics from the Italian Association of Radiotherapists and Oncologists (AIRO) have estimated that more than 3% of the overall Italian radiotherapy annual patients, i.e. more than 3000 new patients per year, would preferably be treated with hadron therapy, but this number is steadily increasing. Pre-selection criteria are defined on the basis of established clinical protocols, and hospitals and clinics in the network adress to CNAO those patients that satisfy the criteria. This paper outlines the project development, the technical aspects of the realisation and commissioning and the clinical issues that are relevant for treatments at CNAO.

Figure 2.1: The CNAO hospital building in Pavia.

2.1 CNAO facility

The construction of CNAO facility was completed at the beginning of 2010 in Pavia. The centre is placed in an area that hosts other hospitals and the university campus, thus allowing the creation of synergies and collaborations. The entrance is shown in fig. 2.1. The large usage of windows allows to bring daylight to most of the areas, an architectural solution to improve the quality of life of operators and patients. The cross section in Fig. 2.2 shows the central cavedium reaching the underground waiting area, the structure of the centre on four levels and the clear distinction between hospital and technical areas. Inside the building the following functional areas are present [23]:

- The outpatient service.
- The imaging service (diagnostics in images and nuclear medicine).
- The therapeutic service (hadron therapy).
- The administrative departments and the offices of personnel.

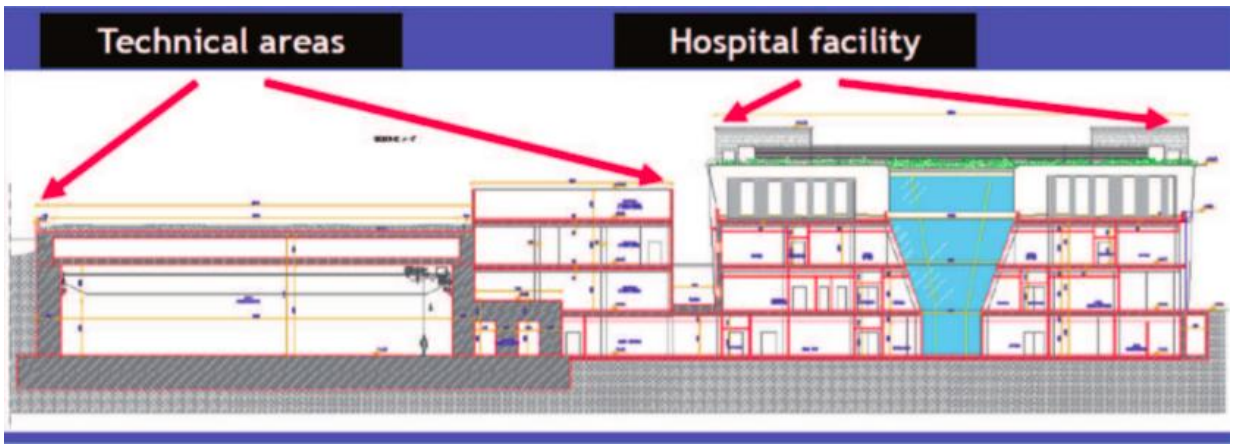

Figure 2.2: Cross-section of the CNAO.

- General services, such as the bar, the conference hall, meeting rooms, and the reading room.
- Technological areas, including electrical power plants, thermomechanical and special plants that provide energy for the building, the central electricity transformation units and the technical areas at the service of high technology.

The space organization envisages the merging of the functions of high users flow on the groundfloor and the basement; all health services are located here. This choice is justified, in the first case, by the immediate accessibility from outside and, secondly, by the need to ensure an appropriate radiation shielding for the rooms used for tumour treatment. Personnel offices, conference and meeting rooms and other service areas are located on the first and second floors. Every day, the medical personnel works on the treatments of clinical trials included in the experimental programme. During the routine operation phase, the medical team counts about 80 people. The Accelerators Department has been completed, and the machine is running 7 days per week, 24 hours a day. During the shifts two persons are continuously present in the main control room.

2.2 CNAO accelerators and beam lines

The main accelerator at CNAO is a synchrotron, a circular accelerator of about 25 m in diameter. The sources, the lines of injection and the linear accelerator are housed inside the ring. Outside the main ring there are four extraction lines, about 50 m each, leading

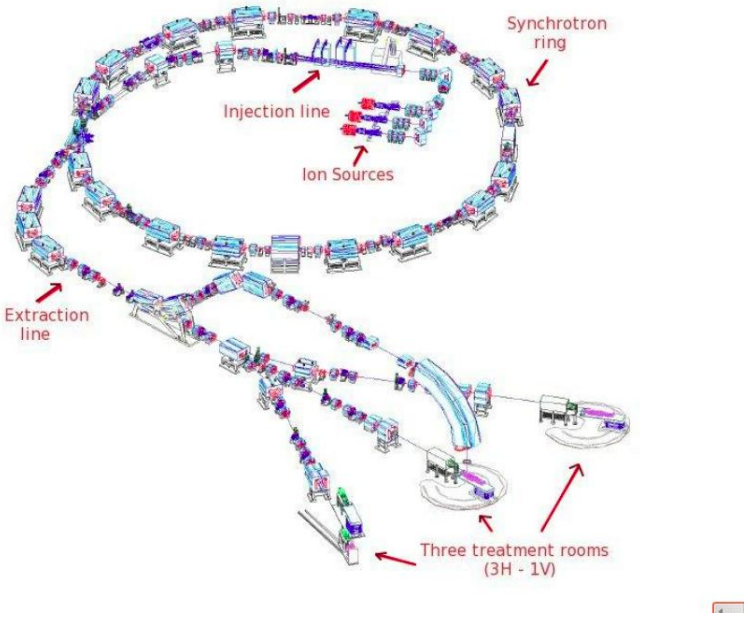

Figure 2.3: View of the CNAO accelerators.

the extracted beam into three treatment rooms. Each of the two side rooms receives a horizontal beam, while the central hall receives both a horizontal and a vertical beam. A view of the complex of accelerators and lines is shown in Fig. 9. CNAO is designed to work with ions with $1 \leq Z \leq 6$ and possibly with oxygen ions, although with reduced penetration. In water, the beam is able to achieve depths between 3 and 27 gcm^{-2} and its intensity is such to administer 2 Gy for a volume of 1 l in about 1 minute. The dose is delivered to the tumour with an active scanning system with a uniformity of $\pm 2.5\%$. The main physical parameters of the beam are reported in table 4. The availability of the machine must be close to 100% in the time reserved for medical use because therapy cannot be interrupted for long periods. The following part of this section is a description of the most meaningful and complex systems of the lines and accelerators.

2.2.1 From sources to injection in the synchrotron ring

At CNAO two identical-sources of type ECR (Electron Cyclotron Resonance) are operating. Each source can produce several kinds of beams simply by changing the gas used to produce plasma and optimizing the settings of certain parameters, such as the RF power and the potential of extraction electrodes.

This way, each source is able to compensate for the possible absence of the other. In normal operation conditions, each source produces only one type of beam, protons or carbon ions, which allows to change quickly the type of accelerated ion. The beam undergoes the following acceleration steps:

- The two ECR (Electron Cyclotron Resonance) sources run continuously and the particle type to be accelerated is selected by changing the LEBT (Low Energy Beam Transfer) magnet settings.

- The LEBT is the line that transports the beam from the sources to the radiofrequency quadrupole (RFQ). The kinetic energy of the beam in LEBT is 8 keV/u, which corresponds to the RFQ injection energy.

- The RFQ has an output energy from of 400 keV/u and provides a suitable beam to be accelerated by the LINAC.

- Then the LINAC accelerates the beam of 400 keV/u to 7 MeV/u in one 3.8 m long tank. It is composed of four accelerating sections among which three triplets of quadrupoles for beam focusing are housed. Immediately after the tank of the LINAC, there is a fourth triplet which focuses the beam onto the stripping foil. Bunches of C 6+ or protons are completely produced by this latter.

- The MEBT transports the beam from the stripping foil to the synchrotron.

- The synchrotron has a diameter of about 25 m. Protons and carbons are injected at 7 MeV/u and accelerated to energies between 60 MeV and 230 MeV for protons and between 120 MeV/u and 400 MeV/u for carbon ions. In the synchrotron there are 16 dipoles and 24 quadrupoles. The beam acceleration is provided by a single RF cavity which acts in four phases:

  - beam adiabatic capture
  - acceleration
  - preparation of the beam for extraction
  - stabilization of the extracted beam

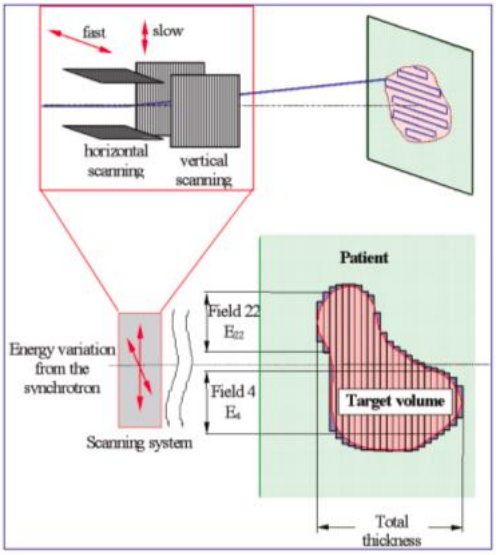

Figure 2.4: Principle of active dose distribution.

Capture and acceleration occur by tuning the cavity to the revolution frequency of the beam (using a harmonic number h = 1) and synchronizing it with the energy increase and the magnetic field value. At the end of the acceleration, the beam must be prepared for extraction.

- The HEBT (High Energy Beam Transfer) transports the extracted beam to the three treatment rooms through four lines, one of these treatment rooms having both a horizontal and a vertical line. HEBT is equipped with a system, called chopper, to dump the beam when necessary.

2.2.2 The dose delivery system

CNAO is designed for a fully active dose distribution system. This means that the tumour is ideally divided into "slices", i.e. into regions that are reached by particles of the same energy. Each slice is then irradiated by "painting" it with a pencil beam, somehow as it happens ona a TV screen for the reconstruction of the image. The concept is illustrated in fig. 2.4. This way, the beam is directed to the various points of the tumour by varying its position without adding additional thicknesses on the path of the beam that can lower its quality.

Energy is varied by the synchrotron to choose the slice, and the beam moves within

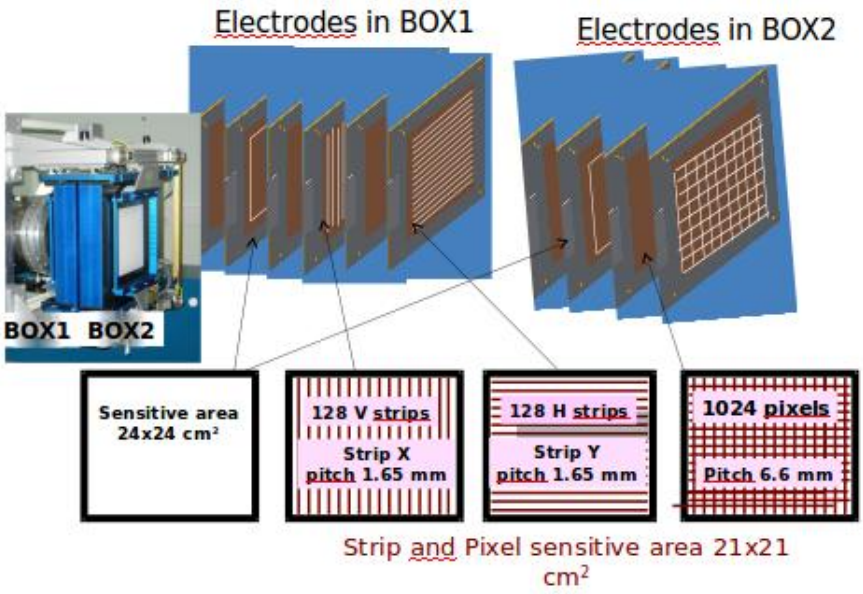

Figure 2.5: Schematization of the CNAO monitoring system placed upstream the patient.

the slice thanks to the finely laminated *scanning magnets*. The maximum speed with which the beam can be moved by the scanning magnets is 20 m/s. The position of the beam is controlled in real time thanks to a system of monitors that measure the beam position and the number of particles received by each voxel. This system (illustrated in fig. 2.5) is used both to decide when the foreseen dose for each voxel has been reached and to correct the position of the beam by acting on the scanning magnets. There are two identical measurement systems and each of the two detectors (Box1 and Box2) in sequence measures and controls separately the beam parameters: position, profile and number of particles. Discrepancies in the measurements lead to fast beam interruption by acting on the chopper magnets in very short times. Finally, it is worth mentioning that all along the beam path there are sensors that measure and control the characteristics of the particle beams. Moreover, the entire complex is managed by a complex control system that was designed to automatically guide irradiaton of the patient and avoid all human actions, which are sources of potential errors and inaccuracies.

Chapter 3

Hadron therapy treatment planning

Radiation treatment planning is the process of planning the appropriate treatment of external beam radiotherapy or internal brachytherapy for a cancer patient. The medical team consists of radiation oncologists, radiation therapists, medical physicists and medical dosimetrists.

Typically, medical imaging (i.e., X-ray computed tomography often the primary image set for treatment planning, magnetic resonance imaging excellent secondary image set for soft tissue contouring, and positron emission tomography less commonly used and reserved for cases where specific uptake studies can enhance planning target volume delineation) is used to create a virtual patient for a computer-aided design procedure. Treatment simulations are used to plan the geometric, radiological, and dosimetric aspects of the therapy using radiation transport simulations and optimization. For *intensity modulated radiation therapy* (IMRT), this process involves selecting the appropriate beam (photons, and perhaps protons), energy (e.g. 6 MV, 18 MV) and arrangements. The more formal optimization processes are typically referred to as *forward planning* and *inverse planning* [7] [11]. Plans are often assessed with the aid of *dose-volume histograms* (DVH), allowing the clinician to evaluate the uniformity of the dose to the diseased tissue (tumor) while sparing healthy structures.

Today, treatment planning is almost entirely computer based, using patient computed tomography (CT) data sets. Modern treatment planning systems provide tools for multimodality image matching, also known as image coregistration or fusion.

3.1 Ion therapy development

3.1.1 Forward and inverse planning

Forward planning is a technique used in external-beam radiotherapy to produce a treatment plan. In forward planning,a dosimetrist organizes beams into a radiotherapy treatment planning system which can deliver sufficient radiation to a tumour while both sparing critical organs and minimising the dose to healthy tissue. The required decisions include how many radiation beams will be used, which angle each beam will be delivered from, whether to use attenuating wedges, and which multileaf collimator configuration will be used to shape the radiation from each beam. Once the treatment planner has made an initial plan, the treatment planning system calculates the required monitor units to deliver a prescribed dose to a specific area in the patient which depends on beam modifiers that include wedges, specialized collimation, field sizes, tumor depth, etc. The information from a prior CT scan of the patient allows more accurate modeling of the radiation behaviour as it travels through the patient's tissues. Different dose prediction models are available, including pencil beam, convolution-superposition and monte carlo simulation, with precision versus computation time being the relevant trade-off. This type of planning is used for the majority of external-beam radiotherapy treatments, but it is only sufficient to handle relatively simple cases-cases in which the tumour has a simple shape and is not near any critical organs. For more sophisticated plans, inverse planning is used to create an intensity-modulated treatment plan. This is now also used as a part of post-mastectomy radiotherapy (PMRT) planning.

Inverse planning is a technique used to design a radiotherapy treatment plan. A radiation oncologist defines a patient's critical organs and tumor, while a dosimetrist gives target doses and importance factors for each. Then an optimisation program is run to find the treatment plan which best matches all the input criteria. In contrast to the manual trial-and-error process known in oncology as "forward planning", "inverse planning" uses the optimiser to solve the Inverse Problem as set up by the dosimetrist. Outside of the oncology field, this procedure might be described as "automated planning".

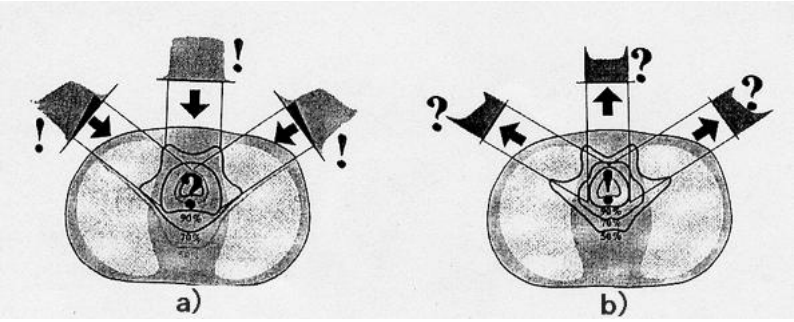

Figure 3.1: Graphic representation of forward (a) and inverse (b) planning.

3.1.2 Intensity Modulated Proton Therapy

The origins of the term *Intensity-Modulated Radiotherapy* (IMRT) are rather obscure, but there is no doubt that this technique has revolutionized radiotherapy practice [2]. However, the term is rather misleading; for most protons, IMRT delivery systems actually modulate fluence (i.e. the total number of particles delivered per unit of area) by varying the dwell time of the beam at a location, rather than directly modulating intensity (the number of particles delivered per unit of area per unit of time). More importantly, however, the success of IMRT lies not in the process of modulation itself, but in the ability of the IMRT treatment planning and delivery system to deliver arbitrarily complex fluence patterns from each field. Therefore, IMRT as a delivery method was only realized after the inclusion into the planning process of algorithms to calculate the fluence patterns and the development of devices such as dynamic multileaf collimators that allow fluence patterns to be delivered.

Pencil beam scanning for ions is a dynamic delivery technique that relies on the modulation of energy and fluence, by varying the dwell time of the beam or by varying the beam intensity, and on an optimization algorithm in the treatment planning process by which fluences and energies can be calculated. IMRT only achieves fluence modulation on the plane which is orthogonal to the beam direction; IMRT is therefore a "two-dimensional" optimization problem where, given the treatment plan constraints, the fluence at a point in that plain is optimized. IMPT, in contrast, has an additional degree of freedom provided by the beam energy, which allows the pristine Bragg peak to be positioned along the beam direction. Therefore, an IMPT field modulates the fluence and position of each pristine Bragg peak, and achieves "three dimensional" optimization within a target

volume. A single IMPT field can therefore achieve full dose conformation to the target, albeit perhaps not optimal compared to the use of multiple fields.

There are two distinct techniques to calculate pencil beam scanned plans. The first is defined as *Single Field, Uniform Dose* (SFUD) planning. In this approach, the fluences are calculated and optimized individually for each field of a plan, with the sole constraint of achieving a homogeneous dose across the whole target volume from each individual field. The second technique is IMPT.

Altough it is always difficult to completely distinguish one delivery method from the others, the term *intensity-modulated proton therapy* was first coined by Lomax in 1999. Using the analogy with photon IMRT, it is defined in that paper as a method where "... a number of individually inhomogeneous (in dose) fields are calculated in such a way that, when combined, these fields deliver a homogeneous and conformal dose to the target volume while simultaneously reducing dose to selected normal tissue types."

The key here is the definition of inhomogeneous fields that differentiates this delivery technique from SFUD pencil beam scanning. In practice, the major operational difference between the two techniques lies in the optimization process, with all Bragg peaks of all fields of an IMPT treatment being simultaneously optimized with common constraints to the targets and surrounding critical organs. The result is a set of (sometimes highly) inhomogeneous dose distributions, which provides the desired target coverage only when all fields are combined (thus, the case of partial treatment becomes problematic).

Perhaps the best way to illustrate the rather subtle difference between SFUD and IMPT treatments is with an example. Consider the dose distributions shown in Fig. 3.2 [2]. From left to right are shown dose distributions calculated to the same pelvic Ewing's sarcoma using passive scattering, pencil beam scanning using the SFUD approach and IMPT. The bottom row shows three-field plans calculated using the same field directions for the three different delivery modes, while the top row shows the anterior field of each plan alone.

The dose distribution for the anterior field for passie scattering does not appear to be very conformal (Fig. 3.2 top-left panel). Altough we have a very homogeneous dose across the planning target volume (PTV) (the yellow contour), and a sharp dose falloff at the distal and lateral aspects of the PTV, it is clear that the high dose (>90%) region covers most of the normal tissues in the proximal path of the beam. As the range modulation is performed before the scattering foils, it is impossible to vary the extent (in depth) of the

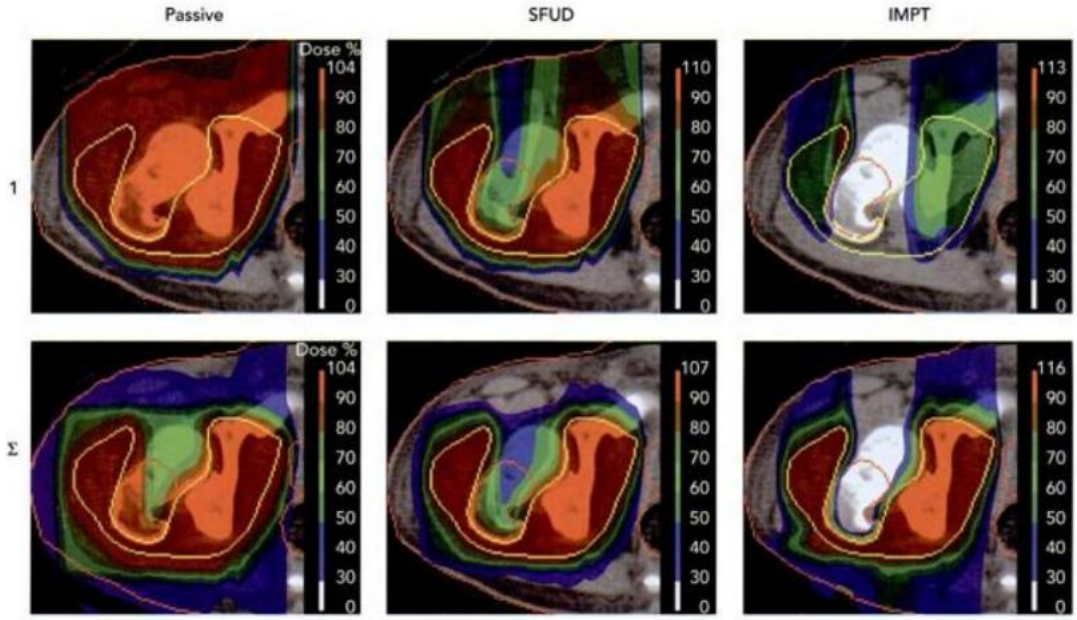

Figure 3.2: Three-field plans for passive scattering, SFUD and IMPT. The top row shows the anterior field of each plan, while the bottom row shows the combined distribution for all three fields. Dose levels are from 90% (red) through to 30% (blue) [2].

SOBP across th field. Therefore, in order to ensure a homogeneous coverage of the PTV, the extent of the SOBP must be the same as the longest extent of the PTV along the beam direction. When the extent of SOBP is applied to narrower portions of the target, the high dose region extends well beyond the proximal portion of the PTV, and even back the patient's surface. Only when multiple beams are applied is the conformation to the target improved, with some sparing of the femoral head then being achieved (3.2, bottom-left panel).

Figure 3.2 shows the equivalent field and plan for an SFUD pencil beam scanning treatment. Altough not strictly correct, it is peraphs convenient for this discussion to consider the SFUD technique to be a method by which variable extent SOBP pencil beams can be applied across the PTV. That is, where the extent of the PTV is narrow, a narrow SOBP can be delivered, where it is broad, a correspondingly broader SOBP can be delivered. The SOBP is therefore tailored exactly to the extent of the PTV along each ray at the proximal and distal extents. The excessive dose delivered to the proximal tissues as a result of the use of a fixed extent SOBP is therefore reduced. The result is a 3-D conformal

dose, which, when considering the full plan, lead to considerablyimproved sparing of the femoral head and a significantly reduced integral dose to all surrounding normal tissues (compare the 30% isodose in the bottom, left and middle panels of Fig. 3.2.
Now consider the IMPT results in Fig. 3.2, which shows the equivalent anterior field and three field plans. As with SFUD planning, IMPT requires an optimization procedure to determine the weights of all the Bragg peaks delivered from each peak, with the major diference to SFUD planning being that the Bragg peaks from all field are optimized simultaneously. The result is that each indvidual field delivers a very inhomogeneous dose distribution, as indicated in the top-right panel of Fig. 3.2. When we combine the anterior field with the other two fields, with similarly inhomogeneous dose distributions (not shown), we obtain the three field dose distribution shown in the lower-right image of figure 3.2. A highly conformal and homogeneous dose is still delivered to the PTV, but with near total sparing of the femoral head. In contrast to the differencebetween passive scattering and SFUD delivery, however, the difference in integral dose going from SFUD to IMPT treatments is negligible, in that the low-to-mid level doses have been simply redistribuited in comparison to the distribution of the SFUD plan (bottom-middle panel of Fig. 3.2).
In summary, the potential advantages of pencil beam scanning, using SFUD or IMPT, over passive scattering are twofold. First, the use of scanning allows for an efficient delivery of the high dose to the target volume, thereby reducing integral dose to all normal tissues. Second, the simultaneous optimization of fields allows to deliver highly inhomogeneous, but optimized, single fields, which in turn give more flexibility in where exactly the residual dose is delivered to normal tissues.

3.1.3 Spot scanning

In scanning beam techniques, magnets deflect and steer the proton beam. Under computer control, the beam "paints" the treatment volume, voxel by voxel, in successive layers. The depth of penetration of the Bragg peak is adjusted by varying the energy of the beam before it enters the gantry (Fig. 3.3) [16] [25].

In nearly all cases, scanning does not require any collimator, compensator, or other beam-modifying device. A narrow mono-energetic beam paints the target volume in layers, steered by magnets. Typically with scanning, there are no modifying devices to

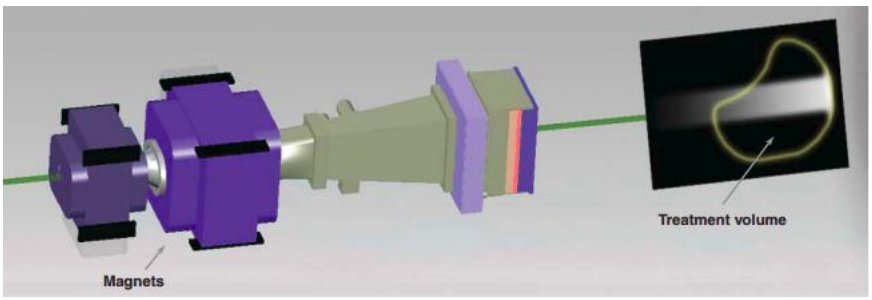

Figure 3.3: Scanning diagram

custom-make or store after treatment, making scanning a greener treatment option.

Without scattering material, scanning naturally produces fewer neutrons and reduces the integral dose to the patient. The smaller the treatment volume and the lower the integral dose, the better the patient is likely to tolerate treatment. Proton therapy delivers lower doses to healthy tissue than external beam therapy with X rays, and scanning delivers a lower dose than other proton delivery methods.

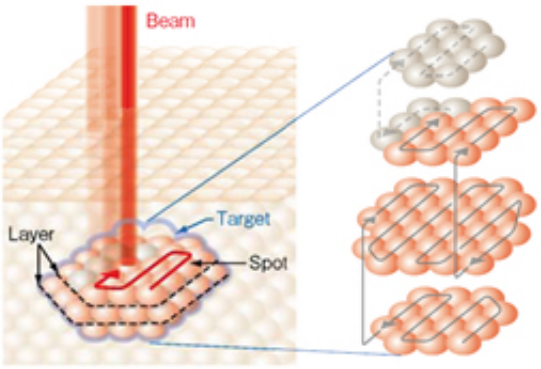

Scanning makes IMPT possible. With scanning, dose distributions can be varied voxel by voxel. By varying the beam intensity or the speed of scan, or both, dose is painted non uniformly on a field-by-field basis to yeld an overall uniform target dose.

3.2 Carbon ion radiobiology

The use of carbon ions in radiotherapy has many potential advantages, arising both from the physical aspects of their energy deposition and from biological phenomena resulting from the high density of energy deposition. In contrast to conventional photon radiations, where the dose distribution in the patient is primarily characterized by an exponential decline in dose with depth, charged particles present a phenomenon known as the Bragg peak. Particles at high energy deposit relatively little energy as they enter an absorbing

material but tend to deposit extremely large amounts of energy in a very narrow peak, the Bragg peak, as they reach the end of their range (Fig. 3.4) [13]. The depth and magnitude of this Bragg peak is determined by the mass and charge, as well as the initial energy of the particle.
For carbon ions, the high rate of energy loss towards the end of the particle range results in a dramatic increase of the LET. While the Bragg peak is extremely narrow for a monoenergetic beam of particles, a variety of techniques can be used to moderate the energy and thus the range of the incident particles. The layering of a succession of Bragg peaks with varying intensity can thus result in the spreading of high dose over a sufficiently wide region to encompass a target volume (tumour) at a selected depth (SOBP) (Fig. 3.4). Spreading of the Bragg peak results in a lowering of the average LET over the SOBP, but this LET is still much higher than for photons and also for the particles in the entrance region of the beam. The result of all this is that the absorbed dose distribution of ions is as good as or better than that of protons, and superior to that of photons. When the biologically weighted absorbed dose is considered, this superiority is further enhanced.

The high LET seen at the end of particle ranges not only affects the absorbed dose distribution, but also marks consequences for the response of biological systems to that dose. Among these known biological consequences there is a reduction in the oxygen enhancement ratio (OER) and in cell cycle sensitivity variation seen with photon radiation. Reduction in the OER may represent an advantage in the treatment of certain tumour types, suspected of possessing radiation resistant regions containing hypoxic cells. Reduction in the variation of cell cycle sensitivity may also be advantageous in the tratment of certain tumour types, notably slowly growing tumours.
In addition to a reduction in the OER and in variation in cell cycle sensitivity seen with ion radiation, a major advantage or concern with the use of high LET radiations is their increased efficiency in producing cell death and a variety of other biological phenomena. This may be an advantagewhen considering the absorbed dose in the cancer cell population, and a disadvantage when considering the absorbed dose in normal tissue. Both issues are of concern. The concept of RBE has been introduced to account for the increased efficiency of high LET radiation if compared to photons. As defined, the RBE is a simple concept, however, its apparent simplicity is deceptive. RBE cannot be uniquely defined for a given radiation. The RBE of a given radiation type will vary with particle type and energy, dose, dose per fraction, degree of oxygenation, cell or tissue type, bio-

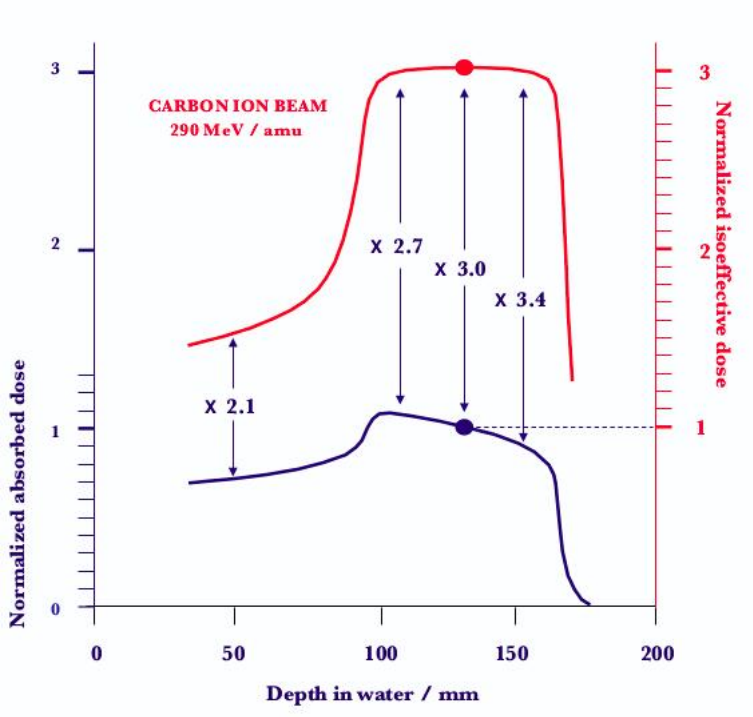

Figure 3.4: Comparison of the absorbed dose and isoeffective dose variations with depth in a carbon ion beam. Carbon ion irradiation of a PTV located between 100 and 160 mm in depth using a 290 MeV/amu beam. The RBE of a carbon beam increases significantly with depth. Therefore, in order to obtain a uniform isoeffective dose (plateau) across the SOBP, the absorbed dose needs to be adapted (modulated) and decrease with depth.

logical end point, etc. The case of ion irradiation is particularly complex and the RBE is a strong function of position within the treatment beam.

3.2.1 Increased RBE

RBE values for various high LET radiations have been determined for many biological systems, and a great number of generalizations can be drawn from the results.
The first of these generalizations is that RBE tends to increase with increasing LET. As energy decreases, LET increases for all particles, so a second generalization is that, for any particle, RBE generally increases as particle energy decreases, except in the region of "overkill".
Fig. 3.5 shows RBE values as a function of LET for cell survival, measured for two cell lines using three different ion beams at different points in SOBPs. Once again, RBE increases with LET but appears to reach a maximum at LET values of approximately 100-200 $keV/\mu m$ before declining in the "overkill" region where the amount of energy deposited in a cell by a single particle traversal is more than the amount required to kill the cell. Fig. 3.6 also shows variation in RBE as a function of LET at various point in SOBPs of carbon, neon, silicon and argon ion. Once again, RBE is seen to peak for LET values of approximately 100-300 $keV/\mu m$ [13].

Figures 3.5 and 3.6 [13] both demonstrate that even at the same value of LET_∞, RBE is a function of ion type. This is a result of differences in the fine structure of energy deposition for different particle types even at the same LET and indicates that LET, while often adequate, is not a perfect predictor for RBE.
In addition to increasing when LET increases and when particle energy decreases, RBE also increases with decreasing dose per fraction (this is essential for partial treatment considerations) and is higher for some late responding tissues than for early responding ones. These findings can be assumed to apply to all tissues irradiaed with high LET radiations and in particular, to a greater or lesser extent, to all tumour or normal tissues in the SOBP region of an ion beam.

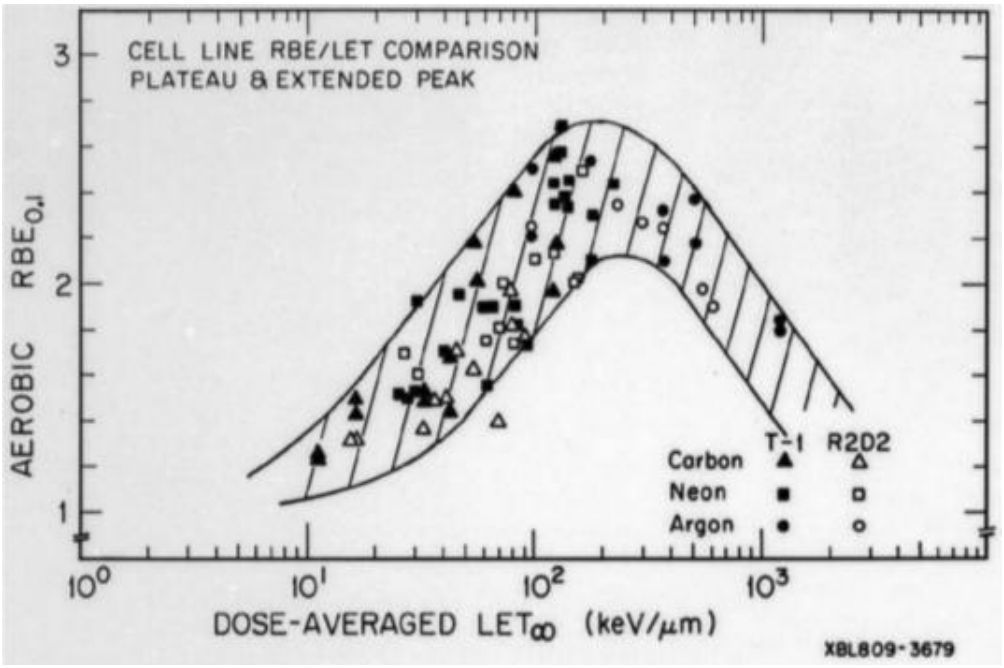

Figure 3.5: RBE of cell survival for T-1 and R2D2 cells as a function of LET measured at various points in SOBPs for carbon, neon and argon ions. The cells were irradiated under aerobic conditions and the end point was 10% cell survived.

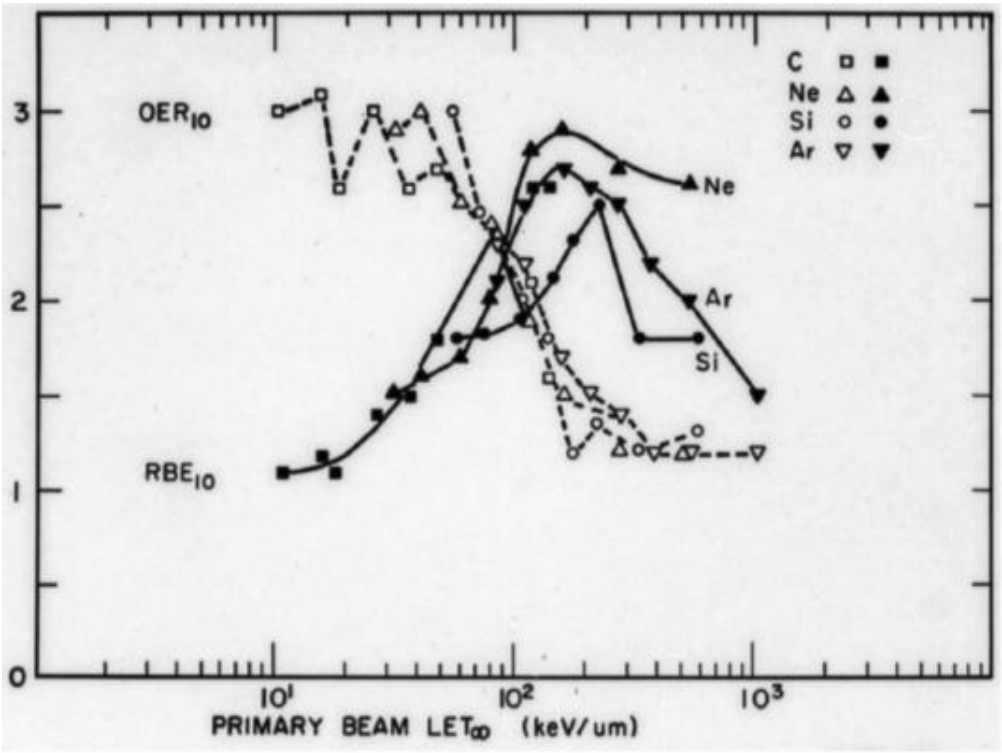

Figure 3.6: Variation of OER as a function of LET measured at various points in SOBPs of carbon, neon, silicon and argon ions.

3.2.2 Rationale for ion therapy

The potential advantages of ions can be summarized in four points [13]

- The physical selectivity of ion beams is comparable to, or better than, the best low LET therapy techniques. The penumbra is narrow and the dose ratio between the SOBP and entrance plateau is better than with the best low LET radiation (protons). Nuclear fragmentation of the ion beams is a potential disadvantage because some energy is deposited beyond the Bragg peak. However, this aspect is probably not clinically significant because the dose is low and the fragments are lower LET particles.

- The LET in the ion beam, and consequently the RBE, increases with depth, and this increases the ratio of the biologically weighted doses between the SOBP and the entrance plateau. The RBE is comparable to neutrons, but the physical dose selectivity is vastly improved for ions.

- At the level of the SOBP, where the PTV is located, high LET makes heavy ion beams specifically effective for the tratment of some tumour types that are resistant to low LET radiation.

- After fractionated irradiation, there is reduced possibility for repair for cells in the PTV located in the SOBP, because the LET is highest there. In contrast the normal tissues located outside the SOBP, in the entrance plateau region, are exposed to lower LET radiation and thus may benefit from an increased repair opportunity. Therefore, from a radiobiological point of view, fractionation in ion therapy should bring a significant advantage and should be exploited. It is recognized, however, that this radiobiological advantage may be balanced by the advantage of reducing treatment times to reduce the effect of tumour cell repopulation, and also by some economic considerations.

While ions appear to have potential advantages for the treatment of many tumour types, it would be wise to use some caution. It has been pointed out that the physical dose in the SOBP is significantly greater than in the entrance plateau and that the biological weighting factor will increase the effect of this dose, due to the high LET in the SOBP. It has also been pointed out that LET increases with depth in the SOBP. All of the above

would appear to be advantages for the treatment of tumours wholly contained within the SOBP. However, it cannot be assumed that the radiobiological effects seen in the entrance plateau, where the LET may be in excess of $20 kev/\mu m$, are characteristic of low LET radiations.

Table 3.1 [13] shows RBE values measured for several biological systems at several points in a spread out beam of carbon ions as well as at the entrance. The table indicates that RBE increases with depth in the SOBP but also shows a very high value for RBE in the entrance region. The apparently high RBE value shown in the entrance region was derived from a preliminary skin experiment and more recent experiments suggest that the RBE in the entrance region is approximately 1.5, in agreement with the data shown in figure 3.5. Both indicate that care must be taken in assuming values of RBE in the entrance region of an ion beam. In addition, the RBE in the entrance plateau may be a function of the type of scattering and beam modulation used with any ion beam.

Position	LET [1] $(keV/\mu m)$	RBE values		
		Single fraction		Four fraction
		Cell culture	Skin reaction	Skin reaction
Entrance SOBP (6 cm)	22	1.8	2.0	-
Proximal	42	2.1	2.1	2.3
	45	2.2	2.2	-
Middle	48	2.2	2.3	-
	55	2.4	2.3	-
Distal	65	2.6	2.3	2.9
	80[a]	2.8	2.4	3.1
Distal fall-off	100	-	-	3.5

Table 3.1: RBE values of modulated 290 MeV/amu carbon ions beams of the heavy ion medical accelerator relative to photon radiation.

3.3 The Local Effect Model

Complex models are needed in hadron therapy to predict the biological effect of radiation in order to make a rigorous treatment planning. However, the complexity of the radio-chemical and radio-biological mechanisms involved in the formation of biological damage complicates the creation of such models. Nowadays the model used at CNAO is the *local effect model*, LEM [14][15].
The Local Effect Model aims to derive the biological effects of ion radiation from the response of cells or tissues to photon radiation, thus efficiently exploiting the large data base collected with conventional radiation. It makes use of the concept of the "local dose", which is defined as the expectation value of the energy deposition at any position in the radiation field for a given pattern of particle trajectories. The main assumption of the LEM is that equal local doses should lead to equal local effects, independent on the radiation quality. This local dose is derived from an amorphous track structure representation of the energy deposition as a function of the radial distance to the particle trajectory. The effectiveness of particles is thus calculated based on the microscopic local dose distribution pattern of ion traversals within the cell nucleus, assuming the nucleus to be the sensitive target for the observed radiation effects. (Fig. 3.7) [6].

In the first implementation of the model (LEM I) (Scholz et al. 1997) the local biological effect for a local dose d_{loc} is derived directly from the corresponding photon dose response curve denoted as $S_\gamma(D)$, where S represents the survival at dose D. This response curve is represented by the linear-quadratic (LQ) parameters α_γ and β_γ for the specific biological endpoint under consideration, which are known from experiments or clinical data. Since the linear-quadratic description is only valid for doses in the order of 5 – 10 Gy (Astrahan 2008), a correction for S(D) was introduced in order to account for a transition to a linear shape at higher doses $D > D_t$, where D_t denotes the "threshold" dose for the transition. For the prediction of cell killing, the biological effectiveness of any ion radiation field can then be derived from the quantity

$$N_{l,ion}^{-} = \int \frac{-\ln S_X(d(x,y,z))}{V_{nuc}} dV_{nuc} \tag{3.1}$$

where SX(D) represents the effect after photon radiation as a function of dose D, d(x,y,z) is the distribution of the local dose within the critical target, assumed to be the cell nucleus,

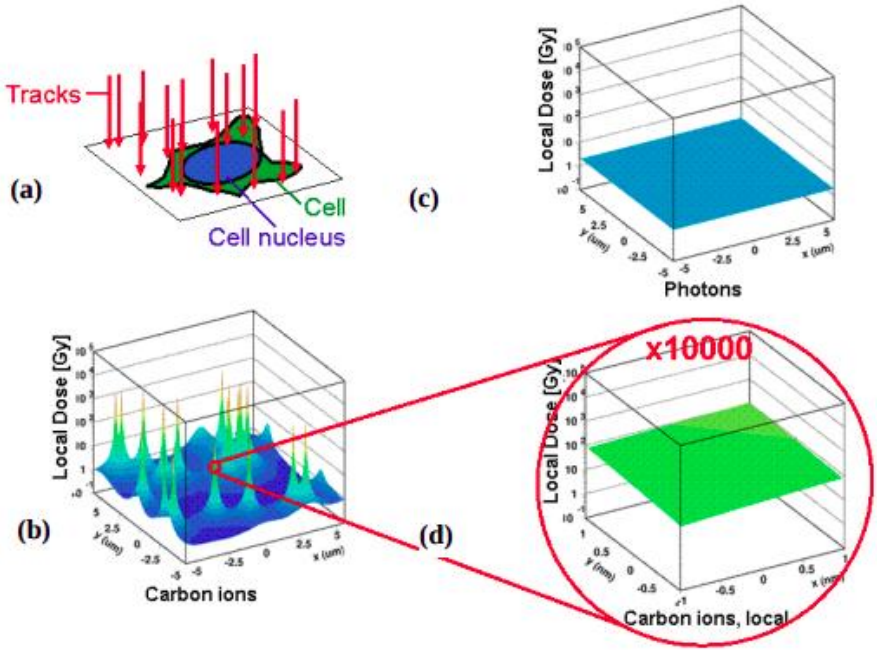

Figure 3.7: Comparison of the microscopic local dose distributions of carbon ions and photons for the same macroscopic dose of 2 Gy. For a random distribution of particle traversals through a cell as depicted in (a) the corresponding local dose distribution is characterized by extremely high spikes close to the particle trajectory (b). In contrast, for photons the distributions is expected to be flat (c). Locally, i.e. in nm dimensions, the distributions of particles can also be approximated by a flat distribution (d), thus allowing the link to the photon distribution.

and V_{nuc} is the volume of the cell nucleus. The term $-\ln S_X(D)$ can be interpreted as the mean number of lethal events produced per cell by photons at a dose D; the integrand in eq. 3.1 thus represents a local density of lethal events at a given position (x,y,z) in the nucleus. Integration of this event density over the volume of the nucleus for a given local dose distribution pattern deposited by particle traversals results in the mean number of lethal events $N_{l,ion}$ per cell induced by these traversals.

Assuming a Poissonian distribution of the number of lethal events around this mean value, the surviving fraction is determined by the fraction of cells with no lethal events and thus by

$$S_{ion} = e^{-\bar{N_{l,ion}}} \tag{3.2}$$

By comparison with the photon dose D_γ leading to the same survival, i.e. $S_\gamma = S_{ion}$, RBE values can then be derived from

$$RBE = \frac{D_\gamma}{D_{ion}}\Big|_{isoeffect} \tag{3.3}$$

The full integration would be too time consuming for purposes of therapy planning; therefore, approximations have been introduced, which are described in more detail in (Scholz et al. 1997, Krämer et al. 2000b, Scholz et al. 2006).

Although the predictions of the LEM I were in reasonable agreement with experimental and clinical data, e.g. for carbon ion irradiation in a spread-out Bragg peak (SOBP), where deviations were in the order of 10-20% for therapy relevant conditions, larger systematic deviations were observed for high-energy, low-LET ions and lighter ions, e.g. protons or helium ions, when using the model parameters optimized for the description of carbon ions. Consequently, improvements have been implemented, aiming at reducing these systematic differences. In the LEM II (Elsässer et al. 2007), the increased yield of DSB, resulting from the induction of DNA single strand breaks in close vicinity (<25 base pair, bp), is taken into account, leading to a further enhancement of the biological effects at very high local doses (>1000 Gy). Furthermore, since a considerable fraction of the biological damage is induced by the indirect effect, the effects of radical diffusion have been considered in more detail in the LEM II, that led to a "wash out" of the extremely spiked local dose distribution in the particle track center.

A further refinement was achieved with the implementation of a more detailed track structure description, now including an energy dependent extension of the track core (LEM III, (Elsässer et al. 2008)). This dependence on energy further increased the gradient of

RBE along the penetration depth and, with that, led to a better agreement of the model predictions with experimental data.

A key feature of the earlier versions LEM I-LEM III as described above is the direct link between local dose deposition pattern and the photon dose response curve the observable endpoint under consideration. In the recently reported extension (LEM IV, (Elsässer et al. 2010)), an intermediate step is introduced, on the premise that a cell final biological response to radiation is directly linked to the initial spatial DNA damage distribution induced by radiation rather than the local dose distribution itself. We assume that the microscopic spatial distribution of DNA damage, namely double strand breaks (DSB) and in particular their local density, represents the relevant measure determining the fate of a cell after radiation insult. Furthermore, in line with the general concepts of the LEM, we assume that similar DSB patterns should lead to similar effects, independent of the radiation quality leading to these patterns.
Although of course a strong correlation between the energy deposition pattern and the spatial damage distribution pattern is expected and thus the distinction made above seems to be quite subtle, actually under certain conditions these two views lead to significantly different conclusions. This can be illustrated by means of the examples shown in Fig. 3.8 [6].

The figure schematically compares the microscopic dose distribution (left side) respectively for low and high energetic carbon ions of comparable macroscopic dose levels, respectively, with the corresponding distribution of double strand breaks. Having very high LET, the local dose distribution for low energetic ions is extremely peaked, and the high number of DSB are concentrated along the particle trajectory, as a result of the extremely high local dose deposition and the narrow track diamater. Here, both the high local dose distribution as well as the clustered DSB distribution intuitively indicate an enhanced effectiveness of the carbon ions. This picture changes when analyzing distributions for the high energetic ions. Here, the local dose still shows significant peaks at the center of the individual tracks, although the space between individual tracks is now filled with a "bath" of low local doses which originate from the overlap of the individual tracks outer regions, which have a comparably large diameter at these high energies. However, assuming that, for example, at these low LET values an individual particle produces only

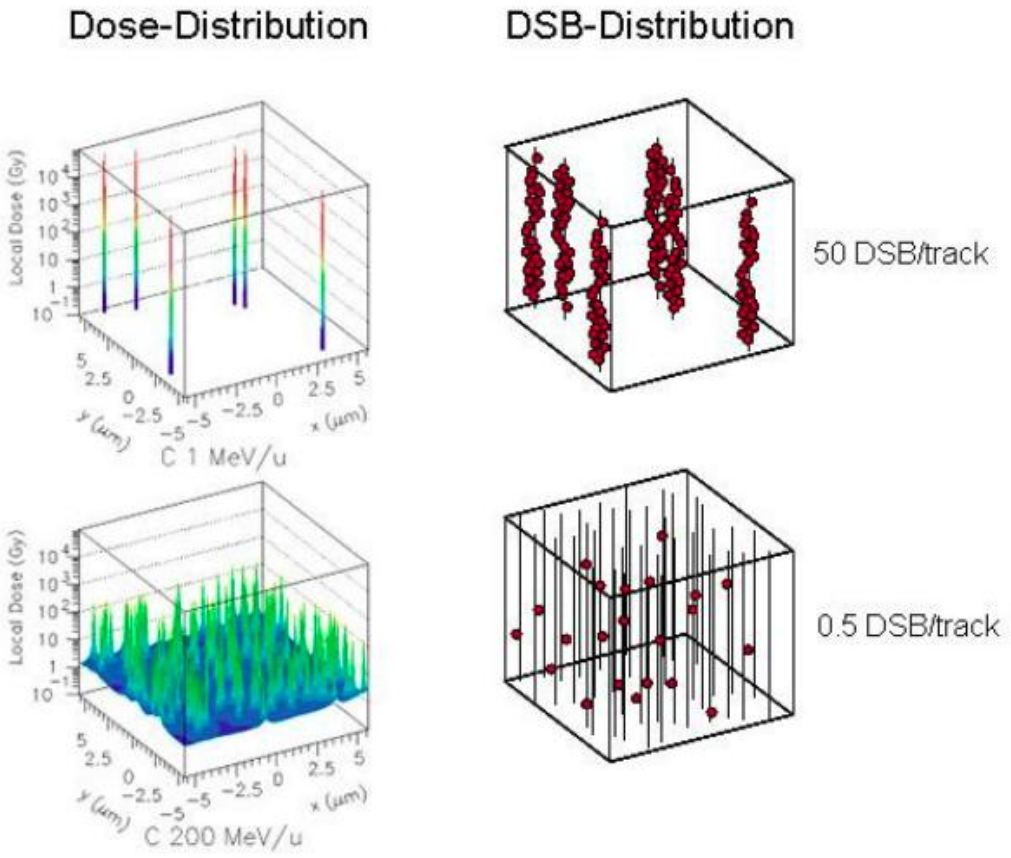

Figure 3.8: Schematic comparison of the local dose distributions (left) and corresponding spatial DSB distributions (right) for low energetic (top) and high energetic (bottom) carbon ions. Assumed DSB yields are 50 DSB and 0.5 DSB for the low energetic and high energetic ions, respectively.

0.5 DSB on average, the resulting pattern of DSB obeys a random distribution according to the random pattern of particle traversals. Now, different conclusions can be drawn from the local dose deposition pattern and the DSB pattern. The spikes in the local dose distribution would still suggest an increased effectiveness of the particles. However, since the DSB pattern is random, it cannot be distinguished from the pattern that would be induced by photon radiation, and thus the same effectiveness is expected on the basis of the DSB distribution. Since the cell actually responds to the damage induced by the particle traversals, but not directly to the energy deposition, the spatial DSB distribution pattern is considered to be the more relevant measure to assess the effectiveness of different radiation qualities. The induction of clustered damages is an important aspect that is reflected in the spatial DSB distribution pattern. In order to assess the similarity of DSB distributions, specific measures have to be defined. In the LEM IV, these are related to the structure of chromatin organization in the cell nucleus. It is assumed that the so called "giant loops" of DNA (Yokota et al. 1995, Solovjeva et al. 1998), comprising about 2 Megabase pairs (Mbp) of DNA length, represent the critical structure of DNA (Ostashevsky1998, Johnston et al. 1998). We then distinguish two types of damage: when a single DSB is induced in such a loop structure ("isolated DSB", iDSB), and when two or more DSB are induced ("clustered DSB", cDSB). It is hypothesized that cDSB leads to a significant higher probability of cell killing if compared to iDSB, since for iDSB the DNA on both sides of the DSB is still attached to the nuclear matrix, and thus repair is expected to be facilitated in this case. In contrast, for cDSB one or more DNA fragments can be removed from the loop, being no longer attached to the nuclear matrix and thus difficult to repair.(Fig. 3.9).

Assuming that induced damage in different DNA loops can be considered to act independently, the total number of loops with iDSB and cDSB represents a measure of the clustering of the DSB induced by a given dose deposition, as defined by the cluster-index C:

$$C = \frac{N_{cDSB}}{N_{iDSB} + N_{cDSB}} \tag{3.4}$$

where N_{cDSB} and N_{iDSB} represent respectively the number of loops with isolated and clustered DSB.

Calculation of the spatial DSB distribution is based on the local dose derived from the radial dose profile described above and used already for the previous versions of the LEM. Assuming a homogenous distribution of the DNA within the nucleus as a first approxi-

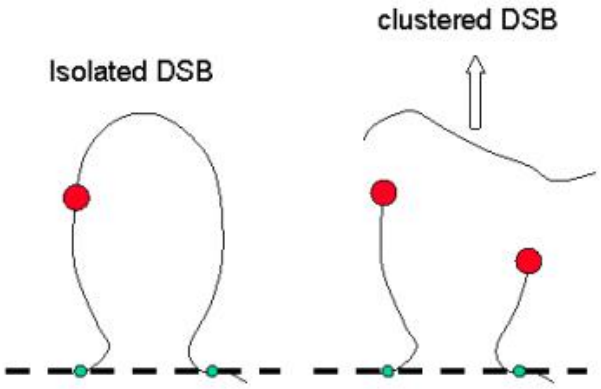

Figure 3.9: Schematic representation of the chromatin giant loop structure (adapted from Yokota et al.) and the consequence of isolated or clustered DSB within loops. For simplicity, only the essential topology of chromatin loop structure is shown; the actual conformation of individual loops includes additional complicated 3-dimensional folding.

mation, the mean number of DSB in any small subvolume of the nucleus can be derived from experimental photon data, which indicate that the yield of radiation-induced DSB is approximately 30 DSB/Gy/cell. Based on the local average number of DSB, spatial DSB distributions are then determined by means of Monte-Carlo techniques, i.e. actual DSB distributions are determined by considering the amorphous track structure pattern as the probability density distribution of DSB.
Assuming a homogenous distribution of DNA within the nucleus, the amount of DNA contained in a loop (approx. 2 Mbp) can be attributed to a subvolume of the nucleus, based on the knowledge of the total DNA content (approx. 6×10^9 Mbp in mammalian cells) and the typical volume of the nucleus (approx. 500 μm^3). In order to determine the number of isolated and clustered DSB, the cell nucleus is divided into cubic shaped subvolumes with 540 nm side length, corresponding to the volume covered by a 2 Mbp DNA content when assuming a homogenous distribution of DNA within the nucleus. The number of DSB in each subvolume is determined according to the local dose distribution within the subvolume, and the subvolumes are then classified as isolated DSB or clustered DSB if exactly one DSB or two or more DSB are induced in a subvolume, respectively.
In order to determine the biological effect of a given spatial DSB pattern, in a first step the photon dose that leads to the same damage complexity C, i.e. the same relative composition of iDSB and cDSB, is determined. In a second step, the effect produced by that

photon dose is appropriately scaled according to the total number of iDSB or cDSB that are induced by a particle traversal and the photon dose, respectively. As a result, the number of lethal events induced by a single particle traversal is obtained. This procedure allows calculation of the effect of a single particle traversal, defining the effectiveness at low doses and thus the α_I term of the linear-quadratic representation of the dose response curve. The β_I-term can then be estimated according to the approximation described in (Krämer et al. 2006). This approximation has been introduced since full simulations of dose response curves would be infeasible for applications in the framework of treatment planning; this was mainly due to the extremely time consuming calculations.
The concept of LEM IV also allows implementation of a detailed, full simulation for arbitrary random particle traversal patterns (Friedrich et al. 2012). Compared to single particle approximations, higher β-values are typically predicted in the intermediate LET region, and work is in progress to analyse in more detail the impact of these differences on the level of track-segment conditions as well as for clinical applications using spread-out Bragg peaks.

For treatment planning, an accurate prediction of RBE for tumor cell killing and normal tissue effects is essential. The model has thus been validated based on large experimental data sets (Elsässer et al. 2008, Elsässer et al. 2010, Friedrich et al. 2012b). Fig. 3.10 shows a comparison of model predictions with experimental data obtained with helium and carbon ions for the different model versions. Interestingly, the model improvements had little effect on the shape of the RBE-LET-relationship at high LET values beyond the maximum of RBE. The main impact is observed in the rising part of the RBE-LET-curve, where essentially the gradient is affected, which consequently also affects the rise of RBE with penetration depth in a typical spread out Bragg peak (SOBP). In general, for the most recent implementation (LEM IV) a very good agreement is observed between the predictions and the experimental data.

Compared to normal tissue toxicity, application of the LEM needs some generalization because typically normal tissue responses cannot be easily traced back to effects of cell killing, in particular for tissues like CNS where cell proliferation normally does not occur and thus cell survival is not defined in the sense of the clonogenic assay. However, dose response curves for normal tissue effects also typically can be described in terms of the linear-quadratic model, and thus hypothetical "survival" curves can be constructed from

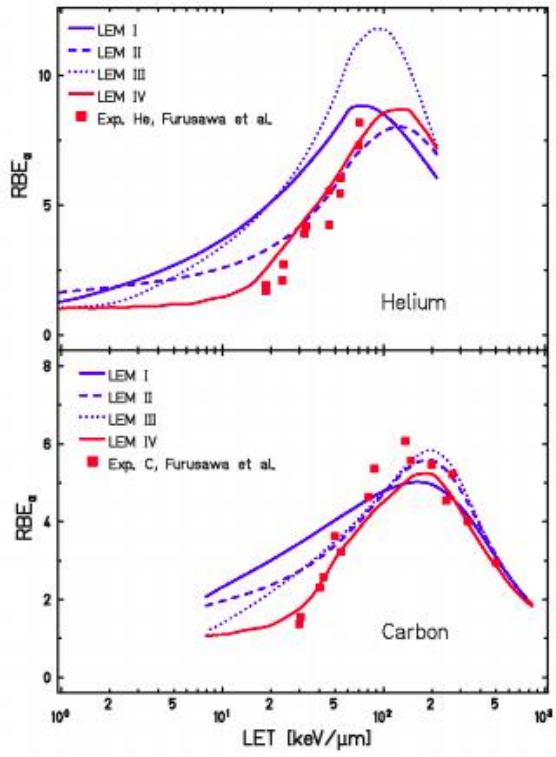

Figure 3.10: Comparison of RBE predictions for different LEM versions with experimental data for He irradition (top) and C irradation (bottom). Experimental data were taken from Furusawa et al. (2000).

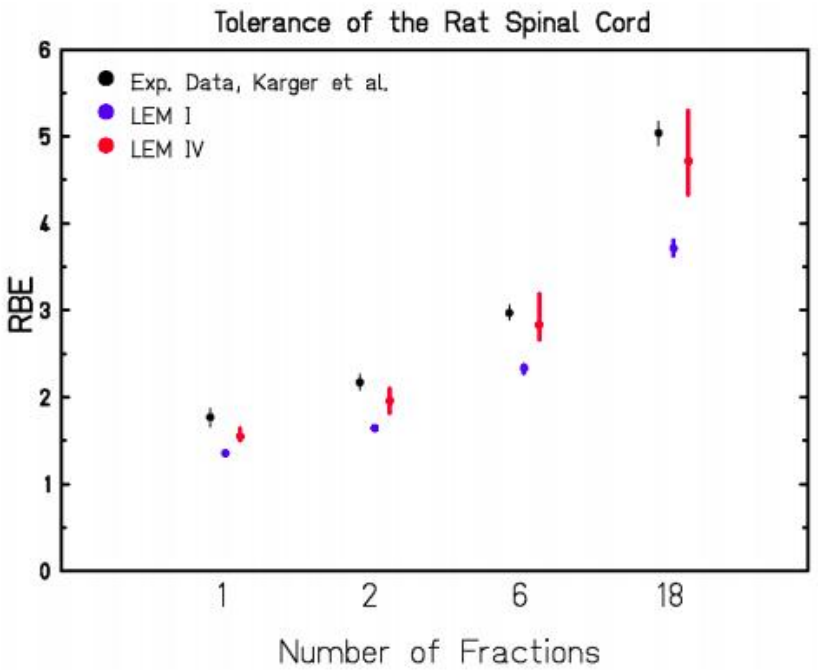

Figure 3.11: Predictions of LEM I and LEM IV for the RBE for the tolerance of the rat spinal cord in comparison to experimental data reported by Karger et al. Redrawn after Grün et al., PMB 2012. Vertical bars for experimental RBE values represent error bars; vertical bars for LEM calculations represent uncertainties due to positioning uncertainties of +/- 1mm of the spinal cord and the RBE gradient within the spread-out Bragg peak.

the known α, β or α/β -values, and then the corresponding RBE values can be calculated in analogy to the procedure applied for cell killing. Since the CNS represents a critical tissue which frequently limits the dose given to the tumor, such as in the case of head and neck tumors, as they were mainly treated within the pilot project, tolerance of the spinal cord has been studied in pre-clinical in-vivo experiments (Debus et al. 2003, Karger et al. 2006). Fig. 3.11 presents a comparison of the RBE values predicted by the LEM IV, assuming an α/β-value for photon radiation of 2 Gy, with the experimental data as reported by Karger et al. (2006). A significant improvement is achieved with the most recent implementation of the LEM (Grün et al. 2012).

Chapter 4

Material and methods

The aim of my thesis was to study the effect of partial irradiation on real patients treated with carbon ions at CNAO. Several quantities contribute to the effectiveness of a treatment and are taken into account by each Treatment Planning System to provide the optimum irradiation setup.

4.1 The Treatment Planning System

The TPS is a software which helps the physician to perform the treatment planning, via the simulation and visualization of different irradiation scenarios and the capability to search for optimal solutions. It is a complex tool, which receives as input the information on patient anatomy as provided by the Computer Tomography (CT) data, the delineation of the target and of the surrounding organs, the beam set-up and the prescription of the wanted effect, and performs an inverse planning. The TPS task is completed when it finds the set of beamlets intensities, energies and directions necessary to satisfy at best the prescription.
This is not an easy task, in carbon ion therapy a uniform damaging of tumour cells is not obtained by simply requiring a constant dose delivery on the target, because a flat dose SOBP does not necessarily correspond to a flat biological effect. In fact, the information of delivered dose alone is not sufficient to determine the biological effectiveness of a carbon ion beam: a beam composed by ions of low kinetic energy is more efficient in inactivating cells than another beam depositing the same dose but with ions of higher kinetic energy, for the reasons explained in the thesis. Since the beam characteristics

(distribution of kinetic energies and ion species) change during tissue penetration (due to energy loss, energy loss straggling and fragmentation) and since in each point a superposition of many beams occurs, the TPS must compute the inactivation probability relative to the cells in a certain location on the basis of the statistical knowledge of how many and which particles have passed by.
The TPS seeks the solution in an iterative way: starting from an initial hypothesis on the beamlets intensities, the program computes for each point of interest the particles spectra and estimates the corresponding biological effect; if the result satisfies the prescription, then the TPS can terminate the execution and return to the physician the information on the used beams; otherwise, the program must vary opportunely the beams intensities and repeat the biological effect evaluation, until the specifications are met or the maximum number of iterations is reached. It is important to underline that the physician will typically specify conflicting prescriptions, since he desires to escalate the dose over the tumour, in the meantime asking to maintain limited the dose in the entrance path and over the surrounding organs. Therefore, the mathematical cost function that quantifies the distance of a certain irradiation effect from what the physician required is generally non-linear and complex, and needs to be treated in the field of multi-objective optimization.
It is also required that the evaluation lasts a reasonable time, of the order of minutes, so that the TPS can constitute an interactive tool for the radiotherapist. The medical physicist can then use it to run several trials, enforcing more or less restricted prescriptions. To achieve these fast elaboration capabilities, the TPS usually relies on approximate models or on pre-computed results, both for physical and radiobiological evaluation purposes. As already underlined, the radiobiological effects estimate is one of the biggest conceptual problems that the TPS has to face.

The TPS in use at CNAO is provided by Siemens and its commercial name is *Syngo RT Planning*, which is also in clinical use at the Heidelberg Ion Therapy Center (HIT), Germany. Siemens software, in 2011, when the CNAO started the clinical treatments, was the unique available CE certified commercial product, able to elaborate treatment plans for protons and carbon ions beams delivered with the modulated scanning technique. It is a very sophisticated software, whose main task is to calculate optimal treatment solutions. It is able to acquire patient anatomical data (through TAC images or MR),

convert data from TAC in water-equivalent material, simulate and optimize the absorbed and effective dose distribution in the region of interest. Beyond many other features, the software main task is to produce treatment plans structured on three steps:

- Read the patient's CT-data
- Choose the positions of the pencil beams within the target
- Determine for each pencil beam the number of particles necessary to produce a dose distribution according to the prescribed dose.

TPSs for hadron therapy are typically based on analytical codes and external databases for the description of nuclear and electromagnetic interactions of hadrons in water. A large database is requested so it is necessary to integrate measurements with Monte Carlo simulations. The most relevant data for hadron therapy are:

- DDD (Depth Dose Distribution).
- Lateral dose profile of individual pencil beams.
- Conversion tables between Hounsfield Units (HU) and range in water, which permit the reading of CT images.

Moreover we describe here some additional inputs:

CT-data and VOIs. An important input to each TPS is the CT image of the patient. Resolution of CT is usually about 1 mm in x- and y-direction and 3 mm in z-direction, which is the thickness of a CT slice. Such an elementary volume having these dimensions is called voxel. To every voxel is assigned one value: the Hounsfield Unit (HU), which represents the X-ray attenuation in a material and it can be related to the density of that voxel. The HU s are defined as:

$$HU = \left(\frac{\bar{\mu}}{\bar{\mu}_{H_2O}} - 1 \right) \cdot 1000 \tag{4.1}$$

where $\bar{\mu}$ and $\bar{\mu}_{H_2O}$ are the mean values of the attenuation coefficient of tissue and water, respectively. Therefore the CT number is a CT-scanner- dependent quantity with fixed values for water, 0, and air, -1000. Using an external database, i.e. water equivalent path length (WEPL) versus HU, the TPS calculates Bragg peak

positions on the CT of the patient. Additional information needed by the software are the positions and the volumes of the target and of the critical structures, which are called VOIs (Volume Of Interest). Each VOI, for example the tumor, is defined in each CT slice by a physician. VOIs may also be defined in healthy tissue, representing critical structures like the brain stem or the optical nerve. This critical structures are called OAR (*Organ At Risk*).

RBE-table. The RBE-tables contain all data relevant to calculate the biological effective dose for a certain tissue type, as a function of energy and particle species. With these informations the biological effect for complex ion fields can be evaluated according to the LEM model, described in chapter 3. For proton beam the RBE-value is fixed at value 1.1.

Accelerator-table. The accelerator-table provides to the TPS the available energies and associated focus, i.e. dimensions, and intensities. Beam fluence optimization is based on the information in this table. At CNAO are available 147 energies. The energy range for Carbon ion beams is 120-400 MeV/u, for proton beams the energy ranges from 63 MeV up to 250 MeV,

Dose values. As a result of the treatment planning a dose matrix contains the 3D-dose distributions of biological dose.

Dose volume histogram. Instead of inspecting the entire CT to access the quality of a treatment plan, a DVH (Dose Volume Histogram) allows fast control of the optimization results. Percentage of a volume is plotted versus received dose (see Fig. 4.1).

4.1.1 DEK

DEK, *Dose Engine Kernel*, is basically a proton/carbon ion TPS kernel developed and validated by INFN of Torino, in collaboration with the Ion Beam Application (IBA) Company [19]. This kernel is focused on spot scanning techniques. It is able to compute the physical and radiobiological effectiveness of a certain treatment configuration, accepting as inputs the anatomy of the patient and the beams set-up (forward planning). Additionally, DEK provides the inverse planning process to create the optimum beams

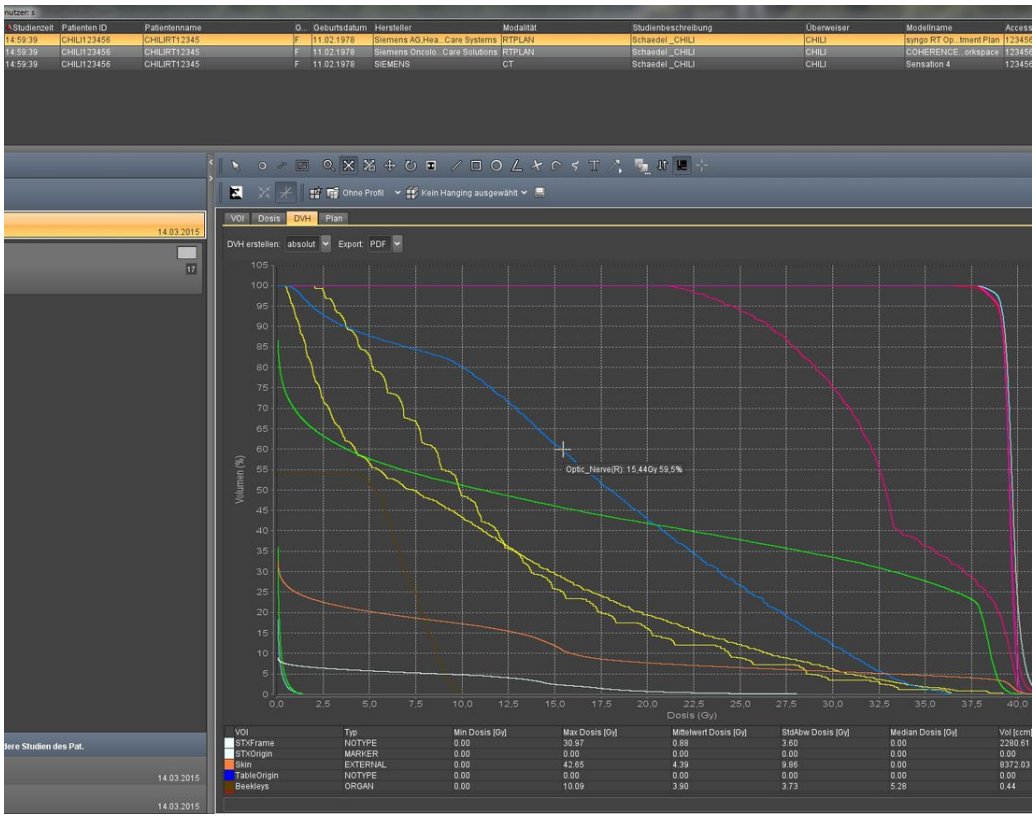

Figure 4.1: Example of Dose Volume Histogram performed by Syngo.

characteristics starting from the physician's prescription and different inputs defined by the user.
The DEK is a TPS kernel in the sense that performs the TPS core computations, while it is not intended to provide a graphical interface nor any support for setting patient contours, beams configuration and prescription. Instead, these features have been a crucial part of my work to use DEK to study the partial doses. DEK has been chosen because of its versatility and availability as a research tool at the INFN of Torino.

DEK is a code able to estimate the probability of cell survival in each volume element traversed by the beam, depending on the characteristics of both ion beams and tissue.
DEK allows the forward dose calculation and the following quantities can be saved and studied:

Physical dose: Hadron absorbed dose is a physical dose quantity D representing the mean energy imparted to matter per unit mass by ionizing radiation.

$$D = \frac{d\bar{\epsilon}}{dm} \tag{4.2}$$

The International System of units uses Gray [Gy] to measure the absorbed dose and 1 Gy corresponds to $1J/1kg$, joules per kilogram.

The physical dose given to each voxel $\{i, j, k\}$ of the computing grid selected within the CT volume, is the superposition of the dose delivered by all the beams l which pass through it:

$$D_{ijkl} = \phi_l D^{(0)}_{ijkl} \tag{4.3}$$

where ϕ_l is the fluence of the l beam, and the total dose is

$$D_{ijk} = \sum_l D_{ijkl} \tag{4.4}$$

RBE: The relative biological effectiveness, RBE, is defined as the ratio of the dose D_X administered with X rays and the dose D given with ions that correspond to the same cell survival S. The RBE is an empirical value that varies depending on the particles, energies involved, and which biological effects are observed.

The relative biological effectiveness for radiation of type R on a tissue of type T is traditionally defined as the ratio

$$RBE = \frac{D_X}{D_R} \tag{4.5}$$

where D_X is a reference absorbed dose of radiation of a standard type X, usually the dose of X-rays of 250 kV, and D_R is the absorbed dose of radiation of type R that causes the same amount of biological damage. Both doses are quantified by the amount of energy absorbed in the cells.

The knowledge of the carbon ions RBE becomes essential for the calculation of the biological dose. We saw in the previous chapter the complexity of the RBE due to its dependence on the dose itself, the LET and several other factors.
The RBE provides a mathematical framework to compare different treatment modalities. It refers to the isoeffective ratio of the dose deposited by a reference radiation to that of carbon ion irradiation in one fraction, d_p (with p standing for particle). In the context of the linear quadratic model, the RBE can be calculated using the LQ-parameters α_p and β_p for particles and α_X and β_X for the reference radiation (x-rays),

$$RBE = \frac{-\alpha_X + \sqrt{\alpha_X^2 - 4\beta_X(\alpha_p d_p + \beta_p d_p^2)}}{2\beta_X d_p} \tag{4.6}$$

The induced cellular damage, and thus the LQ-model parameters, strongly depends on the linear energy transfer of the respective radiation. The parameters α_p and β_p for each ion type and energy level are estimated from biological modeling approaches, e.g, the local effect model (LEM) described in the previous chapter.
For an accurate modeling of both, the delivered physical dose and the biological effectiveness of a carbon ion beam, it is essential to consider its specific fragment and energy spectrum. For a multienergetic beam of energies E, constituting of a range of fragments Z, α_p and β_p at each voxel i in a patient are the dose averaged sum of the contributions from each pristine Bragg peak,

$$\alpha_p(i) = \frac{\sum_Z \int_0^\infty \alpha(Z,E) \cdot \Phi(i,Z,E) \cdot S_p(Z,E) dE}{\sum_Z \int_0^\infty \Phi(i,Z,E) \cdot S_p(Z,E) dE} \tag{4.7}$$

$$\sqrt{\beta_p(i)} = \frac{\sum_Z \int_0^\infty \beta(Z,E) \cdot \Phi(i,Z,E) \cdot S_p(Z,E) dE}{\sum_Z \int_0^\infty \Phi(i,Z,E) \cdot S_p(Z,E) dE} \tag{4.8}$$

Here, $S_p(Z, E)$ refers to the stopping power and the fragmenta spectra are denoted by $\Phi(Z, E)$ Using this representation of the LQ-model parameters, the RBE as given in Eq. 4.6 varies across the volume of interest.

Biological Dose: The biological dose defined as the product of hadron absorbed dose, D, and hadron RBE

$$D_{bio} = D \times RBE \tag{4.9}$$

is introduced to estimate the photon dose that would produce the same therapeutic effect as the hadron absorbed dose, D, given under identical conditions.

Survival: In the context of the linear-quadratic model, the surviving fraction of clonogenic cells in a tumor, S, is solely determined by the biological effect ϵ, wich can be calculated for each voxel i:

$$S(\epsilon) = e^{\epsilon}, \quad \epsilon_i = \alpha_{p_i} d_{p_i} + \beta_{p_i} d_{p_i}^2 \tag{4.10}$$

LET: The linear energy transfer, LET, describes the action of radiation upon matter. It describes how much energy an ionising particle transfers to the material transversed per unit distance. LET depends on the nature of the radiation as well as on the material traversed.

$$L = \frac{dE}{dl} \tag{4.11}$$

where dE is the local energy loss due to collisions for a charged particle along a track segment dl. LET is habitually expressed in $keV \cdot \mu m^{-1}$.

The biological dose, the RBE and the survival distributions for total fraction irradiation and for partial irradiations have been computed for 2 CNAO patients.

At present stage DEK is not able to read DICOM files. Inputs have to be written in a proprietary format that will be specified in what follows. The evaluation results are saved in proprietary files as well.
The DEK is entirely written in C++ and it is executed on a Linux machine.

4.1.2 DICOM and DEK formats

Syngo generates a file with the characteristics of the beams used by the accelerator and by the dose delivery to perform the treatment.
The standard TPS output files are in *DICOM* (Digital Imaging and Communications in Medicin) which is the international standard for medical images and related information (ISO 12052). It defines the formats for medical images that can be exchanged with the data and quality necessary for clinical use. With tens of thousands of imaging devices in use, DICOM is one of the most widely deployed healthcare messaging standards in the world.

The RTPlan.dcm provided by the Syngo TPS with the beam's characteristics has to be converted into the "*.beams" format required by DEK to run. A dedicated MATLAB script has been developed for this work, to create the "*.beams" files for different partial irradiations, starting from the whole RTPlan.dcm.
The format of the "*.beams" file has to be the following:

```
numberOfBeams
x_iso  y_iso  z_iso  gantryAngle  patientAngle  fluence  energy  deflX  deflY  x_s  y_s  z_s
x_iso  y_iso  z_iso  gantryAngle  patientAngle  fluence  energy  deflX  deflY  x_s  y_s  z_s
x_iso  y_iso  z_iso  gantryAngle  patientAngle  fluence  energy  deflX  deflY  x_s  y_s  z_s
...
```

The field *numberOfBeams* indicates the number of beams listed in the next rows, one for each beam (or spot). The rows that follows are one for each spot. Each row contains:

- The (x_{iso}, y_{iso}, z_{iso}) coordinates in mm of the isocenter in the CT reference system.
- The indication of the gantry orientation through the Gantry Angle.
- The indication of the patient orientation through the Patient Support Angle.
- The indication of the number of primaries delivered by the beam.
- The specification of nominal beam energy in MeV/u.
- The X- and Y-coordinates in the IEC Gantry reference system of the intersection of the isocenter plane z = 0 with the beam axis.
- optional : the (x_s , y_s, z_s) coordinates in mm of the beam spot position in the CT reference frame; they can be omitted.

By changing the number of beams or their characteristics we are able to study the effect of these variations on the dose distributions using DEK calculation.
In the next paragraph the use of DEK to study the effect of partial irradiation is described.

4.2 Partial treatment delivery

In the treatment plan, the total dose is divided into fractions and each daily fraction is usually characterized by one, two or three fields.
As I have described in section (3.1), the techniques for planning with active scanning protons are the Single Field, Uniform Dose (SFUD) and Intensity Modulated Proton Therapy (IMPT), that establish the number and characteristics of the fields. The former is the combination of individually optimized fields, each delivering (more or less) homogenous dose across the target volume. The latter is the simultaneous optimisation of all Bragg peaks from all fields (with or without additional dose constraints to neighbouring critical structures).

The dose fractionation optimize the cost-benefits ratio of the treatment plan.

4.2.1 Dose fractionation

Efficacy of fractionation is based on the so called 4 Rs:

- Repair of sublethal damage: Cells exposed to sparse radiation experience sublethal injury that can be repaired, so cell killing requires a greater total dose when given in several fractions. Fractionation allows for repair of injured normal tissue and gives a potential therapeutic advantage over tumor cells.
- Reoxygenation: Hypoxic cells require more radiation to kill.
- Redistribution: Position in cell cycle at time of radiation determines sensitivity
  - S phase is radioresistant
  - G_2 phase delay results in increased radiation resistance

  Fractionated hadron therapy redistributes cells, rapidly cycling cells like mucosa, skin are more sensitive, slower cyclers like connective tissue, brain are spared.

- Repopulation: Determines the length and timing of therapy course

Dividing a dose into several fractions both spares normal tissues and damages the tumor. Former there is repair of sublethal damage between dose fractions and cells are able to repopulate. Latter there is a damage to the tumor because of the reoxygenation of tumor environment and the reassortment of cells into radiosensitive phases of the cell cycle between dose fraction. Prolongation of treatment reduces early reactions, however, excessive prolongation allows surviving tumor cells to proliferate.

During a session, may happens that for some reason, for instance a patient related problem or a machine failure, the total planned dose is not completely executed, in this case we speak of *partial dose irradiation*.
If the missed dose will be delivered to the patient in another day the total physical dose distribution over all the fractions will not change. The effects on biological dose distributions are not trivial and a tool to investigate them would be useful for physicists and physicians to take decisions. One goal of this work was to implement a research tool based on DEK to easy evaluation of partial irradiation. The expected biological effects are discussed in the next paragraph.

4.2.2 Dose recalculation

As mentioned before, DEK can compute the forward dose calculation from the Syngo TPS planned beams parameters, using the "*.beams" files as input to DEK.
We can divide the beams files containing a certain number of fields in n subgroups, where n is the number of the fields. The field is characterized by a specific value of the gantry angle and patient support angle.
The output doses are stored in "**.values.3d*" files (Fig 4.2), filled with the values of the required quantities.
DEK can compute both the total and the partial treatment depending on the *beams* used as input, while the Syngo TPS is not equipped with the Forward Computation option on external input. This is why the work of this thesis is also an interesting work from the clinical usefulness point of view.
The data in the values file are expressed as a 3D matrix, which elements contain the measured quantity delivered to the corresponding voxel.

```
N_x   'X[mm]'   'INTERVAL'
x_1   x_2   ...   x_{N_x + 1}
N_y   'Y[mm]'   'INTERVAL'
y_1   y_2   ...   y_{N_y + 1}
N_z   'Z[mm]'   'INTERVAL'
z_1   z_2   ...   z_{N_z + 1}
N_values   'valueTag_1'   'valueTag_2'   ...   'valueTag_{N_values}'
'BINARY'
value_1(x_1 < x < x_2, y_1 < y < y_2, z_1 < z < z_2) [double]
value_2(x_1 < x < x_2, y_1 < y < y_2, z_1 < z < z_2) [double]
 ...
value_{N_values}(x_1 < x < x_2, y_1 < y < y_2, z_1 < z < z_2) [double]
...
value_1(x_2 < x < x_3, y_1 < y < y_2, z_1 < z < z_2) [double]
...
value_1(x_1 < x < x_2, y_2 < y < y_3, z_1 < z < z_2) [double]
...
value_1(x_1 < x < x_2, y_1 < y < y_2, z_2 < z < z_3) [double]
...
```

Figure 4.2: Example of a *values* file, format of the DEK output.

MATLAB scripts have been developed for graphical display of these radiobiological quantities calculated by DEK.

We show the physical dose, the biological dose, the RBE, the cell survival fraction and the LET for a CNAO patient (A140376) on one slice of the volume passing through the isocenter, expressed in mm, in Fig. 4.3, 4.4, 4.5, 4.6 and 4.7 respectively. Thanks to DEK, it is possible to consider the fields and their effects, both individually and combined.

In Fig 4.8 the dose distribution profiles for a single row of the central plane (representing dose values in function of the increasing depth) can be seen. As expected, the physical dose for combined fields equals the sum of the physical doses for each beam. Due to the non linearity of RBE, however, the sum of biological doses calculated independently for each beam is higher than the biological dose for the total planned irradiation.

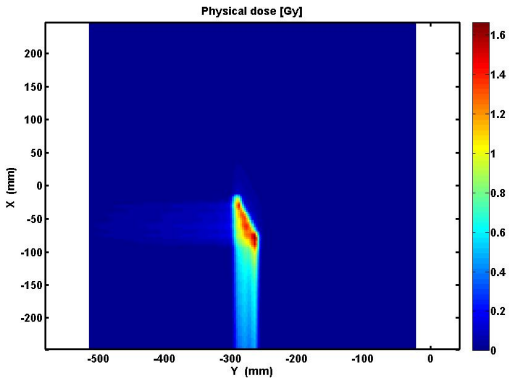

(a) Total

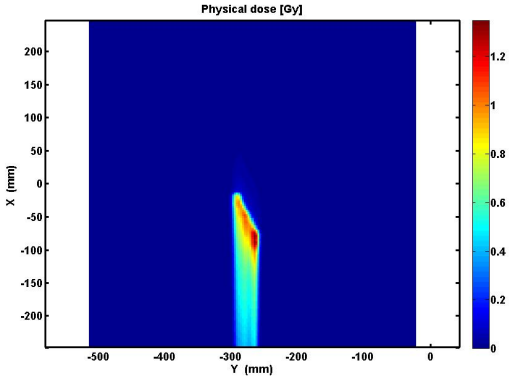

(b) Field A

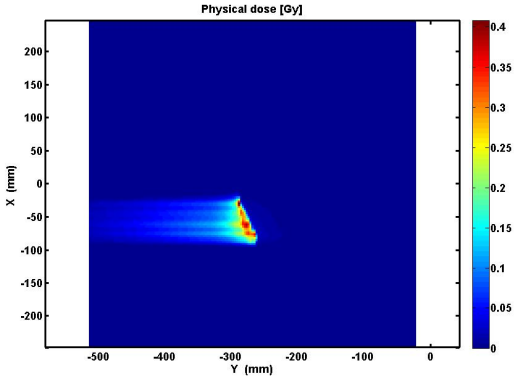

(c) Field B

Figure 4.3: Physical dose [Gy] for total irradiation (a) and for the individual fields (b) (c) of one slice of the volume [mm] ($z = cost$) through the isocenter. With DEK it is possible to evaluate the absorbed dose released by each field individually. Note that the path of entering radiation can be seen as a weaker trace before the target volume. One beam being weaker than the other, in the graph for total delivered dose one of the tracks is almost indestinguishable.

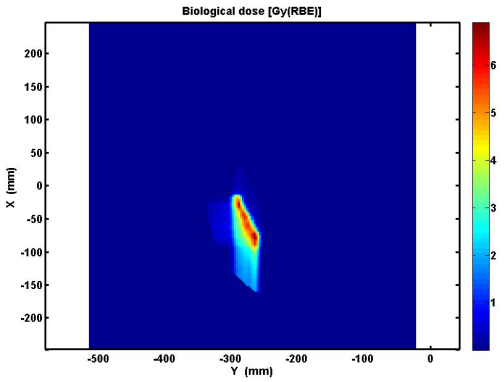

(a) Total

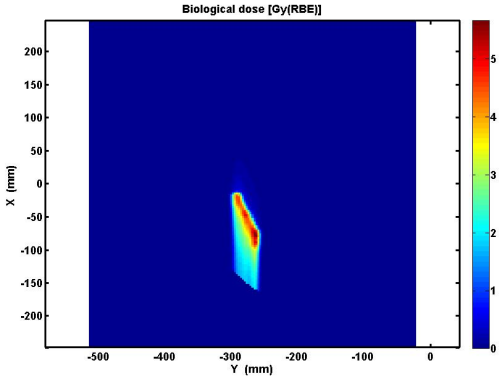

(b) Field A

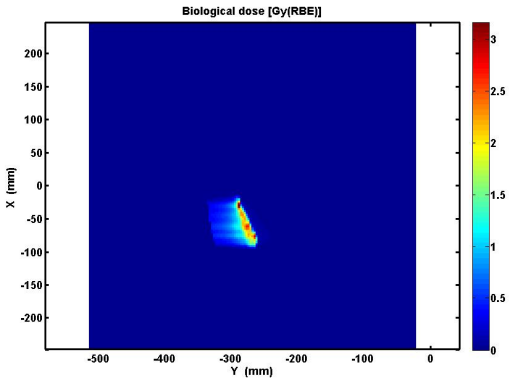

(c) Field B

Figure 4.4: Biological dose [Gy(RBE)] for total irradiation (a) and for the fields taken into account individually (b) (c) of one slice of the volume [mm] ($z = cost$) through the isocenter. With DEK it is possible to evaluate the biological dose released by each field individually. Note that the path of entering radiation can be seen as a weaker trace before the target volume. One beam being weaker than the other, in the graph for total delivered dose one of the tracks is almost indestinguishable.

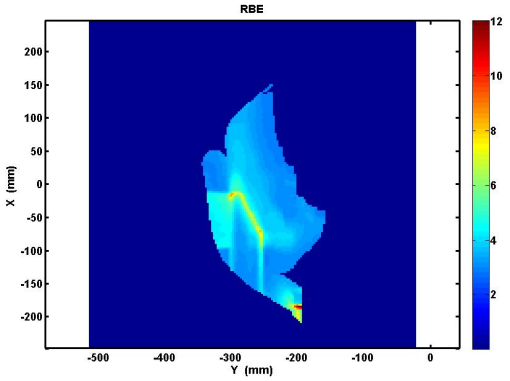

(a) Total

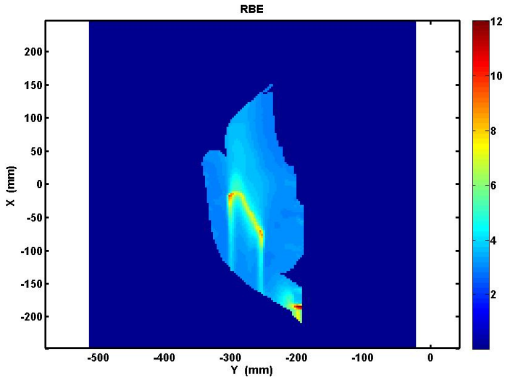

(b) Field A

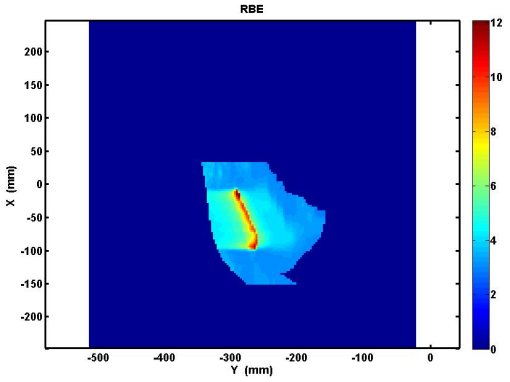

(c) Field B

Figure 4.5: RBE for total irradiation (a) and for the fields taken into account individually (b) (c) of one slice of the volume [mm] ($z = cost$) through the isocenter. With DEK it is possible to evaluate the RBE released by each field individually. Note that RBE is higher for B field due to its lower intensity.

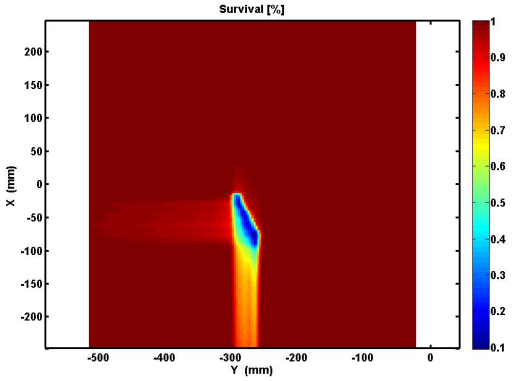

(a) Total

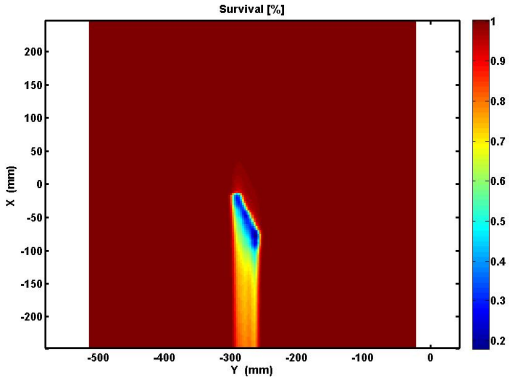

(b) Field A

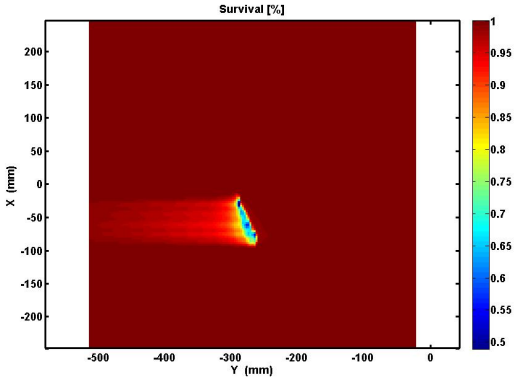

(c) Field B

Figure 4.6: Cells survival fraction [%] for total irradiation (a) and for the fields taken into account individually (b) (c) of one slice of the volume [mm] ($z = cost$) through the isocenter. With DEK it is possible to evaluate the cell survival fraction for each field individually.

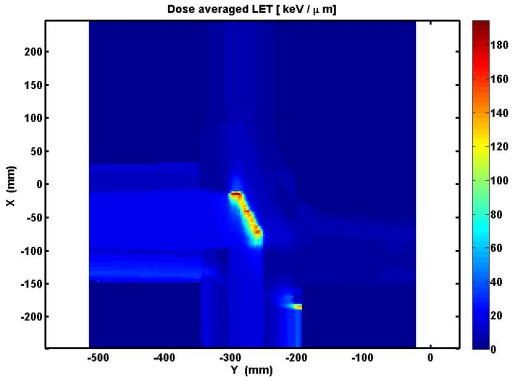

(a) Total

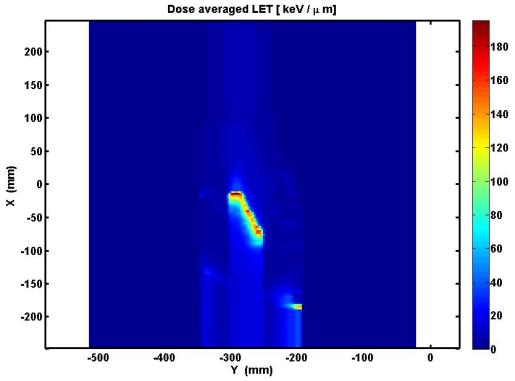

(b) Field A

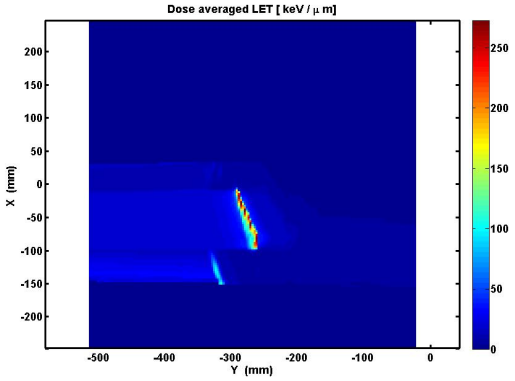

(c) Field B

Figure 4.7: Dose averaged LET [Gy/μm] for total irradiation (a) and for the fields taken into account individually (b) (c) of one slice of the volume [mm] ($z = cost$) through the isocenter. With DEK it is possible to evaluate the LET of each field individually.

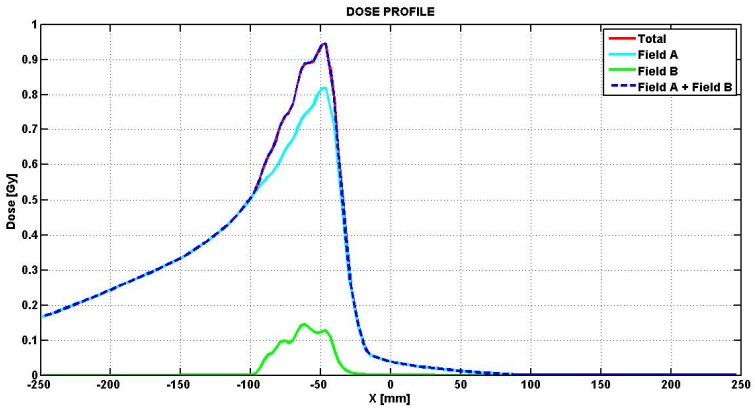

(a) Physical dose

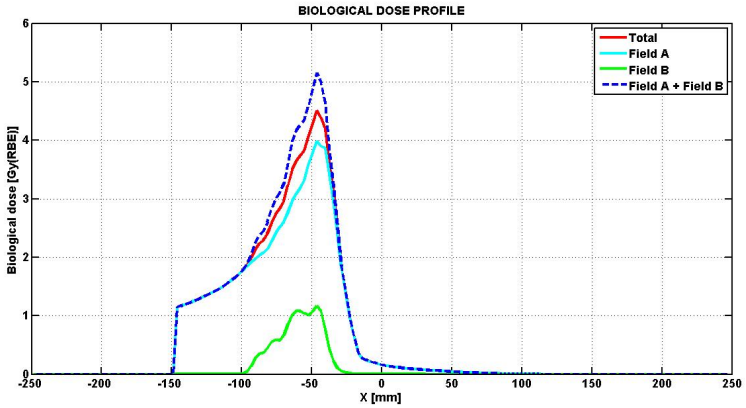

(b) Biological dose

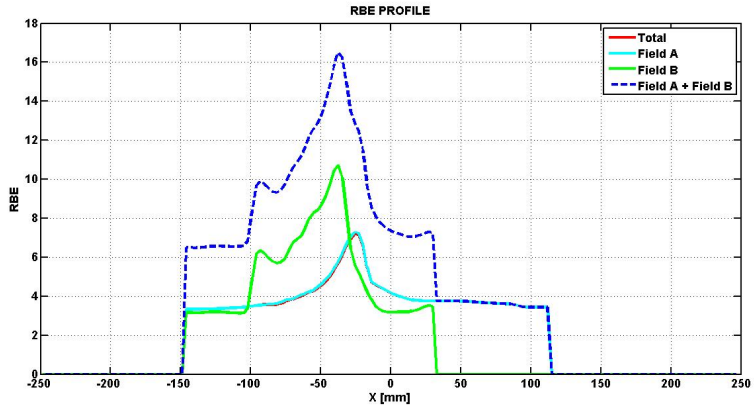

(c) RBE

Figure 4.8: Physical dose [Gy] (a), biological dose [Gy(RBE)] (b) and RBE (c) profile for a row of the central plane [mm] through the isocenter for total irradiation, the two fields taken into account individually and the sum of the two fields. Note that because of the different RBE, the sum of the biological dose of the two fields is greater than the total irradiation.

4.3 Dose Volume Histogram comparison

The purpose of my thesis is to build a tool to evaluate partial dose distributions and compare them with the full planned dose.
The Dose Volume Histogram, **DVH**, allows graphic visualization of how much percentage of the desired organ volume took at least a prescribed amount of dose, this allows the doctor evaluating how good a dose distribution is. In the case of partial irradiation I want to show how much the partial biological doses deviates form the total ones.

DVH summarizes 3D dose distributions in a graphical 2D format. In modern radiation therapy, 3D dose distributions are typically created in a computerized TPS based on a 3D reconstruction of a CT scan. The "volumes" referred to in DVH analysis is a target of radiation treatment, a healthy organ nearby a target, or an arbitrary structure [3].
DVHs can be visualized in either of two ways: *differential* DVHs or *cumulative* DVHs (Fig. 4.9 shows an example). A DVH is created by first determining the size of the dose bins of the histogram. Bins can be of arbitrary size, e.g. 0-1 Gy, 1.001-2 Gy, 2.001-3 Gy, etc. In a differential DVH, bar or column height indicates the volume of structure receiving a dose given by the bin. Bin doses are along the horizontal axis, and structure volumes (either percent or absolute volumes) are on the vertical. The differential DVH takes the appearance of a typical histogram.
The cumulative DVH is plotted with bin doses along the horizontal axis, as well. However, the column height of the first bin (0-1 Gy, e.g.) represents the volume of structure receiving greater than or equal to that dose. The column height of the second bin (1.001-2 Gy, e.g.) represents the volume of structure receiving greater than or equal to that dose, etc. With very fine (small) bin sizes, the cumulative DVH takes on the appearance of a smooth line graph. The lines always slope and start from top-left to bottom-right. For a structure receiving a very homogenous dose (100% of the volume receiving exactly 10 Gy, for example) the cumulative DVH will appear as a horizontal line at the top of the graph, at 100% volume as plotted vertically, with a vertical drop at 10 Gy on the horizontal axis.
A DVH used clinically usually includes all structures and targets of interest in the radiotherapy plan, each line plotted with a different color, represents a different structure, as shown in Fig. 4.9. The vertical axis is almost always plotted as percent volume (rather

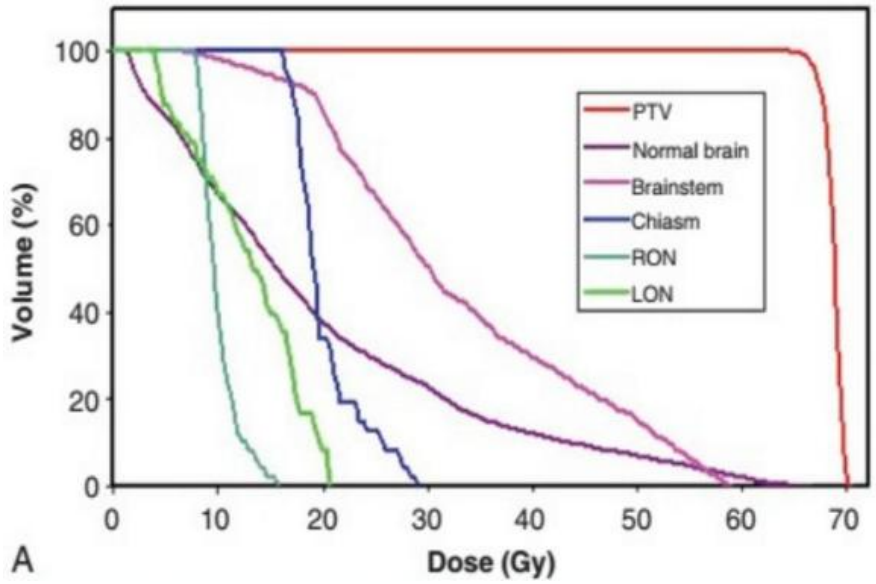

(a) Cumulative DVH

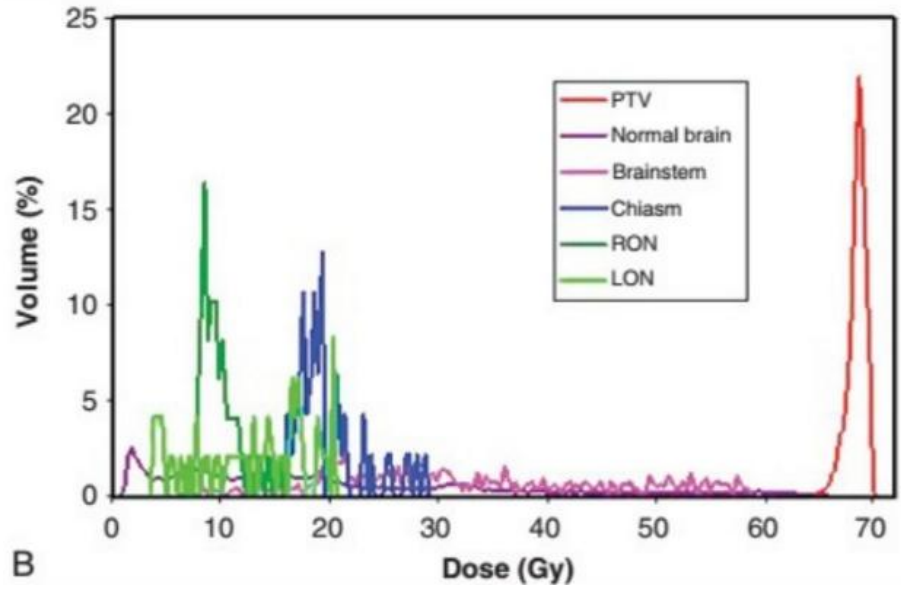

(b) Differential DVH

Figure 4.9: Example of a cumulative (a) and differential (b) DVH for the same plan.

than absolute volume), as well. A drawback of the DVH methodology is that it offers no spatial information, i.e., a DVH does not show where within a structure a dose is received.

Structures and targets

As introduced in ICRU Reports 50, 62 71 and 78, several volumes and margins related to both tumor and normal tissues have been defined for use in the treatment planning and reporting processes. Delineation of these volumes is an obligatory step in the planning process, as absorbed dose cannot be prescribed, recorded and reported without specification of target volumes and volumes of normal tissues at risk.
The main defined volumes are:

- *Gross tumour volume* (GTV): the gross palpable or visible/demonstrable extent and location of malignant growth. The tumour can be discovered by palpation and application of different medical imaging methods.

- *Clinical target volume* (CTV): The clinical target volume is the volume that contains a demonstrable GTV and/or sub-clinical microscopic malignant disease, which has to be eliminated. This volume thus has to be treated adequately in order to achieve the aim of therapy, cure or palliation. The CTV is an anatomical–clinical volume and is usually determined by the radiation oncologist. The CTV is usually stated as a fixed or variable margin around the GTV (e.g. CTV = GTV + 1 cm margin). Margins will be added to the CTV to create the Planning Target Volume (PTV).

- *Planning target volume* (PTV): The planning target volume is a geometrical concept, and it is defined to select appropriate beam arrangements, taking into consideration the net effect of all possible geometrical variations, in order to ensure that the prescribed dose is actually absorbed in the CTV. The PTV includes CTV and an additional margin for set-up uncertainties (organ motion, systematic errors caused by inaccuracy of patient positioning and machine tolerances). The PTV is linked to the reference frame of the treatment machine and is often described as the CTV plus a fixed or variable margin (e.g.PTV = CTV + 1 cm).

- *Region of interest* (ROI): The region of interest is a user defined region, which is commonly abbreviated as ROI. In radiation therapy: normal tissues whose radiation

sensitivity may significantly influence treatment planning and/or prescribed dose. ICRU 62 gives some new definitions:

- *Internal margin* (IM) - A margin that needs to be added to the Clinical Target Volume (CTV) to form the Planning Target Volume (PTV) to account for any positional errors from the planning information. ICRU Report 62 divided this margin into the Set up Margin (SM) and Internal Margin (IM), in order to separate the contributory sources of positional error into physiological error and set up error, respectively. The IM compensates for physiological variation of the size and shape of the volume (filling of rectum, movements due to respiration).

- *Setup margin* (SM) - The IM incorporates both intra-fraction errors such as that due to respiration, and inter-fraction errors such as that due to weight gain/loss or digestive system changes. SM accounts for all uncertainties in patient-beam positioning and technical factors (patient immobilization, machine stability). The total required margin is SM + IM.

- *Internal target volume* (ITV): accounts for motion of CTV in the patient, does not account for setup uncertainties, ITV = CTV + IM. The PTV in the case of conformal therapy and IMRT have to be determined with formula: PTV = ITV+set-up errors (on the base of on-board imaging).

- *Planning organ at risk volume* (PRV): PRV = OAR + margin (accounts for OAR movements). PTV and PRV may overlap.

I have analyzed the DVHs of some important structures of two CNAO patients. The effect of partial irradiations has been estimated looking the DVHs of the absorbed dose for the PTV and for some organs at risk separately as presented in the Chapter 5.

Patient A140376

The CNAO patient A140376 was treated to cure a chest wall sarcoma. The total prescribed dose on the PTV is of 76.8 Gy(RBE), delivered in 16 fractions of 4.8 Gy(RBE)/day. The total dose is delivered with two fields (field A and field B) perpendicular to each other. The analysis of this patient is described in Chapter 5.

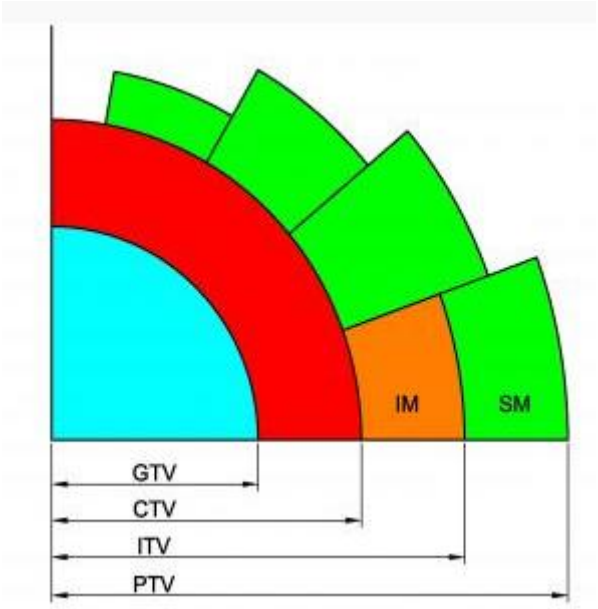

Figure 4.10: Schematisation of some volumes of interest used in a treatment plan.

Patient A150769

The CNAO patient A150769 was treated to cure a a chordoma. The total prescribed dose on the PTV is of 48 Gy(RBE), delivered in 16 fractions of 3 Gy(RBE)/day. The total dose is delivered with two fields (field A and field B) with a Gantry angle of 90° for both the fields and a Patient angle of 160° for the field A and 260° for the field B. The analysis of this patient is described in Chapter 5.

Chapter 5

Results

The figures 5.1, 5.2, 5.5 and 5.6 show the DVHs of PTV for the physical and biological dose for two CNAO patients, A140376 and A150769, in case of total treatment ("Total" in the plots) superimposed to the cases of individual fields ("Field A" and "Field B" in the plots) and to the case of the sum of single fields performed individually ("Field A + Field B" in the plots). In figures 5.3, 5.4, 5.7 and 5.8 are represented the DVHs for the organs at risk (it was taken as reference the liver for patient A140376 and the brain for patient A150769).
The PTV and OAR DVHs that I have calculated show the main characteristic of carbon ions: while the physical dose remains unchanged for the total case and for the sum of the fields taken individually, the biological dose changes. This important carbon ion phenomenon compared to photons and protons is explained by the fact that the physical dose is proportional to the number of deposited particles (and the total number of particles does not vary), while the biological dose, i.e. the physical RBE weighted dose, depends on the dose itself. Specifically we expect greater biological effectiveness at lower doses, and in fact the sum of the fields gives a higher biological dose than the total one.
Furthermore we have to remember that the technique used for the TPS is the intensity modulated proton therapy, IMPT. This technique allows a good dose uniformity over the tumor, as a result of the overlap of two or more not uniform fields, but the single field taken individually is not at all uniform. Therefore from the figures we can see how the DVHs of fields taken individually are covering in a different way the target. In particular in both the analyzed patients, both the fields are required to deliver a uniform dose on the PTV. Looking the Fig. 5.1 and 5.2 the shape and the maximum dose of the two fields

are significantly different. For that reason if one field is not delivered in the scheduled day it will be recovered in a dedicated additional day. The effect of the split of the Total dose in two days can be seen in the curve "Field A + Field B" in the shown DVHs.
In the specific both A140376 and A150769 cases, we can conclude that field B is essential in optimizing the TPS: it makes the dose on PTV uniform and is much less intense than field A, thus gives greater biological effectiveness.

In Tab. 5.1, 5.2, 5.3 and 5.4 the differences between the different DVHs curves are summarized. The therapy goal is to deliver the 100% of the prescribed dose to the 100% of the tumor (or PTV in our figures). Lower values indicate low treatment efficacy. On the contrary if the OAR are considered, the best should be 0 dose on 100% of the OAR volumes. In that case the low dose values on small percentage of volume indicate low toxicity and good treatment.

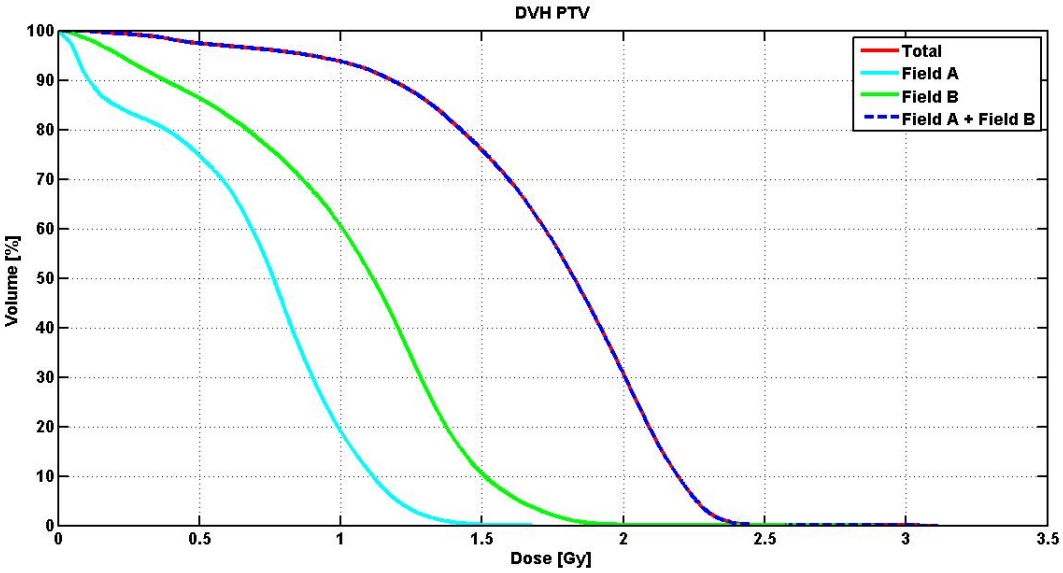

Figure 5.1: PTV DVH of physical dose for patient A140376 in case of total and partial treatment delivery.

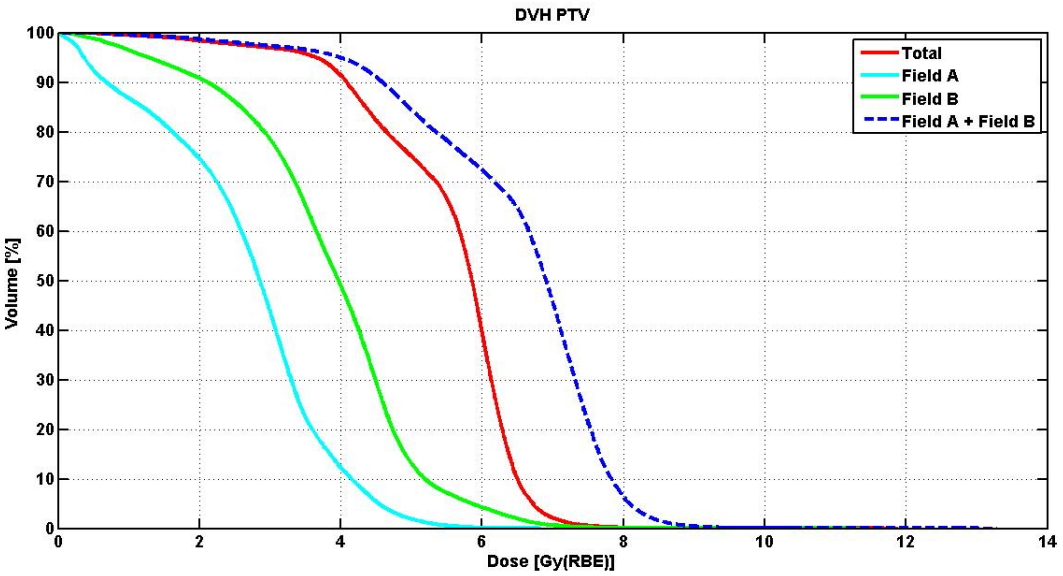

Figure 5.2: PTV DVH of biological dose for patient A140376 in case of total and partial treatment delivery.

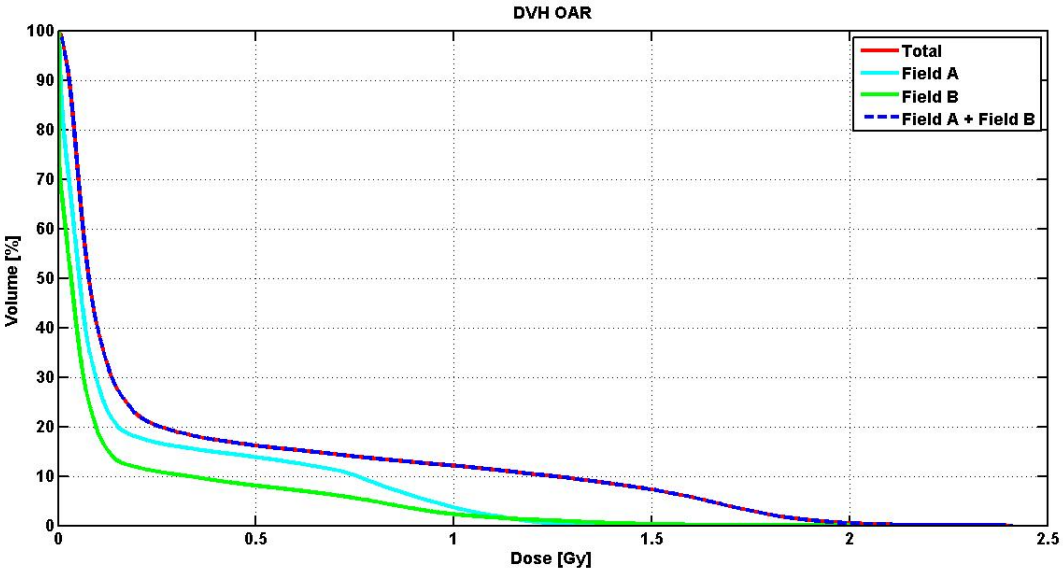

Figure 5.3: OAR (liver) DVH of physical dose for patient A140376 in case of total and partial treatment delivery.

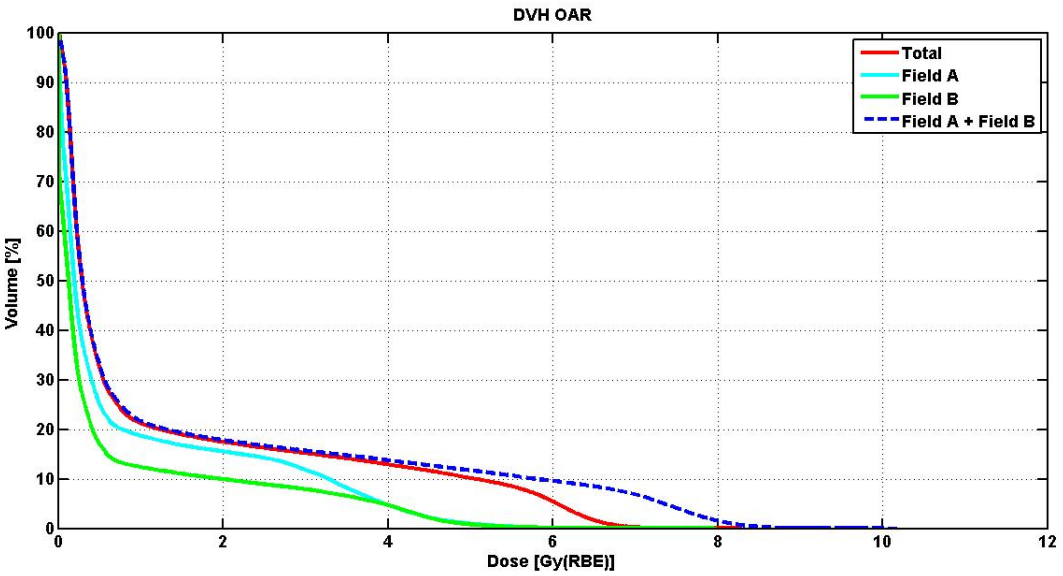

Figure 5.4: OAR (liver) DVH of biological dose for patient A140376 in case of total and partial treatment delivery.

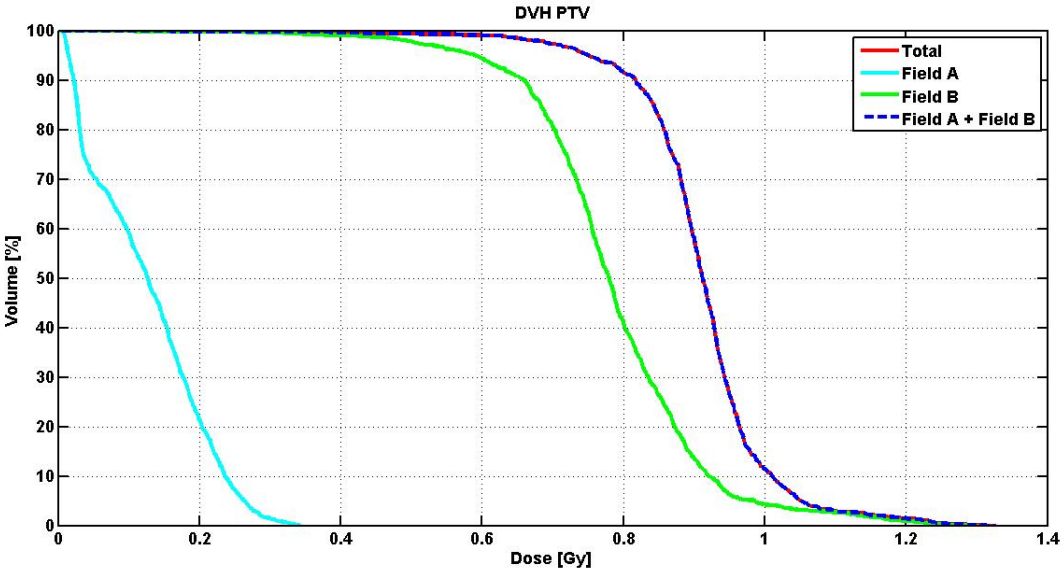

Figure 5.5: PTV DVH of physical dose for patient A150769 in case of total and partial treatment delivery.

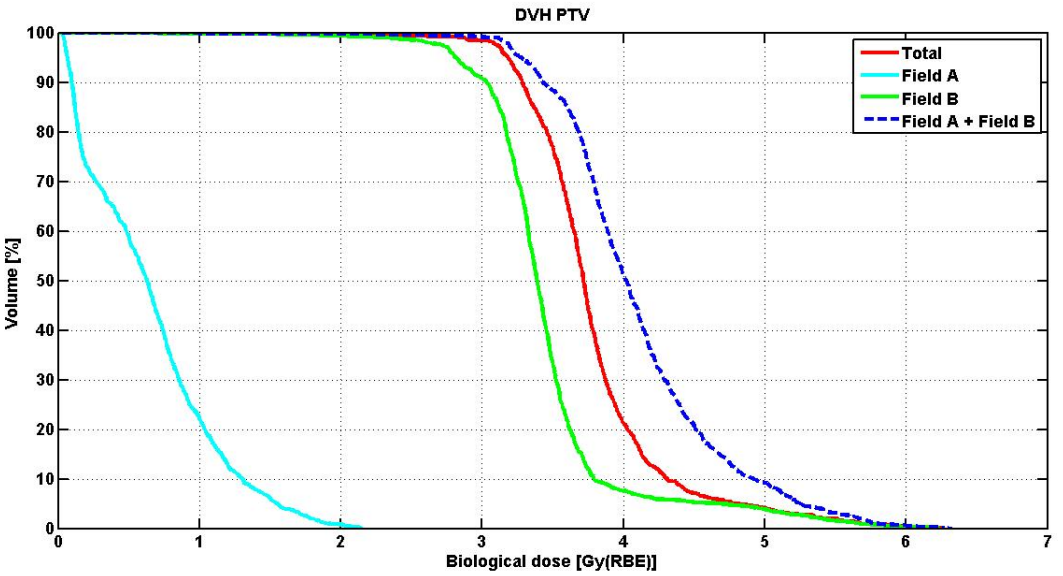

Figure 5.6: PTV DVH of biological dose for patient A150769 in case of total and partial treatment delivery.

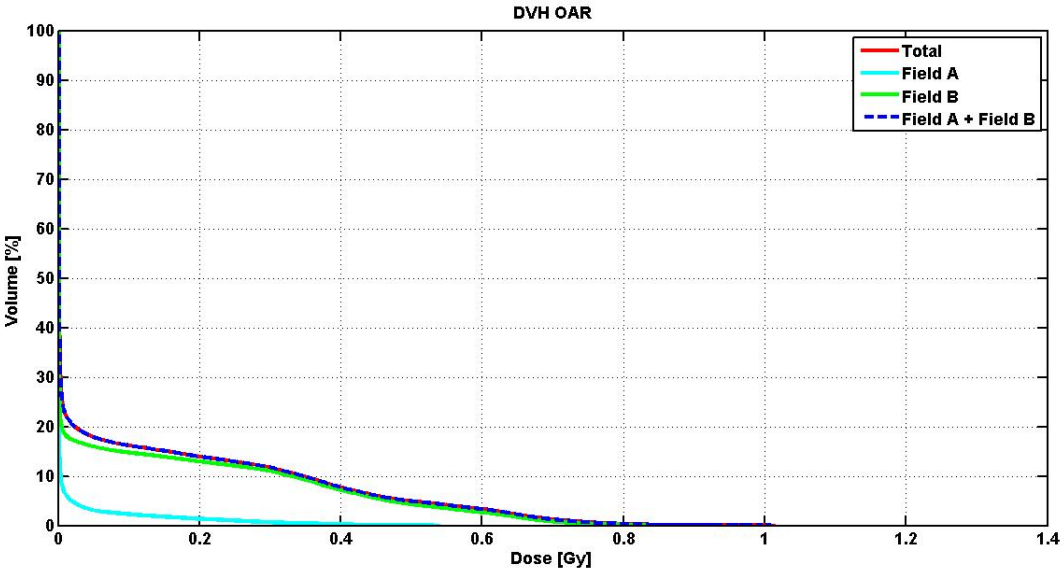

Figure 5.7: OAR (brain) DVH of physical dose for patient A150769 in case of total and partial treatment delivery.

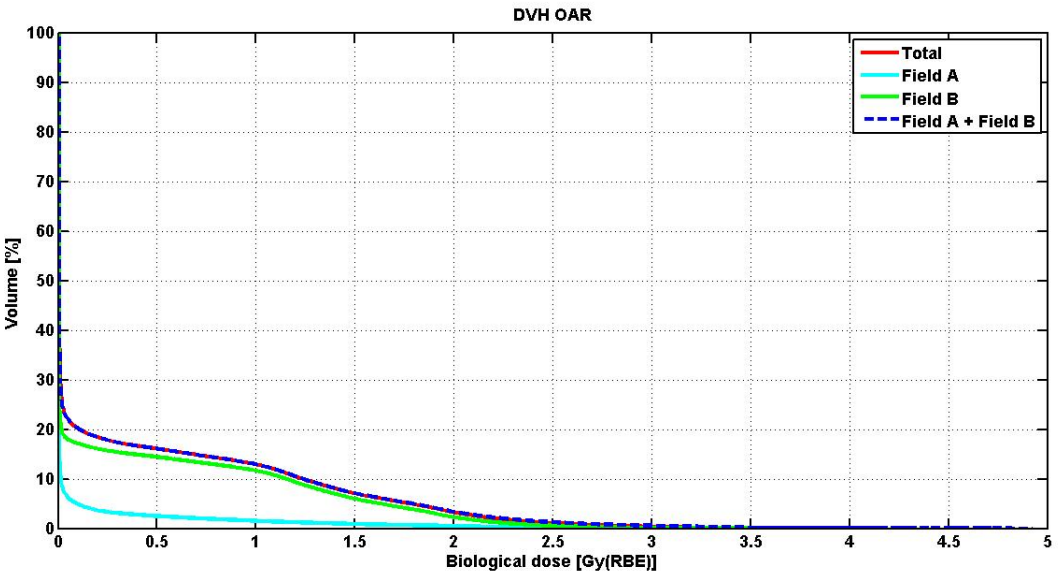

Figure 5.8: OAR (brain) DVH of biological dose for patient A150769 in case of total and partial treatment delivery.

Volume [%]	Total [%]	Field A+B [%]	Field A [%]	Field B [%]
95%	31%	34%	3%	11%
75%	42%	49%	17%	27%
50%	49%	58%	24%	33%
10%	55%	66%	35%	44%
5%	57%	68%	38%	49%
1%	61%	73%	45%	57%

Table 5.1: Some biological dose threshold values for PTV DVH for patient A140376 in case of total and partial treatment delivery, expressed as relative dose respect the prescribed one, assumed to be the max value of the biological dose, $D_{max} = 11.88\,Gy(RBE)$.

Volume [%]	Total [%]	Field A+B [%]	Field A [%]	Field B [%]
95%	1%	1%	0.1%	0%
75%	2%	2%	0.1%	$3 \cdot 10^{-2}$%
50%	3%	4%	2%	1%
10%	61%	70%	40%	24%
5%	73%	89%	48%	48%
1%	80%	98%	60%	59%

Table 5.2: Some physical dose threshold values for the OAR (liver) DVH for patient A140376 in case of total and partial treatment delivery, expressed as relative dose respect the prescribed one, assumed to be the max value of the biological dose, $D_{max} = 8.29\,Gy(RBE)$.

Volume [%]	Total [%]	Field A+B [%]	Field A [%]	Field B [%]
95%	51%	52%	1%	45%
75%	56%	60%	3%	51%
50%	59%	64%	10%	54%
10%	69%	78%	21%	61%
5%	77%	84%	25%	75%
1%	91%	92%	31%	90%

Table 5.3: Some biological dose threshold values for PTV DVH for patient A150769 in case of total and partial treatment delivery, expressed as relative dose respect the prescribed one, assumed to be the max value of the biological dose, $D_{max} = 6.26\,Gy(RBE)$.

Volume [%]	Total [%]	Field A+B [%]	Field A [%]	Field B [%]
95%	0%	0%	0%	0%
75%	$2 \cdot 10^{-5}$%	$2 \cdot 10^{-5}$%	0%	0%
50%	0.05%	0.05%	$2.3 \cdot 10^{-3}$%	0.01%
10%	30%	30%	0.2%	28%
5%	44%	44%	2%	40%
1%	62%	64%	35%	56%

Table 5.4: Some biological dose threshold values for OAR (brain) DVH for patient A150769 in case of total and partial treatment delivery, expressed as relative dose respect the prescribed one, assumed to be the max value of the biological dose, $D_{max} = 4.11\,Gy(RBE)$.

Chapter 6

Conclusions

During a session, may happens that for some reason, for instance a patient related problem or a machine failure, the total planned dose is not completely executed, in this case we speak of *partial dose irradiation*.
If the missed dose will be delivered to the patient in another day the total physical dose distribution over all the fractions will not change. The effects on biological dose distributions are not trivial and a tool to investigate them would be useful for physicists and physicians to take decisions.
One goal of this work was to implement a research tool based on DEK to easy evaluation of partial irradiation.

The codes developed in this thesis, written in MATLAB, made possible to automatically vary the number of DEK input beams to calculate partial doses and to show in a Dose Volume Histogram (DVH) the quality of the expected biological dose distribution for different combinations of partial plans compared with the planned one.
DEK was chosen for its versatility, typical of research products, which allows to calculate the following quantities: the physical dose [Gy], the Relative Biological Effectiveness, RBE, in different tissues, the Biological Dose [Gy(RBE)], cell survival and distribution of Linear Energy Transfer, LET, of the beams used.
The results show an increase of the biological dose in all cases of partial irradiation compared to the physical one, in accordance with the RBE dependence on the dose that appears to be greater for lower total doses. This agreement confirms the correctness of the work, which is the starting point of a more complex instrument, capable of consider-

ing different radiobiological models and all the variables used in them.

The study of the RBE as function of time is also currently studied by several research group [12].
A model considering the properties of carbon ion RBE and its dependence on the time would bring huge benefits in hadron therapy.

Appendix A

Dose recalculation

The dose calculation is performed in R using a forward planning.

CT, contours and 3D data

Patient CT: Assuming to have in the './patient-data/CT/' folder the sequence of DICOM images of patient CT, you can load into memory the complete CT with:

```
ct <- read.3d.dicom (dicom.folder = './patient-data/CT/')
```

The command read.3d.dicom reads directly the CT from DICOM format. The CT is assigned to the object ct.

3D data display (a slice): The objects of class *values* can be displayed with the family of *display.slice* methods. For example, to display the Hounsfield numbers on an axial slice for z = 180 mm:

```
display.slice (ct, z = 180, variable = 'HounsfieldNumber')
```

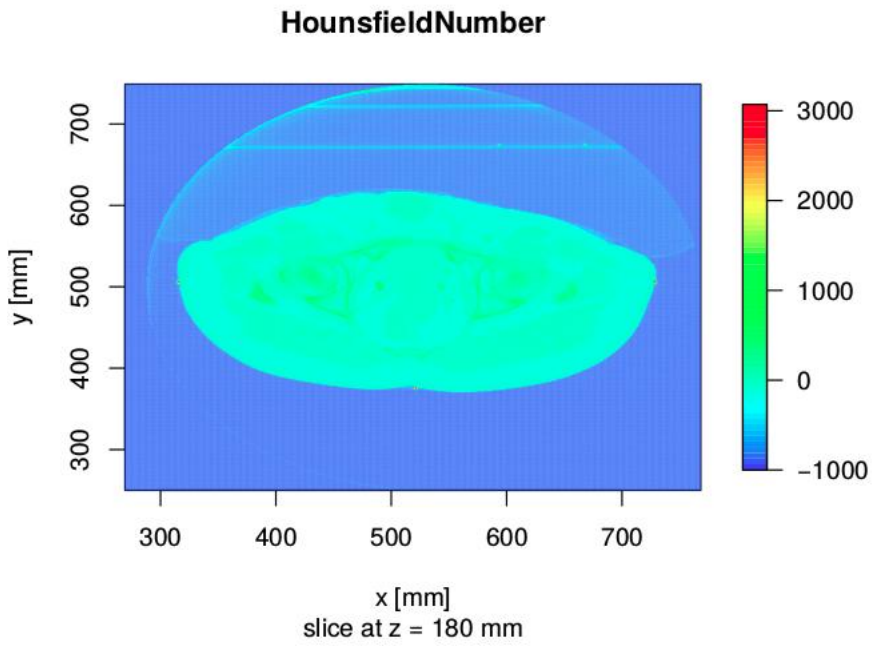

Data patient contours: For the tratment planning we need to identify the volumes of interest (VOI) in CT. This is done by defining the boundaries that circumscribe the VOI, on the axial slice. Rplanit does not have methods to directly define these boundaries (except in the case of simple volumes), so you have to load them from files (DEK format):

contours <- read.contours (file.contours = 'patient-data / CM / cm.contours', CT = ct)

Data Display + CT contours: Having loaded into memory the contours it is possible display them overlapping on axial CT slice using an optional parameter in *display.slice.ct*:

display.slice.ct (ct = ct, contours = contours, HU.window = c (-150, 250), z = 180, invert.y.axis = TRUE)

The contours are displayed in a single color (green by default). It is possible to use different colors for each contour defining them directly in *data.frame contours* (this color information is already present in DICOM, but not in the DEK format). For example these colors are defined (one for each contour) and inserted into *contours*:

display.color <- rainbow (length (unique (contours$contour)))
contours$display.color <- display.color [contours$id + 1]
display.slice.ct (ct = ct, contours = contours, HU.window = c (-150, 250), z = 180, invert.y.axis = TRUE, use.contour.colors = TRUE)

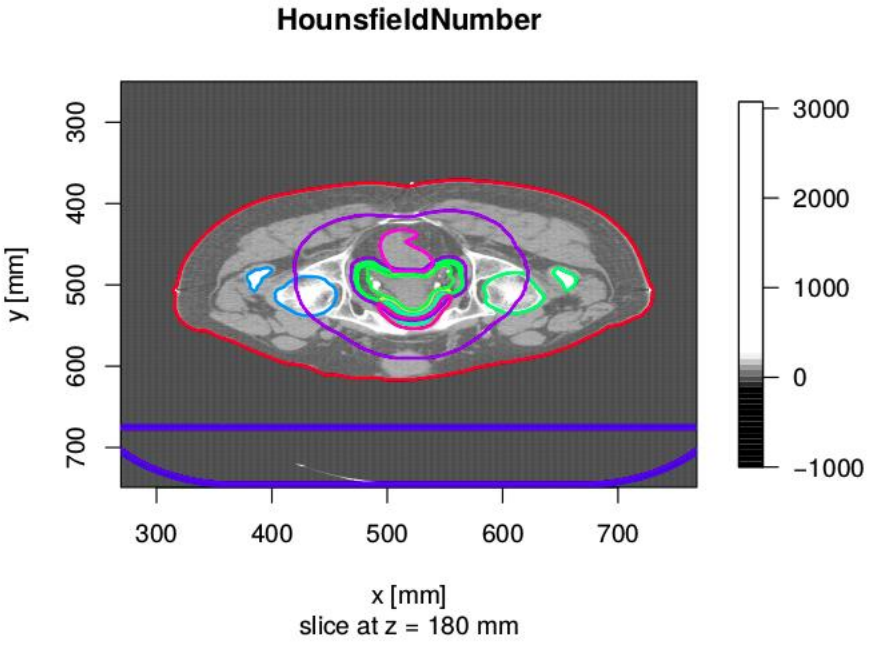

Read / write 3D data and contours: For a more comfortable use CT (or generally the 3D structures) can be saved locally in DEK format with the command:

write.3d (values = ct, file.name = 'ct.3d') # write in file 'ct.3d'
ct <- read.3d (file.name = 'ct.3d') # read 3D data in DEK format

Similarly for the contours you can use *write.contours* and *read.contours* commands. Generally it is always possible to use the *save* and *load* commands directly to save any object in R format.

Treatment plan definition

To carry out the treatment planning we have to define some information.
R organizes this data in a specific data structure called *plan*. You can create a template of this structure with this command, filled with default values:

plan <- create.plan(name = 'plan-example')

Through *create.plan* command, defining the appropriate parameters it's possible directly associate data to their corresponding fields. Once the plan is created, these data can also be added or changed later. In the above example the only data directly entered

is the plan name. The plan name corresponds essentially to the folder name where the simulation input and output data will be saved. For practical purposes it is sufficient to know only the name of the plan to retrieve the required information. For example, to save and load later the plan:

```
save.plan(plan) # the 'plan-example' folder is created and filled
plan <- read.plan ( 'plan-reverse')
```

Patient definition: Information of the patient's geometry are contained in CT and contours. It's possible set these data "hooking" directly objects in *ct* and *contours* memory to the respective plan slots:

```
plan$ct <- ct
plan$contours <- contours
```

In an alternative way it would be possible, instead of directly pass objects, indicate in plan$ctFile and plan$contoursFile the path to their file, previously saved to disk (in DEK format). Or mixed situations.

Radiation fields definition: Fields (*field*) of the radiation treatment are set by defining a specific *data.frame*. Different *field* correspond to different *data.frame* rows. Each *field* is caracterise by a beamline model, by a pair of angles (gantry and patient table), the target volume, from the interspot spacing, an isocenter and an external edge of the target volume coverage.

We want to irradiate the patient with two orthogonal proton fields lying onthe axial plane. The target is the PTV, and we want to cover it with an external 10 mm margin. The margin extension helps to get a more uniform dose coverage in the target volume, at the expense of a small increase in dose around this volume, the healthy part of the patient. It's possible to create the fields requested through the command:

```
fields <- create.field(beamline = 'protonSimple', targetVOI = 'PTV', iecGantryAngle =
c(90, 180), spotsExtensionOutsideTarget = 10)
```

The *create.field* parameters are optional. Where they are not used, they have been left to default values.

The fields object is then "hooked" in the plan:

```
plan$fields <- fields
```

Defining the method of calculation: In this section, we specify the quantities that it's possible to calculate with the simulation, the resolution of the calculation grid and any cut-off.
If we want to calculate the physical dose, and the RBE of a computing grid of voxel dimensions $5 \times 5 \times 5$ mm, it is necessary to modify the object *plan* as follows:

plan$computingValues <- c('Dose [Gy]', 'RBE')
plan$computingGridVoxelSizes <- c(5, 5, 5)

It's possible to define the region volume where you want to calculate the dose and other variables. This region can be a portion of the total volume of the CT. For example, to calculate the dose only in 'BODY':

plan$computingGridCoverageVOI <- 'BODY'

To speed up the calculations (and save memory, mandatory if you are working on remote server) it is possible to define a geometrical radius of the cut-off beyond which the single pencil-beam does not contribute to the total dose. By default, this radius is set to 100 mm. To make a quick sample calculation as example we set the radius to 20 mm:

plan$cutOffRadius <- 20

Alternatively, you can define an effective radius, through the percentage of the total energy released outside this range to neglect, using the field *plan$cutEnergyFraction*.

Forward planning

In order to calculate a forward planning, the complete definition of *beams* must be present in *plan*. While in the inverse-planning the radiation information is taken from *plan$fields*, in the case of forward planning this information is taken from *plan$beams*. This field is automatically filled when you run the inverse-planning with *run.dek.inverse*. If you create a plan from scratch, it is still possible to load an object *beams* with *beams <- read.beams('file.beams')* (DEK format) and "hook" to *plan* with *plan$beams <- Beams*, or alternatively directly with *plan$inputBeamsFile <- 'file.beams'*.
Then we perform forward planning:

plan.out <- read.plan('plan-example')
plan.forw.out <- run.dek.forward(plan.out)

It's finally posible to assess the contribution of each *field*. We have already in the object *beams* the total radiation information, just then split *beams* in the components depending on the gantry angle.

Appendix B

Create DVHs

We have developed some useful MATLAB scripts for analyzing the biological dose. The goal is to create the DVHs, the most effective way for analyzing the dose distribution.
The work flux counts basically 3 steps:

- Convert the DEKGPU dose file to plankit values.3d file
- If VOIs are not present, create the VOIs file
- Compute DVHs

We can convert the DEKGPU dose file to plankit values.3d file thanks to the function *convertDEKGPU2values(valueFilExample,DEKGPUfilename,outfile)*.
This funtion has as input:

- filename of an example values.3d with the coordinate definition (the dose values are not needed).
- file name of the DEKGPU 3D dose
- the name of the out file

and as output:

- file with the dose in DEK values.3d format.

To work in MATLAB we have to load correctly the DEK values with the function *loadValues(fileName, wantFigure)*.
This function has as input

- "*.value.3d"

and as output:

- *variable type struct x, y, z, xTag,yTag,zTag,valuesNames,values(Ndoses,x,y,z)*

We can create VOIs with the function *createVOIs(contourfileName, valuesFilename, createFile, VOIsfileName)*.
This function has as input

- filename of "*.contours.3d"
- file name of "*values.3d" to use as reference for 3D matrix
- if you want to save the file: "y" or "n"
- the name of the file *VOIsfileName*

and as output:

- booleam cell of $\{N_{vois}, x \times y \times z\}$

Then it's possible to load the VOIs with *loadVOIs(fileName)*.
This function has as input

- filename of the vois.3d file

and as output:

- *variable type struct x, y, z, xTag, yTag, zTag, voiNames, isInVOI(VOI,x,y,z)*

Finally, it's possible to compute the DVHs with *computeDVH(voisFileName, valuesFileName)*.
This function has as input

- filename of the vois.3d file
- filename of the values.3d file

and as output:

- *cell arrays*

Bibliography

[1] Sarah C. Bruningk, Florian Kamp, Jan J. Wilkens, 2015, EUD-based biological optimization for carbon ion therapy, Medical Physics 42, pp. 6248-6257

[2] Thomas F. Delaney, Hanne M. Kooy, 2007, *Proton and Charged Particle Radiotherapy*, Lippincott Williams & Wilkins

[3] Drzymala RE, Mohan R, Brewster L, Chu J, et al., 1991, *Dose-volume histograms*, International Journal of Radiation Oncology, Biology and Physics 21, pp. 71-78

[4] Martijn Engelsman, PhD, Marco Schwarz, PhD, Lei Dong, PhD, 2013, *Physics Controversies in Proton Therapy*, Semin Radiat Oncol 23, pp. 88-96

[5] Piero Fossati, Silvia Molinelli, Naruhiru Matsufuji, Mario Ciocca, Alfredo Mirandola, Andrea Mairani, Junetsu Mizoe, Azusa Hasegawa, Reiko Imai, Tadashi Kamada, Roberto Orecchia, Hirohiko Tsujii, 2012, *Dose prescription in carbon ion radiotherapy: a planning study to compare NIRS and LEM approaches with a clinically-oriented strategy*, Phys. Med. Biol. 57 pp. 7543–7554

[6] Thomas Friedrich, Marco Durante, Michael Scholz, 2013, *The Local Effect Model-Principles and Applications*

[7] Galvin, James M; Ezzell, Gary; Eisbrauch, Avraham; Yu, Cedric; Butler, Brian; Xiao, Ying; Rosen, Isaac; Rosenman, Julian; Sharpe, Michael; Xing, Lei; Xia, Ping; Lomax, Tony; Low, Daniel A; Palta, Jatinder, 2004, *Implementing IMRT in clinical practice: a joint document of the American Society for Therapeutic Radiology and*

Oncology and the American Association of Physicists in Medicine, Int J Radiat Oncol Biol Phys. 58, pp. 1616–34

[8] A Gemmel, B Hasch, M Ellerbrock, W K Weyrather,M Kramer, 2008, *Biological dose optimization with multiple ion fields*, Phys. Med. Biol. 53, pp. 6991–7012

[9] S. Giordanengo, M. A. Garella, F. Marchetto, F. Bourhaleb, M. Ciocca, A. Mirandola, V. Monaco, M. A. Hosseini, C. Peroni, R. Sacchi, R. Cirio, and M. Donetti, 2015, *The CNAO dose delivery system for modulated scanning ion beam radiotherapy*, Medical Physics 42, pp. 263-275

[10] R Grun, T Friedrich, T Elsasser, M Kramer 1 , K Zink, C P Karger, M Durante, R Engenhart-Cabillic, M Scholz, 2012, *Impact of enhancements in the local effect model (LEM) on the predicted RBE-weighted target dose distribution in carbon ion therapy*, Phys. Med. Biol. 57, pp. 7261–7274

[11] Hendee W., Ibbott G., Hendee E., 2005, *Radiation Therapy Physics*, Wiley-Liss Publ

[12] Taku Inaniwa, Masao Suzuki, Takuji Furukawa, Yuki Kase, Nobuyuki Kanematsu, Toshiyuki Shirai, Roland B. Hawkins, 2013, *Effects of Dose-Delivery Time Structure on Biological Effectiveness for Therapeutic Carbon-Ion Beams Evaluated with Microdosimetric Kinetic Model*, RADIATION RESEARCH 180, pp. 44-59

[13] International Atomic Energy Agency, IAEA, 2008, *Relative Biological Effectiveness in Ion Beam Therapy*, TECHNICAL REPORTS SERIES No 461

[14] M Kramer, J F Wang, W Weyrathe, 2003, *Biological dosimetry of complex ion radiation fields*, Phys. Med. Biol. 48, pp. 2063–2070

[15] M Kramer, M Scholz, 2000, *Treatment planning for heavy-ion radiotherapy: calculation and optimization of biologically effective dose*, Phys. Med. Biol. 45, pp. 3319–3330

[16] Lomax A, 2007, *An overview of Proton Therapy*, Med. Phys., pp. 2552-2552

[17] Daniel A. Low, William B. Harms, Sasa Mutic,James A. Purdy, May 1998, *A technique for the quantitative evaluation of dose distributions*, Medical Physics, Vol. 25, No. 5, pp. 656-661

[18] G Magro, S Molinelli, A Mairani 3, A Mirandola, D Panizza, S Russo, A Ferrari, F Valvo, P Fossati, M Ciocca, 2015, *Dosimetric accuracy of a treatment planning system for actively scanned proton beams and small target volumes: Monte Carlo and experimental validation*, Phys. Med. Biol. 60, pp. 6865–6880

[19] F. Marchetto, G. Russo, 2012, *Dose Engine Kernel 2.0.0 user manual*

[20] A. Mirandola, S. Molinelli, G. Vilches Freixas, A. Mairani, E. Gallio, D. Panizza, S. Russo, M. Ciocca, M. Donetti, G. Magro, S. Giordanengo, R. Orecchia, 2015, *Dosimetric commissioning and quality assurance of scanned ion beams at the Italian National Center for Oncological Hadron therapy*, Medical Physics 42, pp. 5287-5300

[21] S Molinelli, A Mairani, A Mirandola, G Vilches Freixas, T Tessonnier, S Giordanengo, K Parodi, M Ciocca, R Orecchia, 2013, *Dosimetric accuracy assessment of a treatment plan verification system for scanned proton beam radiotherapy: one-year experimental results and Monte Carlo analysis of the involved uncertainties*, Phys. Med. Biol. 58, pp. 3837–3847

[22] M. P. Morigi, *Applied physics in medicine notes*, Department of Physics, University of Bologna.

[23] S. Rossi, 2011, *The status of CNAO*, Eur. Phys. J. Plus (2011) 126: 78

[24] G Russo, A Attili, G Battistoni, D Bertrand, F Bourhaleb, M Ciocca, F M Milian, S Molinelli, S Muraro, T Orts, P Sala, G Vivaldo, F P Marchetto, *Physical and radiobiological modelling of ion beams in treatment planning through the Beamlet Superposition approach*, Phys. Med. Biol.

[25] E. Shinohara, 2009, *Module 7: Treatment Volumes and Treatment Planning in Proton Therapy*, Oncolink

[26] Tadashi Kamada, Hirohiko Tsujii, Eleanor A Blakely, Jürgen Debus, Wilfried De Neve, Marco Durante, Oliver Jäkel, Ramona Mayer, Roberto Orecchia, Richard Pötter, Stanislav Vatnitsky, William T Chu, 2015, *Carbon ion radiotherapy in Japan: an assessment of 20 years of clinical experience*, Lancet Oncol 16, pp. 93–100

[27] Reid F. Thompson, 2014, *RadOnc: An R Package for Analysis of Dose-Volume Histogram and Three-Dimensional Structural Data*, Journal of Radiation Oncology Informatics, pp. 98-110

[28] Hirohiko Tsujii, Tadashi Kamada,2012, *A Review of Update Clinical Results of Carbon Ion Radiotherapy*, Jpn J Clin Oncol 42, pp. 670-685